NOTE TO USERS

This reproduction is the best copy available

UMI

Colour Reproduction for Reflective Images

by

Wing-Ki Wilkin Chau

A thesis

presented to the University of Waterloo

in fulfilment of the

thesis requirement for the degree of

Doctor of Philosophy

in

Computer Science

Waterloo, Ontario, Canada, 1999

©Wing-Ki Wilkin Chau 1999

National Library of Canada
Acquisitions and Bibliographic Services
395 Wellington Street
Ottawa ON K1A 0N4
Canada

Bibliothèque nationale du Canada
Acquisitions et services bibliographiques
395, rue Wellington
Ottawa ON K1A 0N4
Canada

Your file Votre référence

Our file Notre référence

The author has granted a non-exclusive licence allowing the National Library of Canada to reproduce, loan, distribute or sell copies of this thesis in microform, paper or electronic formats.

L'auteur a accordé une licence non exclusive permettant à la Bibliothèque nationale du Canada de reproduire, prêter, distribuer ou vendre des copies de cette thèse sous la forme de microfiche/film, de reproduction sur papier ou sur format électronique.

The author retains ownership of the copyright in this thesis. Neither the thesis nor substantial extracts from it may be printed or otherwise reproduced without the author's permission.

L'auteur conserve la propriété du droit d'auteur qui protège cette thèse. Ni la thèse ni des extraits substantiels de celle-ci ne doivent être imprimés ou autrement reproduits sans son autorisation.

0-612-38231-1

Canada

The University of Waterloo requires the signatures of all persons using or photocopying this thesis. Please sign below. and give address and date.

Abstract

Because of differences between the colour gamuts of different printing devices, often some colours of an image are not producible by the output device of choice. To handle this problem, gamut mapping is used to make certain that every input colour has a corresponding printable output colour. Gamut mapping is normally done in a trichromatic device-independent space, such as the CIEXYZ, CIELAB or CIELUV colour spaces. The colour coordinates in such spaces can only be computed by assuming a source of illumination. Unfortunately, satisfactory results obtained for one viewing illuminant do not guarantee good results for other illuminants. Using colours specified as spectral reflectances can solve some parts of this illuminant dependency problem.

The basic concepts of colour image reproduction in reflectance space are developed in this thesis. The major reproduction steps for reflective images, including device characterization, gamut mapping, and backward colour transformation are examined. For device characterization, a colour lookup table (CLUT) with nonuniform sampling should be used for better accuracy. Reflectance space gamut mapping based on objective measurement and subjective measurement were investigated. A novel algorithm that preserves the fundamental component of reflectance is developed. Compared to the usual mapping algorithm, projective mapping, the new algorithm consistently produces results with small colour differences between reproduction and original colours for multiple illuminants.

The essential concepts for developing gamut mapping that based on appearance matching in reflectance space are developed. Two gamut mapping algorithms based on perceived colour attributes are provided. Finally, to reduce the high cost of cell extraction associated with nonuniformly sampled CLUTs, a novel algorithm for cell-finding is developed. This algorithm improves the performance of the backward transformation, which must be done once per image pixel.

Acknowledgements

I wish to thank my supervisor, William Cowan, who provided expert and insightful advice to me throughout the work. He has suggested numerous corrections and revisions.

Thanks also to Ian Bell who provided advice to me, and assisted in running the experiments; to Richard Bartels who taught me Computer Graphics courses; to Rob Kroeger for his help on solving countless system adminstration problems during my work as research programme manager; to Steve Mann who provided countless ice cream to release my stress in the lab; and, of course, to my wife, Meg Lui, for her support and patience.

Contents

1 Introduction 1

1.1 Overview 3

2 Colour Image Reproduction Concepts 5

2.1 A Formalism for Colour Image Reproduction 6

2.2 Device Independent Colour Spaces 8

2.3 Gamut Mapping using Tristimulus Colour Spaces 12

2.3.1 Matching Tristimulus Values 13

2.3.2 Matching Colour Appearance 15

2.4 Colour Reproduction and the Human Visual System 19

2.5 Surface Reflectance Spaces 20

2.5.1 Geometric Features of Reflectance Solids 23

2.6 Conclusion 25

3 Device Characterization 27

3.1 Model-based Reflective Characterizations 28

3.1.1 Halftone Images 28

3.1.2 Continuous Tone Images 31

3.1.3 Determining Control Values for a Model 32
3.1.4 Problems Associated with Models 39
3.2 Lookup Table Techniques for Colour Characterization 40
3.2.1 Colour Lookup Table Construction 41
3.2.2 Performance Issues with Colour Lookup Tables 42
3.2.3 Conclusion 44

4 Gamut Mapping in Reflectance Space **45**
4.1 Human Visual Sensitivity Space 46
4.2 Orthogonal Projective Mapping 48
4.2.1 Steps for Orthogonal Projective Mapping 48
4.2.2 Projective Mapping and Colour Matching 49
4.3 Fundamental Component Mapping 54
4.3.1 Basic Concepts of Fundamental Component Mapping 54
4.3.2 Fundamental Component Mapping under Several Illuminants 57
4.4 Experimental Results 59
4.4.1 Illuminant Differences 62
4.4.2 Mapping Results 63
4.5 Conclusions 64

5 Colour Attributes in Reflectance Space **65**
5.1 Constant Hue in Reflectance Space 66
5.1.1 Hue Sensation and Colour Spaces 70
5.1.2 Matching Hue under an Unknown Illuminant 73
5.1.3 Matching Hue with a Single Light Source 77

5.1.4 Matching Hue with Multiple Light Sources 78
5.1.5 Summary 79
5.2 Lightness in Reflectance Space 79
5.2.1 Constant Lightness in Reflectance Space 80
5.2.2 Changes of Lightness Due to Illuminant Changes 82
5.2.3 Lightness Changes for Chromatic Colours 85
5.2.4 Summary 88
5.3 Saturation in Reflectance Space 88
5.3.1 Reflectance and Saturation 88
5.3.2 Summary 91
5.4 Possible Mapping Methods 91
5.4.1 Hue Mapping that Minimizes Surface Metamerism 91
5.4.2 Barycentric Mapping on the Universal Hue Plane 92
5.5 Conclusion 93

6 Device Control Values for Reflective Images **94**
6.1 Backward Transformations Using Colour Lookup Tables 95
6.1.1 Extraction 96
6.1.2 Interpolation 98
6.2 A Fast Extraction Algorithm for the Backward Transformation . . . 102
6.2.1 Basic Idea 102
6.2.2 Gamut Partition 104
6.2.3 Region Detection 109
6.2.4 Point Advancement 110
6.2.5 Performance Analysis of the Algorithm 110

6.2.6 Applying the Extraction Algorithm in Reflectance Space . . 112
6.3 Conclusion 116

7 Conclusion **117**
7.1 Summary of the Thesis 117
7.2 Future Work 121
7.3 Final Conclusions 122

Bibliography **125**

List of Tables

4.1 The average CIELAB colour differences for the fundamental mapping (F.M.) and directed projection (Proj.) under two set of illuminants. 60

4.2 The average CIELAB colour differences for the fundamental mapping (F.M.) and directed projection (Proj.) under two set of illuminants. 61

4.3 Cosine of the principal angles between the fundamental component subspaces of the pairs of illuminants within a set. 62

5.1 Angles between luminous vectors of two light sources 85

6.1 Pseudocode of the extraction algorithm 111

6.2 Compare the expected and worst-case costs of extraction for different algorithms. 111

List of Figures

2.1 Mappings for colour image reproduction. 7

2.2 Colour-matching functions for the CIE Standard observer. 9

2.3 Colour signal of the light reflected from a surface illuminated by a light source. 18

2.4 Various reflectances sets: Producible reflectance set. physical realizable reflectance set. reflectance space. and wavelength space. 22

2.5 Three Dimensional Reflectance Solid. 24

3.1 The assumed light path for Neugebauer equations. 30

3.2 The scaled spectral absorption of the dyes with different concentrations for the DuPont printer used in our experiment. 36

4.1 The residuals spectra of illuminants for projective mapping. 53

4.2 Each reflectance space can be represented as the direct sum of two subspaces and under an illuminant. 55

5.1 Common topological properties for colour attributes. 67

5.2 The constant hue lines for Munsell Value 5 in the chromaticity diagrams 68

5.3 The dominant and complement wavelengths of the colours. 69

5.4 Saturated reflectance corresponding to a reflectance. 74

5.5 The regions of the projection space for two illuminants. 83

5.6 The sizes of regions of a projection space determine the number of useful reflectances available for colour reproduction. 84

5.7 The changing of illuminant has different impact on luminance for different reflectances depending on their relative location in its universal hue plane. 86

5.8 The chromaticity diagram of CIELUV. Saturation increases as colour points are located further away from the lightness axis. 89

6.1 (a) Trilinear interpolation: (b) prism interpolation: and (c) tetrahedral interpolation are shown in the figure. 100

6.2 Regions defined by contour curves of two different inks. 103

6.3 Partition of 2D printer gamut defined by four boundary lines. . . . 105

6.4 Boundary lines that partition the 2D printer gamut. 107

6.5 Boundary planes of gamut partition in 3D colour space. 108

6.6 Projection of an iso-surface on onto a tangent plane. 113

6.7 Projection of printer gamut in a reflectance space. 114

6.8 Orthogonal projection of printer gamut onto a plane. 115

Chapter 1

Introduction

With the advance of digital technology, almost all colour image reproduction processing is now controlled by computer. Most image reproduction processes are variants of the following process. A colour image is first scanned into digital form. The digitized image is then read by a colour matching program to determine the colours to be produced by the output device. Once the output colours are determined, a *backward colour transformation* determines the corresponding control signals to drive the output device.

Even though the reproduction process is described simply by the above three steps, many subtle issues must be resolved in designing a colour reproduction system. For example, after scanning, the colour of each pixel of an image is usually represented by a set of discrete numbers. How does a colour matching program know which set of numbers represents which colour? Worse, the same set of numbers from different input devices often represents more than one colour. Similarly, how does the program know which control signals should be sent to the output device to produce a particular colour? But, the most important issue is how the colour matching program assigns output colours for any given input colours. Because of differences in the ranges of producible colours, or *gamut*, from one device to another, the program must handle situations where input colours cannot be produced by an output device.

The above colour representation problems can be solved effectively using a *device characterization* process. which determines the relationships between device values and an objective. device-independent colour specification. The out of gamut problem is solved by *gamut mapping*. which defines a procedure to map colours between the input and output gamuts. Gamut mapping is best defined in a device-independent colour specification. All input and output colour devices that are characterized for the device independent space can then use the same gamut mapping procedures.

Many gamut mapping techniques have been proposed by researchers throughout the decade. Most of them were developed for the CIE (Commission International de l' Éclairage) standard colour tristimulus spaces. such as the CIEXYZ. CIELAB or CIELUV spaces. Since the tristimulus values in each of these spaces are computed based on the spectral distribution of the sources of illumination. problems arise when illuminants are changed. Two objects that are the same colour under the test illuminant may be different in colour under the viewing illuminant. Therefore. reproductions created for a specific test illuminant may be quite different when seen under a different viewing illuminant. To handle this problem better. some basic understanding of our visual system is needed.

Our visual system has the ability to adapt to changes in illuminant. Illuminant changes usually cause only a moderate change in the colour appearance of an object. The effect of discounting illuminant changes for colour sensation is referred to as *colour constancy*. Without colour constancy. the perceived colour of an object is based solely on the light emitted from the object: conversely, with perfect colour constancy. the perceived colour of an object is based solely on the surface reflectance of the object. It has been shown [Wys86] that our visual system exhibits good colour constancy under daylight illumination. but colour constancy is less effective under artificial illumination.

Because partial colour constancy is normal. neither a gamut mapping that preserves the emitted light reflected from a surface nor one that preserves reflectance information[1] provides a general solution for colour image reproduction. A com-

[1]Clearly, if a reproduction has the exact spectral reflectances of the original, the output image

promise between the two often provides a better result. Thus. it is important to understand gamut mapping techniques that use surface reflectance data. Unfortunately. there is no infrastructure of concepts and techniques available for gamut mapping using reflectance data.

Generating reflective images of real world is not practical with currently availabe input devices. Nevertheless. technology of capturing. editting and creating reflectance information exists and the future availability of reflective images that require high quality reproduction is likely. This thesis develops the basic concepts of colour image reproduction in reflectance space. It studies the major reproduction steps in reflectance space. which including *device characterization. gamut mapping.* and *backward colour transformation.* Several algorithms have been developed for the basic operations of colour image reproduction. With this infrastructure in place. future development of gamut mapping techniques in reflectance space is possible.

1.1 Overview

The thesis is organized in seven chapters. After this introduction. Chapter 2. *Digital Colour Image Reproduction Concepts.* provides background information that is needed to understand the concepts described in the later chapters. It examines the current technology of colour reproduction. and describes different characterizations and gamut mapping techniques for device independent colour spaces based on emitted light. Because the thesis extends these techniques to reflectance specification data. that use high dimensional linear reflectance spaces. the properties of such spaces are also described.

Before any controlled colour reproduction process is undertaken, the characteristics of both input and output devices must be known. Chapter 3, *Device Characterization.* describes *model-based* and the *colour lookup table based* methods

is always identical to the original one. Because of differences in device characteristics. it is almost impossible to obtain such reproduction in general.

for reflective characterizations. Important performance questions relating to accuracy and efficiency are examined for both approaches. Difficulties associated with model-based approaches and problems in constructing effective colour lookup tables are also discussed.

Gamut mapping algorithms can be developed based on objective criterion, such as minimizing a predefined colour difference function, or subjective criterion, such as maintaining perceptual colour attributes. Chapter 4. *Gamut Mapping in Reflectance Space*, develops objective criterion for gamut mapping in reflectance space. The shortcomings of orthogonal projective mapping are presented. Fundamental component mapping, which was developed to solve some of the problems associated with the projective mapping, is described. The two mapping techniques are compared in terms of reproduction accuracy.

To use subjective criteria in reflectance space, the relationship between a reflectance and its colour attributes must be determined. Chapter 5 develops relationships between reflectance and perceptual attributes like *hue*, *lightness*, and *saturation*. Methods for finding reflectances that have the same hue under different illuminants is provided. Two possible gamut mapping techniques based on colour attributes are given.

The high dimensionality of reflectance spaces presents a potential high cost in efficiency for colour reproduction. The backward colour transformation, the most costly operation for colour reproduction, is studied in Chapter 6. A fast extraction algorithm for backward transformation is described, and a performance analysis of the algorithm is presented. Procedures for using the algorithm with reflectance data are given.

Chapter 7 is the conclusion of the thesis. It summerizes the results of the thesis and provides directions for future work.

Chapter 2

Digital Colour Image Reproduction Concepts

The success of colour image reproduction is highly dependent on gamut mapping. Matching tristimulus values or some measurable quantities related to colour appearance, which will be referred as *matching colour appearance* in short, is the most common criterion used when developing gamut mapping algorithms. These algorithms produce satisfactory results for many applications. However, since most of them are developed based on the CIE tristimulus values measured using a predefined illuminant, problems exist when the images are viewed under other illuminants. Because of colour constancy, gamut mappings based on reflectance data, which is independent of viewing illuminant, may be able to improve the results.

In this chapter, the basic concepts of colour image reproduction are described in terms of current colour reproduction technology using device independent colour spaces. The representation of reflectance data in a high dimensional reflectance space is also described. The geometrical features of such reflectance spaces are also presented.

2.1 A Formalism for Colour Image Reproduction

A colour image reproduction process can be represented as a mapping function f that causes an output device to produce to an image that looks as closely as possible to the original image. The function is defined over the domain of all possible input colours, $\mathcal{D}_i^{\cdot}$, and the range of producible colours, $\mathcal{D}_o^{\cdot}$:

$$f : \mathcal{D}_i^{\cdot} \longrightarrow \mathcal{D}_o^{\cdot} .$$

Both $\mathcal{D}_i^{\cdot}$ and $\mathcal{D}_o^{\cdot}$ are the finite sets of colour points associated with the discrete device control values. A calibration function $v : \mathcal{D}^{\cdot} \rightarrow \mathcal{D}$ can be used to map a finite colour set into a continuous device colour space generated from the elements in $\mathcal{D}^{\cdot}$: its inverse $v^{-1} : \mathcal{D} \rightarrow \mathcal{D}^{\cdot}$ discretizes a colour value [Bel96]. The space $\mathcal{D}$ can be partitioned into two sets: one is a device gamut, $\mathcal{G}$, which contains all colours producible by the device, the other set, $\mathcal{D} - \mathcal{G}$, contains all nonproducible colours.

Since colours are usually described by device coordinates, the same colour value on two different devices only rarely produces two perceptually identical colours. This problem is usually handled by representing colours in a device independent colour space, $\mathcal{I}$. Device characterization (described in Chapter 3) is used to define the relationship. In essence, a device characterization determines a continuous function between device coordinate space $\mathcal{D}$ and the colour space $\mathcal{I}$, where $\mathcal{D}$ is viewed as a continuation set of the device control values. That is, for $h^{\cdot} : \mathcal{D}^{\cdot} \rightarrow \mathcal{I}$ and $h : \mathcal{D} \rightarrow \mathcal{I}$, $h(v(x)) = h^{\cdot}(x)$, for every $x \in \mathcal{D}^{\cdot}$, and $\mathcal{I}$ as a continuation of the device gamut. The mapping for the input device characterization is

$$h_i : \mathcal{D}_i \longrightarrow \mathcal{I} ,$$

and the mapping for the output device characterization is

$$h_o : \mathcal{D}_o \longrightarrow \mathcal{I} .$$

To define the mapping f, the inverse of h_o, h_o^{-1}, must be defined first,

$$h_o^{-1} : \mathcal{I} \longrightarrow \mathcal{D}_o , \qquad \text{such that} \qquad h_o^{-1} \circ h_o = e_I$$

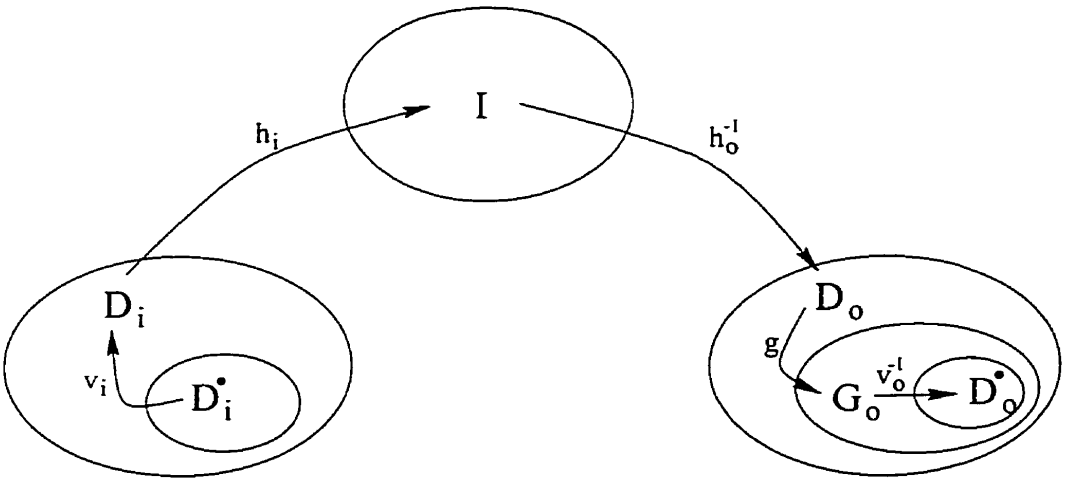


Figure 2.1: Mappings for colour image reproduction. which includes calibration functions (v). device transfer functions (h). and device gamut mapping (g).

where $e_I : \mathcal{I} \rightarrow \mathcal{I}$ is the identity function on $\mathcal{I}$. The inverse mapping h_o^{-1} describes the backward transformation. the most important mapping in colour image reproduction. It can be created empirically from the colour lookup table generated by a set of measured samples. Otherwise. it can be created from a mathematical model of the device *transfer function*. which describes the output response of a device for any given control values.

Ideally. the mapping f can be fully described in terms of v_i, v_o, h_i and h_o^{-1} as

$$f = \mathcal{D}_i^{\cdot} \xrightarrow{v_i} \mathcal{D}_i \xrightarrow{h_i} \mathcal{I} \xrightarrow{h_o^{-1}} \mathcal{D}_o \xrightarrow{v_o^{-1}} \mathcal{D}_o^{\cdot} .$$

However. because of differences in device characteristic. it is quite possible that some input colours are not producible by the output device. An additional mapping can be defined to handle such a situation. Let $\mathcal{G}_o \subset \mathcal{D}_o$ be an output device gamut. A mapping

$$g : \mathcal{D}_o \longrightarrow \mathcal{G}_o$$

maps colours in an output device space to the device gamut is applied before the inverse of v_o. Thus, f becomes

$$f = \mathcal{D}_i^{\cdot} \xrightarrow{v_i} \mathcal{D}_i \xrightarrow{h_i} \mathcal{I} \xrightarrow{h_o^{-1}} \mathcal{D}_o \xrightarrow{g} \mathcal{G}_o \xrightarrow{v_o^{-1}} \mathcal{D}_o^{\cdot} .$$

The function g is often referred as a gamut mapping between the devices. The success of image reproduction depends strongly on the actual form of g (see Figure 2.1).

2.2 Device Independent Colour Spaces

For colour image reproduction as described in the previous section, a device independent colour space is necessary. Many suitable colour spaces have been developed. Some of them define a colour based on its psychophysical properties, such as the CIE colour spaces [CIE78], the Munsell System [Mun46], or the Mutually Opposed Trichromatic Response (MOTR) model [Hun89], while others define descriptive parameters approximating perceived visual attributes, such as HSV [Smi78], Lsα [Lai93]. Most of these colour spaces are derived from or standardized on the CIEXYZ tristimulus space, described in the following paragraph.

Based on colour-matching experiments conducted in 1931 and 1964, the CIE developed a standard colour representation referred as the CIEXYZ colour space [CIE78]. It is the most widely used and recognized colour space. To determine the colour of a light, its colour is compared in appearance to an additive mixture of red, green, and blue primary lights. By adjusting the amounts of the red, green, and blue primary colours, a match is found. The amounts of each primary in the mixture are used to specify the colour. Using a linear transformation, the colour of the light can be represented by its tristimulus values X, Y, and Z. The X, Y, Z values specify the weights of standard primaries defined for the CIE Standard observer. Two lights with the same tristimulus values are perceived as matched in colour when perceived under identical viewing conditions. The tristimulus values

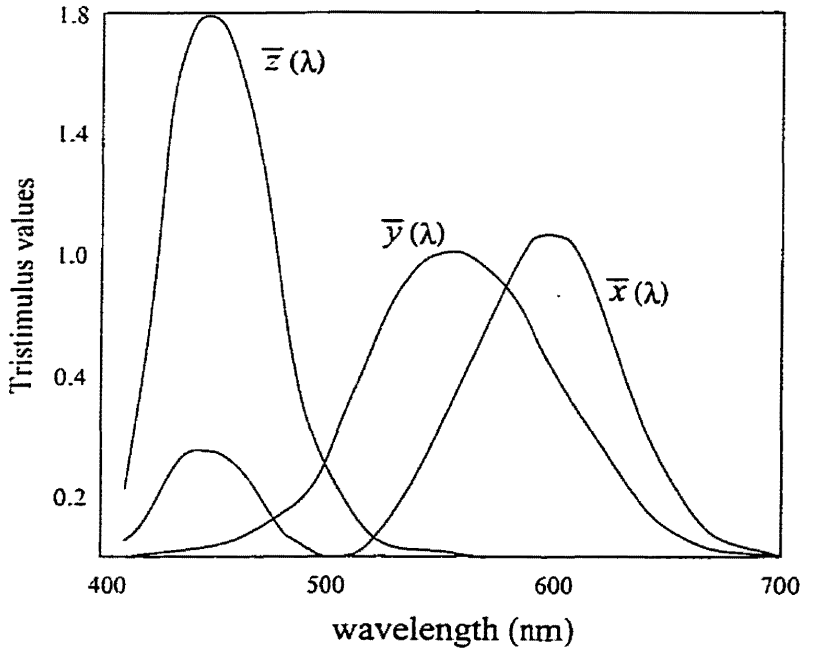


Figure 2.2: Colour-matching functions $\bar{x}(\lambda)$, $\bar{y}(\lambda)$, and $\bar{z}(\lambda)$ for the CIE Standard observer.

of a light, φ_λ, are computed by the following formulas:

$$X = \int_\lambda \varphi_\lambda \bar{x}(\lambda) d\lambda \ . \quad Y = \int_\lambda \varphi_\lambda \bar{y}(\lambda) d\lambda \ . \quad Z = \int_\lambda \varphi_\lambda \bar{z}(\lambda) d\lambda \ .$$

where $\bar{x}(\lambda)$, $\bar{y}(\lambda)$, and $\bar{z}(\lambda)$ are the colour-matching functions (Figure 2.2) [WS82]. The tristimulus values of the reflected light from a surface with reflectance, $\mathbf{r}$, illuminated by Φ_λ are computed by the above formulas with $\varphi_\lambda = r(\lambda)\Phi_\lambda$

$$X = \int_\lambda r(\lambda)\Phi_\lambda \bar{x}(\lambda) d\lambda \ . \quad Y = \int_\lambda r(\lambda)\Phi_\lambda \bar{y}(\lambda) d\lambda \ . \quad Z = \int_\lambda r(\lambda)\Phi_\lambda \bar{z}(\lambda) d\lambda \ .$$

For computer calculations, the tristimulus values are usually approximated by the summation of the N discrete sample points, suitably positioned across the entire visible spectrum. The above equations become

$$X = \sum_{i=1\cdots N} r(\lambda_i)\Phi_{\lambda_i}\bar{x}(\lambda_i) \ . \quad Y = \sum_{i=1\cdots N} r(\lambda_i)\Phi_{\lambda_i}\bar{y}(\lambda_i) \ . \quad Z = \sum_{i=1\cdots N} r(\lambda_i)\Phi_{\lambda_i}\bar{z}(\lambda_i) \ . \tag{2.1}$$

or in matrix form:

$$\mathbf{t} = \mathbf{H}^t \mathbf{E}\, \mathbf{r} \ .$$

where $\mathbf{t} = [X\ Y\ Z]^t$, $\mathbf{H}$ is the $N \times 3$ colour matching matrix given by the discrete CIE colour-matching functions as

$$\mathbf{H}^t = \begin{bmatrix} x(\lambda_1)\ x(\lambda_2)\ \cdots\ x(\lambda_N) \\ y(\lambda_1)\ y(\lambda_2)\ \cdots\ y(\lambda_N) \\ z(\lambda_1)\ z(\lambda_2)\ \cdots\ z(\lambda_N) \end{bmatrix} \ .$$

$\mathbf{E}$ is the $N \times N$ diagonal matrix with Φ_{λ_i} in its (i,i) entry, and $\mathbf{r} = [r(\lambda_1)\ r(\lambda_2)\ \cdots\ r(\lambda_N)]^t$. Notice that even though the XYZ tristimulus values are used for colorimetric specification, they do not tell us the appearance of a colour; instead, their primary function is to determine whether two colours match. Two colours with the same tristimulus values for a given illuminant are perceived as matching in colour when observed in identical viewing conditions.

The most important advantage of using CIEXYZ colour space is its linearity. According to Grassmann's Law, additive mixtures of colour stimuli can be uniquely described using only their tristimulus values [Hun91b]. The colour of a mixture can be expressed as a linear combination of the XYZ values of each individual colour. However, the CIEXYZ colour space has several related disadvantages:

1. There are no well defined geometric functions that describe surfaces of constant saturation or hue.
2. The Euclidean distance in the space does not correlate well with the perception of colour difference.
3. The colour of a surface, specified by its XYZ values, is illuminant dependent.

In an attempt to reduce these problems the CIE defines two uniform colour spaces. The more commonly used of the two is CIELAB. Its coordinates are derived directly from the XYZ tristimulus values using the following nonlinear equations:

$$L^* = 116\left(\frac{Y}{Y_n}\right)^{\frac{1}{3}} - 16 \tag{2.2}$$

$$a^* = 500\left[\left(\frac{X}{X_n}\right)^{\frac{1}{3}} - \left(\frac{Y}{Y_n}\right)^{\frac{1}{3}}\right] \tag{2.3}$$

$$b^* = 200\left[\left(\frac{Y}{Y_n}\right)^{\frac{1}{3}} - \left(\frac{Z}{Z_n}\right)^{\frac{1}{3}}\right] \tag{2.4}$$

where X_n, Y_n, and Z_n are the tristimulus values for a reference white colour.[1] In colour printing, the reference white object is normally the white paper used for printing. The tristimulus values are normalized to offset some of the influence of the illuminant.

The coordinate L^* corresponds roughly to the lightness; a^* to red/green balance; and b^* to green/blue balance. The values of a^* and b^* do not correspond to simple

[1]When X/X_n, Y/Y_n or Z/Z_n are smaller or equal to 0.008856, different equations are used to compute the values of $L*$, $a*$, and $b*$. The exact formula can be found in [WS82, Page 167].

psychophysical properties of the colour. but they can be used to approximate the colour attributes of hue and saturation [Hun95]. The colour difference between two colours can be approximated by the CIELAB colour difference formula:

$$\Delta E_{ab} = \sqrt{\Delta(L^*)^2 + \Delta(a^*)^2 + \Delta(b^*)^2}\,.$$

This formula has been widely used in colour image reproduction research [Kan96. Hun91b. SFB92. HRV97] and is used in this thesis as an objective measurement of colour difference.

Other colour spaces have been defined based on perceptual attributes. The HSV space [Smi78]. and the Lsα space [Lai93] are two such colour spaces. The HSV space approximates the perceptual properties of *hue. saturation.* and *value.* Similarly. the Lsα space defines the coordinates closely related to *hue. saturation.* and *level.* The terms *value* and *level* in these colour spaces correspond to the *lightness* of a colour. Since these spaces are designed for improving user interaction for colour image manipulation. accurate colour representation is not guaranteed. Thus. these colour terms are only defined as perceptually approximate.

2.3 Gamut Mapping using Tristimulus Colour Spaces

Once a colour space is chosen. a gamut mapping algorithm can be developed for the space. In doing so colour image reproduction algorithms are grouped into two different categories based on reproduction criteria. One category tries to preserve the original tristimulus values or similar derived values like L^*, a^*, and b^*. Since two colours with the same tristimulus values invoke similar colour sensations, a reproduction that has tristimulus values similar to those of the original is expected to be good. The difference in tristimulus values between reproduction and original is minimized with respect to a metric function. Based on past experience [Hun95, WG93]. however. good results are obtained only when the output medium and viewing condition are similar to those of original.

When viewing conditions differ. simply matching tristimulus values is frequently inadequate. In this case. a second approach that matches colour appearance is used

[Sch86. VW92. Mac93. Gra95. ML97]. The appearance of a colour is determined using a colour appearance model derived from psychophysical experimentation. Colour appearance is specified in terms of perceived attributes such as lightness. hue. and saturation. During the reproduction process. colours that are close in appearance are used to represent the original colours. Unfortunately. whether an exact model of colour appearance even exists is currently unresolved. and all proposed models have high computation cost. To avoid the high cost. most algorithms use colour attributes that are simply defined in terms of CIE tristimulus values. To handle out-of-gamut colours. the algorithms usually maintain hue. while scaling lightness and chroma to fit into the gamut of the target output device. When the output gamut is very different from the input gamut. this method can produce good results that are not possible using the methods that attempt to preserve the tristimulus values.

2.3.1 Matching Tristimulus Values

Two surfaces with the same spectral reflectance are perceived as being identical in colour under all illuminants because the re-emitted light reflected from them is always identical. As a result. the problem of illuminant dependency can be avoided if the reflectances of a reproduced image are matched with the original ones. Unfortunately. reflectance matched outputs rarely exist because of physical differences in device technology. Instead. methods based on surface metamerism concepts must be used.

Two colours that have the same CIE tristimulus values produce the identical colour sensations when viewed in isolation. Thus. an intuitive approach to colour image reproduction is to obtain the same tristimulus values in the reproduced image as in the original image when both are viewed under the same reference illuminant.

In the abstract. reproduction can occur in the following steps. Convert the colour of an original image from device coordinates to CIEXYZ values. Locate the colour in the output device gamut that has the same tristimulus values as the original. Output that colour. The process is complicated by two problems.

First, the relationship between the colour sensation and the tristimulus values is illuminant dependent: a change of illumination may affect the matching results. Second, because of the differing characteristics of colour devices, the output device can have a different colour gamut than the input image. Thus, a simple match of tristimulus values may be impossible.

To understand the first problem, metamerism must be introduced. Surface metamerism occurs when two spectrally different surface reflectances are perceived as being identical in colour [BS81]. This occurs when the tristimulus values of light re-emitted from the two surfaces are identical. Because the re-emitted light is controlled by both illuminant and surface reflectance, a change of illuminant causes changes of the colour signals reflected from the two surfaces. Problems arise when the viewing illuminant of the reproduction is different from the original. Surfaces that matched in colour for the standard may now be perceived as having distinct colours. Thus, reproduction that is based only on the tristimulus values under a given illuminant does not generate consistent results for other illuminants.

Much research has been done on matching paint colours [Yul67, GB82]. They examine how appearance changes with changes of illuminant and try to produce paints with smooth spectral reflectance that exhibit little metamerism. Even though exact spectral matches are not possible in most cases, stable results can be obtained using reflectance. As shown in Chapter 4, matching colour appearance for multiple illuminants is possible using the fundamental component of a reflectance.

The second problem occurs because output devices have very different gamuts. To illustrate this problem for luminance, consider the reproduction of a photographic transparency as a reflective print. The luminance range of the transparency is ten fold larger than that of reflective printing, so that most colours in the transparency lie outside of the printing gamut in CIEXYZ space [Hun95]. Any matching criteria in XYZ colour space are guaranteed to fail.

The first problem is hard to solve, while the second one can be handled directly either by scaling during gamut mapping, which will be discussed in Section 2.3.2, or by using a normalized colour space. For the luminance example, CIE perceptually uniform spaces, such as CIELUV and CIELAB, use colour coordinates that are

calculated with respect to reference white as shown in Equation 2.2. As a result, the lightness value L^* is normalized with values between 0 to 100. The effect of changing illuminant and luminance range can be offset by this normalization step. If the viewing illuminants do not change much, matching colour values in the perceptually uniform space can produce satisfactory results.

The idea of maintaining tristimulus values is to preserve colour appearance. As discussed above, this strategy may not work well for cross media reproduction because problems related to different viewing environments, and different gamuts of the devices. Even when the above problems can be reduced by using a CIE uniform colour space, the results may not be acceptable because of differences between the colour gamuts of the devices. On the other hand, the colour specification using the tristimulus values is hard to interpret in terms of our colour sensation.

2.3.2 Matching Colour Appearance

When the original and reproduction are viewed in very different environments, it is often more appropriate to match colour appearance than to match tristimulus values. Predicting colour appearance is hard: many researchers have worked for several decades trying to understand how different factors affect perceived colour. The colour of the illuminant, luminance level and surrounding field are some of the important factors that affect the appearance of colour. When the colour of the illuminant changes drastically, the colour of an illuminated object changes somewhat, though the change of an object colour is often less than the change of tristimulus values would suggest, an effect called colour constancy. Luminance level also affects the sensation of colour. For example, colour appears desaturated at low luminance and vivid at high luminance [Hun95, Chapter 5]. The colour and luminance of surrounding areas also affects colour appearance. A grey patch appears lighter or darker depending on whether it is placed on a dark or light background, an effect called simultaneous contrast. Similarly, a grey patch appears greenish on a red background and reddish on a green background, effect called chromatic contrast.

In addition to the factors described above, other conditions such as viewing

angle and adaptation level also influence colour sensation. To accurately determine colour appearance, all factors must be taken into account. Unfortunately, a comprehensive understanding of these factors and their interactions is not available. Many colour appearance models, such as the Hunt model [Hun91a, Hun94b], the Nayatani model [NTS90], the Guth ATD model [Gut91], and RLAB [Fai91, Fai93], have been developed to explain some appearance phenomena, but using these models for colour reproduction is uncommon because of problems related to accuracy and efficiency [BF95]. Instead, existing colour image reproduction algorithms [SW91, Gua92, HB93, WAB94, Gra95] tend to use the colour attributes, normally derived directly from the CIE tristimulus values, to try to retain the appearance of an original image.

Unlike tristimulus value matching algorithms, appearance matching algorithms are not based on objective measurements. Instead they adopt rules of thumb commonly used in the graphics arts community to produce satisfactory output. A typical set [SCB88] is the following :

1. Preserve the grey axis of the image.
2. Maximize luminance contrast.
3. Reduce the number of out-of-gamut colours.
4. Minimize shifts of hue and saturation.
5. Maximize colour saturation.

Such principles are used as general guidelines when developing gamut mapping algorithms for digital image reproduction. Other properties, such as preserving detail in both light and dark regions, mapping distinct input colours to distinct output colours [SW91], and maintaining smooth transitions between neighbouring colours [Gua92], are also important. Such guidelines cannot be followed rigidly, because conflicts exist between some rules. For example, luminance contrast can often be increased only at the cost of increasing out-of-gamut colours in dark regions: sometimes increasing saturation causes large shifts of saturation from the

original image. Thus. compromises are made when designing a gamut mapping algorithm.

Gordon. Holub. and Poe [GHP87] proposed a very simple gamut mapping algorithm. They first mapped neutral colours to output neutrals. then tried to preserve colour difference by compressing saturation in each constant lightness plane using a constant scaling factor. The scaling factors were derived from the largest discrepancies between the input and output saturation on the constant lightness planes. As a result. the input gamut was compressed to fit inside the output gamut. This approach achieves the first. third and fourth principles stated above. while ignoring the second and fifth. The results suffer severe compression of tonal and chromatic range. To alleviate the problem. the authors suggest using the input image gamut instead of the device gamut to compute the scaling factors.

Stone. Cowan. and Beatty [SCB88] used the above principles to develop a set of heuristic transformations for digital image reproduction. The image gamuts are first translated. scaled. and rotated to align the gray axes. followed by an umbrella transformation to conform with the target gamut. Any remaining out-of-gamut colours are then projected onto the gamut boundary. The parameters of the transformations are determined interactively image by image. Since the method uses the XYZ colour space. which is not perceptually uniform. the transformations have different perceptual effects on different regions of the colour space. To produce high quality results. the trade-offs among the reproduction principles had to be made carefully for each image. As discovered by Gordon et al. [GHP87], only some reproduction rules can be followed.

These two algorithms provide a reference model for the process of designing gamut mappings. The reference model first ensures that the neutral colours are mapped correctly before chromatic components are introduced. Further transformations are defined to map the input colours into the output gamut while trying to minimize the hue changes and maintain colour relationships.

Even after decades of research. there is no general solution for gamut mapping. Gentile *el at.* [GWA90] compared several techniques for handling out-of-gamut colours. Their results showed that clipping algorithms, which project out-of-gamut

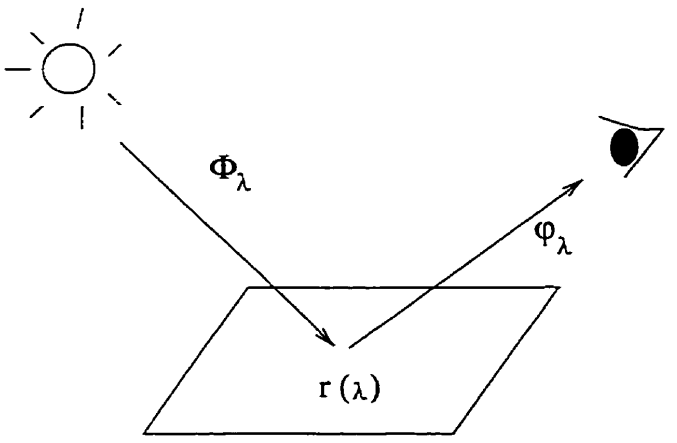


Figure 2.3: Colour signal, φ_λ, is the light reflected from a surface, $r(\lambda)$, illuminated by a light source, Φ_λ.

colours to the output gamut boundary, are preferred to piecewise linear compression algorithms, which scale the image gamut to fit into the output gamut. Morovic and Luo [ML97] evaluated different gamut mapping algorithms using a psychophysical experiment. They showed that some algorithms have better overall performance than others, but, there is no single algorithm that consistently outperforms the others.

Almost all currently available colour image reproduction algorithms are based on CIE tristimulus values. As a result, they work only for a predefined illuminant. To avoid this problem, an illuminant independent colour space is needed.

2.4 Colour Reproduction and the Human Visual System

Before considering which colour space is better for colour image reproduction, it is beneficial to understand how the human visual system perceives colour. As shown in Figure 2.3, the colour signal reflected from a surface is jointly determined by the illuminant, Φ_λ, and the surface spectral reflectance, $r(\lambda)$. The colour signal, φ_λ, is expressed as

$$\varphi_\lambda = \Phi_\lambda r(\lambda) \ .$$

Thus, changes in illuminant can lead to considerable changes in reflected light. However, illuminant changes only cause a moderate change in the colour appearance of an object [LM71, PS86]. Effects based adaptation and contrast, which allow colour appearance to remain approximately constant under different illuminants are referred to as *colour constancy*.

Consider a scenario where an observer looks at a colour patch surrounded by a constant background under an arbitrary illuminant. Let the CIE chromaticity (the normalized XYZ tristimulus values) of the colour patch be (x, y). Now change the illuminant so that the chromaticity of the colour patch becomes (x', y'). If the patch now has the same colour appearance as any colour patches that have chromaticity (x', y') under the old illuminant, the visual system did not adjust to the changes in illuminant at all. In such a case, there is no colour constancy. In contrast, if our visual system had perfect colour constancy, then the colour appearance of the patch under the new illuminant would be same as before: it's colour appearance would be the same as that of patches having chromaticity (x,y) under the old illuminant and changes in illuminant are completely compensated by the visual system. In fact, our visual system exhibits good colour constancy under daylight illumination, but colour constancy is imperfect under artificial illumination such as tungsten or fluorescent lamps [WS82]. The inconsistency can be explained using Bayesian colour constancy theory [BF97], which states that our visual system compensates

for changes of illuminant based on prior probability distributions of natural illuminants and surfaces that exist in the world. This illuminant compensation functions perform poorly for artificial illuminants.

When the visual system has no colour constancy, algorithms that preserve the colour signal reflected from a surface are the best solutions for colour image reproduction. On the other hand, when the visual system exhibits perfect colour constancy, then algorithms that preserve surface reflectance are the best general solution for colour image reproduction.

Our visual systems exhibit good, but imperfect, colour constancy. Therefore, a colour reproduction algorithm should use information of illuminant and reflectance. It is important to investigate colour reproduction based on reflectance, so as to provide the basis for future algorithms related to partial colour constancy.

2.5 Surface Reflectance Spaces

To use reflectance data for colour image reproduction, a compact vision-oriented representation is needed for reflectance data. Reflectance is a continuous function over the visible spectrum. It is normally approximated by values of the function at a finite set of wavelengths, evenly sampled across the visible spectrum between 400nm to 700nm. A typical spacing is 10nm, at which each reflectance is represented by 31 values. The amount of data becomes so large that it is impractical for a colour image reproduction system to handle and equally-weighted parts of the data are not equally salient for human vision. The recent development of linear surface reflectance models [MW86, Wan87, HFD90, D'Z92, Bok97] showed that much of this data is redundant, leading to representations compact enough for colour image reproduction. (Even though a good non-linear reflectance model [Fun93] exists, its computational cost is high and the model is not considered in this thesis.) Using a linear reflectance model, each surface reflectance is approximated by a linear model with a small number of parameters. The reflectances are expressed as the weighted

sum of basis functions as follows:

$$r(\lambda) = \alpha_1 r_1(\lambda) + \alpha_2 r_2(\lambda) + \cdots + \alpha_N r_N(\lambda) \ .$$

where $r_i(\lambda)$, $i = 1, \cdots, N$, are the basis spectra, and the α_i are the weights of the basis spectra that describe a particular reflectance. The vector of the weights $(\alpha_1, \alpha_2, \cdots, \alpha_N)$ can be used to represent the reflectance.

Singular value decomposition (SVD) is the usual method for finding the basis spectra of a set of surface reflectances. The resulting basis spectra are then orthonormal. It has been shown that most useful sets of surface reflectances are effectively approximated by a small number of basis spectra. Maloney showed that 99% of the variance in the set of reflectances published by Krinov [Kri47] can be described by three basis spectra. Dannemailler [Dan92] reported a similar result using ideal-observer analysis for surfaces of naturally-occurring objects. Vrhel *et al.* [VGI94] analyzed the errors with different number of basis spectra for the spectral reflectance of Munsell chips, paints and various natural materials, and concluded that fewer than seven basis spectra are sufficient to model the reflectance.

A linear reflectance space is defined to be the space spanned by the basis spectra. With N basis spectra, the reflectance space is a N-dimensional linear space over a real field. As the basis spectra may have negative values in some regions and values above 1 in others, they are not directly related to any physical surface reflectance. All physically valid reflectances must satisfy the condition:

$$0 \leq r(\lambda) \leq 1 \ .$$

for every visible wavelength. The set of points that correspond to the physical reflectances defines a region in the space are referred as the *reflectance solid* [Pae94].

The ideal white reflectance (where $r(\lambda) = 1$) does not necessarily exist for a given basis spectra, and hence some grey reflectances ($r(\lambda) = c$) do not lie in the reflectance solid. Thus, neutral colours, which must be preserved in colour image reproduction, may not be accurately represented by the basis spectra. To avoid this problem, Paeth created a modified SVD to compute the basis spectra [Pae94]. It ensures that the ideal white reflectance is the first basis spectrum and that

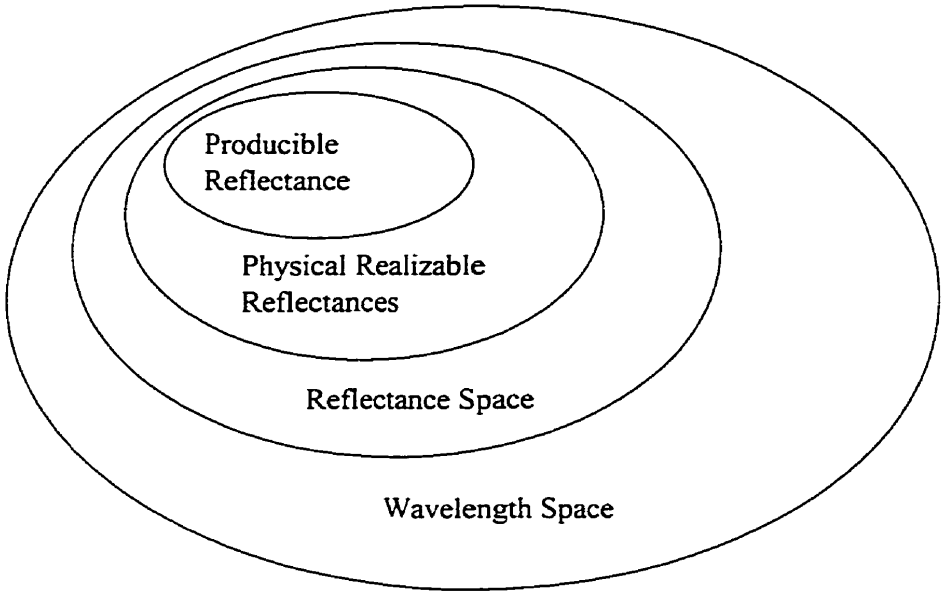


Figure 2.4: Various reflectances sets. They are producible reflectance set $\mathcal{R}_c$, physical realizable reflectance set $\mathcal{R}_p$, reflectance space $\mathcal{R}_{D_i}$, and wavelength space $\mathcal{W}$. The relationship between these sets is $\mathcal{R}_c \subset \mathcal{R}_p \subset \mathcal{R}_{D_i} \subset \mathcal{W}$

orthogonality of the basis is maintained. The ideal neutral colour reflectances are then represented in reflectance coordinates as $(c, 0, \cdots, 0)$. As shown in Chapter 5, neutral reflectances are important for describing relationships between a reflectance and its colour attributes. Therefore, the reflectance spaces described in the thesis are computed using Paeth's modified SVD.

Throughout the thesis, several important sets of reflectances are encountered. They are defined below.

Wavelength space, $\mathcal{W}$. A linear space having delta functions, one at each sample wavelength, as basis elements and coordinates any element of $\mathcal{R}$. The reflectances in the space may or may not be physically realizable.

Reflectance space, $\mathcal{R}_D$. A linear space with basis reflectances derived by modified SVD from the set of reflectances produced by an output device D, and weights any element of $\mathcal{R}$. The reflectances in the space may or may not be physically realizable.

Physical reflectances in $\mathcal{R}_D$, $\mathcal{R}_p$. The set of reflectances in $\mathcal{R}$ that are physically realizable.

Producible reflectances in $\mathcal{R}_D$, $\mathcal{R}_c$. The set of reflectances in $\mathcal{R}_p$ that can actually be produced by the colour device D.

The relationship between these sets (Figure 2.4) can be expressed as

$$\mathcal{R}_c \subset \mathcal{R}_p \subset \mathcal{R}_{D_i} \subset \mathcal{W} .$$

2.5.1 Geometric Features of Reflectance Solids

The geometric properties of reflectance solids were studied extensively by Paeth [Pae94]. With the modified reflectance basis, the reflectance solid can be visualized as two cone-shaped objects with their bases joining together (Figure 2.5). The

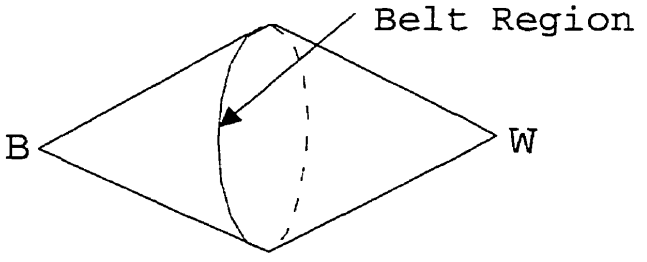


Figure 2.5: Three Dimensional Reflectance Solid. It contains all the physical realizable reflectances. The black apex (B) corresponds to the reflectance with zero reflectivity over the entire visible spectrum. and the white apex (W) corresponds to the ideal white reflectance with unit reflectivity over the entire visible spectrum. The points in the belt region correspond to the reflectances having simultaneous minimum and maximum values in the visible spectrum.

left apex B in the figure is the *black apex* and corresponds to the colour with zero reflectivity over the entire visible spectrum. i.e., $r(\lambda) = 0$. It is associated with the origin of the reflectance space. The right apex W is the *white apex* and corresponds to the ideal white colour, which has unit reflectivity over the entire visible spectrum. i.e., $r(\lambda) = 1$. The left end of the solid containing the black apex in the figure is called *dark cone*, while the right end is called *light cone*. The surface of the solid defines all reflectances which have at least one wavelength λ_i at which $r(\lambda_i) = 0$ or $r(\lambda_i) = 1$. Specifically, for any reflectance on the dark cone surface, there is at least one wavelength λ_i at which $r(\lambda_i) = 0$, and for any reflectance on the light cone surface there is at least one wavelength λ_i at which $r(\lambda_i) = 1$. The intersection of the dark cone and the light cone is the *belt region* of a solid. It is a $N - 2$ dimensional subset of the N dimensional reflectance space. The points in the belt region correspond to the reflectances having simultaneous minimum and maximum values in the visible spectrum, i.e., at least two different wavelength λ_i and λ_j at which $r(\lambda_i) = 0$ and $r(\lambda_j) = 1$ (Figure 2.5).

The surface geometry of any reflectance solid is described uniquely by the convex hull of the belt region and the two apices. Thus a reflectance solid is fully specified by the points in the belt region plus the black and white apices in the solid.

As described in Chapter 5, the above properties are useful when describing the relationship between reflectance and its colour attributes.

2.6 Conclusion

A formalism for colour image reproduction process was described. The image reproduction process was defined as the composition of three functions. Two of them are obtained from device characterizations, which define the relationship between the device control values and the corresponding colour values, and the third one is a gamut mapping, which defines the mapping between the input and output colours. Gamut mapping is usually defined for a device independent space so that it can be used by all devices characterized for the space.

Two gamut mapping approaches have been used. One is defined as a minimization problem, such as minimizing CIELAB colour difference. The other is defined as a perceptual trade-off, such as balancing contrast and saturation. Current techniques base both approaches on measurements in a device independent space, usually derived from CIE tristimulus values. The resulting algorithms are computed with respect to a predefined illuminant, so that reproduction can be unsatisfactory when different illuminants are used. Thus, illuminant independent colour specification is worth investigating, and colour constancy suggests that surface reflectance may be an interesting alternative.

It has been shown that surface reflectances can be adequately approximated by linear models. In a linear model, reflectances are represented by its coordinates in a reflectance space. By using modified SVD, a reflectance space with the ideal white reflectance as its first basis spectrum can be constructed. It has some nice properties that are useful for defining relationships between a reflectance and its colour attributes.

Chapter 3

Device Characterization

Successful colour reproduction depends on precise control of the relationship between device control values and the corresponding output colours. Device characterization is the process that determines such relationships. For devices where the transfer function is known. a mathematical model can be created to represent the transfer function and used for characterization. This approach is referred as model-based characterization. Otherwise. a colour lookup table (CLUT) generated from empirical data is used for characterization. This practice is referred as lookup-table characterization.

In model-based characterization. a model is first chosen to represent a device transfer function. A few output samples are then measured to estimate the model parameters. The accuracy of this approach depends on how well the chosen model agrees with the true device transfer function: its efficiency depends on how complicated the model is.

In lookup-table characterization. output samples distributed across the entire device gamut are measured. The control values used to create the samples and the corresponding colorimetric data are used to construct the CLUT. The output value for a given control value is approximated by interpolating among points in the CLUT. The accuracy of approximation depends on the sampling and interpolation

techniques being used: its efficiency depends on the searching technique to locate target points in the CLUT and on the complexity of the interpolation algorithm.

The characterization process defines forward and backward transformations. The forward transformation converts device control values to corresponding output colour values. The backward transformation determines device control values that produce given colour values. The accuracy and computational costs of these colour transformations are affected by the calibration approach being used. In this chapter, the concepts of different characterization approaches are described, and the costs associated with each approach are discussed.

3.1 Model-based Reflective Characterizations

Most of the mathematical models of colour printing devices are based on one of two colour mixing theories: additive mixing for halftone images and subtractive mixing for continuous tone ones. Developed decades ago, these models have stood the test of time, and still provide colour printing models that are indispensable for digital printing.

3.1.1 Halftone Images

Numerous models have been proposed for the halftone printing process. Most are derived from the Neugebauer model and Yule-Nielsen refinement of it. Neugebauer observed that cyan, magenta and yellow inks printed on white paper produce eight different colours. In addition to the three primary colours, cyan, magenta, and yellow, red is produced by combining magenta and yellow, green by cyan and yellow, blue by cyan and magenta, black by all three primaries, and white with no ink at all. Each of the eight colours covers a fraction of the printed area. Areas combine spatially by additive mixture to form the perceived colour. Analogously, Neugebauer suggested that the reflectances in an halftone image can be described by the weighted sum of the reflectance of the dominant colours. The weights are

associated with the areas covered by individual colours. The Neugebauer equation is

$$\begin{aligned} r(\lambda) &= a_w r_w(\lambda) + a_c r_c(\lambda) + a_m r_m(\lambda) + a_y r_y(\lambda) + \\ & \quad a_r r_r(\lambda) + a_g r_g(\lambda) + a_b r_b(\lambda) + a_k r_k(\lambda) \ . \end{aligned}$$

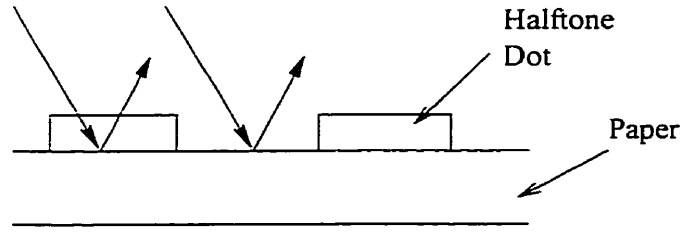
where a_i and $r_i(\lambda)$ are respectively the area coverage and reflectance of the colour i. The area coverage can be determined by the Demichel's dot overlap model [Yul67. Chapter 10]. which uses a joint probability model to compute the individual areas. With p_i the fraction of a unit area covered by primary i. the area coverage of each colour is

$$\begin{aligned} a_w &= (1-p_c)(1-p_m)(1-p_y) \\ a_c &= p_c(1-p_m)(1-p_y) \\ a_m &= p_m(1-p_c)(1-p_y) \\ a_y &= p_y(1-p_c)(1-p_m) \\ a_r &= p_m p_y(1-p_c) \\ a_g &= p_c p_y(1-p_m) \\ a_b &= p_c p_m(1-p_y) \\ a_k &= p_c p_m p_y \ . \end{aligned}$$

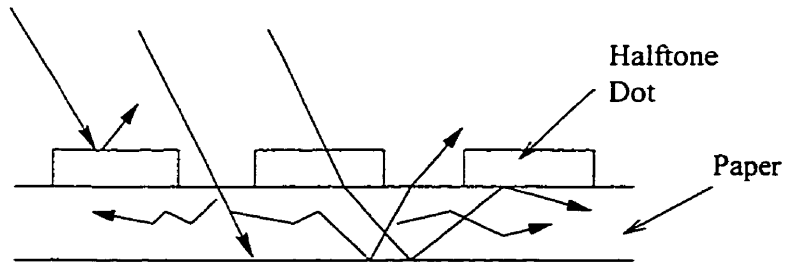
The Neugebauer equations provide a relatively easy method to determine the halftone colours. They are derived on the assumption that light emerges from the paper at the point where it enters. However. some light scatters laterally inside the medium before returning to the surface. an important inaccuracy in the model. (Figure 3.1) To correct this problem. Yule and Nielsen [YN51] proposed a model that takes into consideration light penetration and scattering, and derived the halftone equation to compute reflectance of a halftone area $r(\lambda)$. The equation is given as

$$r(\lambda) = r_s(\lambda) + r_m(\lambda)(\,1 - r_s(\lambda)\,)[\,1 - a(1 - t_i(\lambda))\,]^n \ .$$

where $r_m(\lambda)$ is the reflectance of the medium. $r_s(\lambda)$ is the surface reflection at the air-ink interface. a is the dot area coverage. $t_i(\lambda)$ is the transmittance of the



(a)



(b)

Figure 3.1: Light Path. (a) Neugebauer equations assume that light emerges from the paper at the point where it enters. (b) In reality, some light scatters around before returning to the surface.

ink i. and n is the empirical Yule-Nielsen value based on the fitting of sampling data. To further improve the halftone model. Clapper and Yule [CY55] proposed a halftone equation that takes into account the effects of multiple-scattering. internal-reflection. and ink transmission.

3.1.2 Continuous Tone Images

Two different models are used to match colours for continuous tone images. The Bouguer-Beer Law is used for transparent media such as colour film and transparencies. while the Kubelka-Munk Law is used for translucent and opaque media [All80].

The Bouguer-Beer Law states that the transmittance. $T(\lambda)$. of a transparent medium of thickness X is given by

$$T(\lambda) = I(\lambda)/I_o(\lambda) = \exp(-K(\lambda)X) \ .$$

where $I_o(\lambda)$ is the light intensity entering the medium. and $I(\lambda)$ is the light intensity leaving the medium. $K(\lambda)$ is the absorption coefficient of the medium. Since $K(\lambda)$ is proportional to the concentration of colorant. it can be expressed as $K(\lambda) = c\,k(\lambda)$. with c the concentration of colorant and $k(\lambda)$ be the absorption of a unit concentration of the colorant. When multiple colorants are present. $K(\lambda)$ is the linear function

$$K(\lambda) = k_m(\lambda) + c_1k_1(\lambda) + c_2k_2(\lambda) + \cdots + c_ik_i(\lambda) \ ,$$

where $k_m(\lambda)$ is the absorption coefficient of the uncoloured medium. $k_i(\lambda)$ the unit absorption coefficient and c_i the concentration of the ith colorant.

The Bouguer-Beer Law cannot be used for translucent and opaque media since it ignores light scattering within the medium. Based on the assumption that light is absorbed and scattered only perpendicularly to the surface of the medium. Kubelka and Munk derived an equation to compute the reflectance of a translucent film. Once the absorption coefficient. $K(\lambda)$. the scattering coefficient. $S(\lambda)$. the film

thickness, X, and the reflectance of the background, $R_g(\lambda)$, are known. The reflectance of the film can be expressed as

$$R(\lambda) = \frac{1 - R_g(\lambda)\,[\,a(\lambda) - b(\lambda)\,\coth(\,b(\lambda)S(\lambda)X\,)\,]}{a(\lambda) - R_g(\lambda) + b(\lambda)\,\coth(\,b(\lambda)S(\lambda)X\,)}\,. \tag{3.1}$$

where

$$a(\lambda) = 1 + K(\lambda)/S(\lambda)$$

$$b(\lambda) = \left[\,(K(\lambda)/S(\lambda))^2 + 2\,(K(\lambda)/S(\lambda))\,\right]^{1/2}$$

$$\coth(\,b(\lambda)S(\lambda)X\,) = \frac{\exp(\,b(\lambda)S(\lambda)X\,) + \exp(\,-b(\lambda)S(\lambda)X\,)}{\exp(\,b(\lambda)S(\lambda)X\,) - \exp(\,-b(\lambda)S(\lambda)X\,)}\,.$$

If the medium has infinite thickness, the above equation can be simplied as

$$R(\lambda) = 1 + K(\lambda)/S(\lambda) - \left[\,(\,K(\lambda)/S(\lambda)\,)^2 + 2\,(\,K(\lambda)/S(\lambda)\,)\,\right]^{1/2}.$$

Since only the single constant ratio of $K(\lambda)/S(\lambda)$ is needed to describe the medium, this equation is referred as the single-constant KM theory. For multiple colorants, the constant $K(\lambda)/S(\lambda)$ is obtained by summing the ratio for each individual colorant weighted by the concentration of the colorant:

$$\begin{aligned} K(\lambda)/S(\lambda) \;=\; & (\,k(\lambda)/s(\lambda)\,)_m + c_1(\,k(\lambda)/s(\lambda)\,)_1 + c_2(\,k(\lambda)/s(\lambda)\,)_2 + \\ & \cdots + c_n(\,k(\lambda)/s(\lambda)\,)_n\,. \end{aligned}$$

where $(\,k(\lambda)/s(\lambda)\,)_m$ is the absorption and scattering ratio for the substrate, c_i and $(\,k(\lambda)/s(\lambda)\,)_i$ is the concentration and the absorption and scattering ratio of the colorant i, respectively. When the coloured layer is transparent on an opaque medium, i.e., the scattering coefficient $S(\lambda)$ approaches zero, then Equation 3.1 can be simplified to

$$R(\lambda) = R_g(\lambda)\,\exp(-2K(\lambda)X)\,. \tag{3.2}$$

3.1.3 Determining Control Values for a Model

Models like those described above are used to develop the device model. In addition, a set of parameters must be measured to describe the qualities of the particular

device. For example. dot area coverages. ink transmittances. and the Yule-Nielsen value have to be determined for devices that produce halftone images: spectral absorptions of the dyes. dye concentrations. and medium reflectance have to be determined for continuous tone devices. To complete the model of a device. these parameters are derived empirically from samples of the device output.

For purposes of illustration. the steps used to obtain the parameters of the model of our dye diffusion thermal printer are described in this section. First. consider the printer model. developed by Berns [Ber93]. which is based on Kubelka-Munk theory. Since the Kubelka-Munk theory assumes there is no refractive index discontinuity between the coloured layer and its medium. the Saunderson correction for refractive index discontinuity is applied to the measured reflectance before any calculation. The correction is expressed as

$$R(\lambda) = \frac{R_{measured}(\lambda)}{(1-k_1)(1-k_2) + k_2 R_{measured}(\lambda)} ,$$

where k_1 is the Fresnel reflection coefficient based on the refractive indices of the receiver layer and air. and k_2 is the diffuse internal reflection coefficient.

Assuming the paper medium to be opaque. Equation 3.2 is used to compute reflectances. Since the medium thickness is constant. the term $K(\lambda)X$ can be combined into a single term $K_{mixture}(\lambda)$. The equation is rewritten as

$$R(\lambda) = R_g(\lambda)\ \exp(-2K_{mixture}(\lambda)) . \tag{3.3}$$

Its inverse is

$$K_{mixture}(\lambda) = -0.5\ ln\left(\frac{R(\lambda)}{R_g(\lambda)}\right) . \tag{3.4}$$

The spectral absorption of any mixture is assumed to be the sum of the absorptions of each dye:

$$K_{mixture}(\lambda) = K_{cyan}(\lambda) + K_{magenta}(\lambda) + K_{yellow}(\lambda) ,$$

and the relative spectral absorption are independent of concentration:

$$\begin{aligned} K_{cyan}(\lambda) &= c_c K_{cyan.max}(\lambda) \\ K_{magenta}(\lambda) &= c_m K_{magenta.max}(\lambda) \\ K_{yellow}(\lambda) &= c_y K_{yellow.max}(\lambda) , \end{aligned} \tag{3.5}$$

where c_i is the concentration for dye i. Thus, the relative spectral absorption can be determined once the concentrations are known. c_i is determined by the device control value. Assuming that the channels to be independent of each other, Berns suggested that the concentrations can be approximated by third-order polynomials as

$$\begin{aligned} c_c &= a_{11}d_c + a_{12}d_c^2 + a_{13}d_c^3 \,. \\ c_m &= a_{21}d_m + a_{22}d_m^2 + a_{23}d_m^3 \,. \\ c_y &= a_{31}d_y + a_{32}d_y^2 + a_{33}d_y^3 \,. \end{aligned} \tag{3.6}$$

where d_i is the normalized control value of dye i. Since dye diffuses when heated, two phenomena, diffuse back and dye transfer inhibition, affect the actual amount of dye being transferred on the medium. Diffuse back occurs when previously transferred dye diffuses back onto the supply. Transfer inhibition, which reduces the amount of dye transferred, depending on the amount of dye already transferred onto the print medium. As a result, the estimated concentrations, c_i, are different from the actual concentrations, $c_{i,actual}$, transferred onto the medium. The following relationships are hypothesized:

$$\begin{aligned} c_{c,actual} &= \beta_{1,0} + \beta_{1,1}c_c + \beta_{1,2}c_c^2 + \beta_{1,3}c_m + \beta_{1,4}c_y + \beta_{1,5}c_c c_m + \beta_{1,6}c_c c_y \,. \\ c_{c,actual} &= \beta_{2,0} + \beta_{2,1}c_m + \beta_{2,2}c_m^2 + \beta_{2,3}c_c + \beta_{2,4}c_y + \beta_{2,5}c_m c_c + \beta_{2,6}c_m c_y \,. \\ c_{c,actual} &= \beta_{3,0} + \beta_{3,1}c_y + \beta_{3,2}c_y^2 + \beta_{3,3}c_c + \beta_{3,4}c_m + \beta_{3,5}c_y c_c + \beta_{3,6}c_y c_m \,. \end{aligned} \tag{3.7}$$

With the above complete model, the relationship between control value and output reflectance is determined by the following procedure:

1. measure the reflectances of a set of output samples,
2. apply the Saunderson correction to the reflectances,
3. determine the spectral absorption using Equation 3.4,
4. compute the maximum spectral absorption, $K_{i,max}(\lambda)$, in Equation 3.5, of each dye for the samples with single dye.

5. calculate the concentrations, c_i, of single dye samples.

6. compute the coefficients, $a_{i,j}$, in Equation 3.6 by applying multiple-linear regression on the control values and their corresponding concentrations obtained from (5).

7. using the modified Newton-Raphson iteration method [All80], determine the actual concentrations of dyes for each sample.

8. determine the coefficients, $\beta_{n,m}$, in Equation 3.7.

Once the coefficients $a_{i,j}$ in Equation 3.6 and $\beta_{n,m}$ in Equation 3.7 are found, reflectances corresponding to any given control value (d_c, d_m, d_y) can be determined by the model.

Following the above procedure, we obtained the parameters of the model for our DuPont 4Cast printer. To estimate the parameters, the reflectances of 216 ($6 \times 6 \times 6$) evenly spaced samples were measured. The measured reflectances were then normalized by the paper white. As the result, the spectrum of $R_g(\lambda)$ in Equation 3.3 is unity. The normalized spectral absorption of each dye is shown in Figure 3.2.

As expected, the coefficients of $a_{i,j}$ and $\beta_{n,m}$ of our printer are quite different from the ones published by Berns. In our experiment Equation 3.6 was:

$$\begin{aligned} c_c &= 0.2488d_c + 1.7821d_c^2 - 1.0276d_c^3 , \\ c_m &= 0.1594d_m + 1.7615d_m^2 - 0.9204d_m^3 , \\ c_y &= 1.1740d_y - 1.1241d_y^2 + 0.9461d_y^3 , \end{aligned}$$

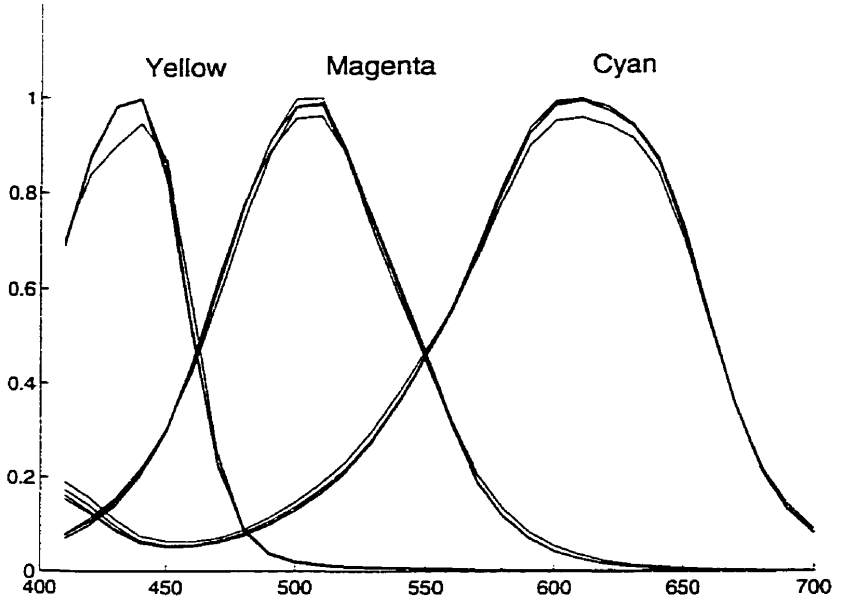


Figure 3.2: The scaled spectral absorption of the dyes with different concentrations for the DuPont printer used in our experiment. The absorptions of different cencentrations for each dye differ by scaling factors. The assumption of relative spectral absorption invariant with concentration is met.

and Equation 3.7 was

$$\begin{aligned} c_{c.actual} &= -0.0056 + 1.0331c_c - 0.0288c_c^2 + 0.0045c_m + 0.0057c_y \\ &\quad -0.0003c_c c_m + 0.0038c_c c_y \ . \\ c_{m.actual} &= 0.0085 + 0.8340c_m + 0.0898c_m^2 - 0.0029c_c - 0.0089c_y \\ &\quad -0.2812c_m c_c + 0.0490c_m c_y \ . \\ c_{y.actual} &= -0.0359 + 1.0063c_y - 0.0269c_y^2 + 0.0040c_c + 0.0044c_m \\ &\quad -0.1889c_y c_c - 0.1480c_y c_m \ . \end{aligned}$$

Ignoring the smaller values of the interaction terms (corresponding to coefficients $\beta_{i.3}$ to $\beta_{i.6}$ in Equation 3.7 where i referes to the colorant). the above equation becomes

$$\begin{aligned} c_{c.actual} &= -0.0056 + 1.0331c_c - 0.0288c_c^2 \ . \\ c_{m.actual} &= 0.0085 + 0.8340c_m + 0.0898c_m^2 - 0.2812c_m c_c \ . \\ c_{y.actual} &= -0.0359 + 1.0063c_y - 0.0269c_y^2 - 0.1889c_y c_c - 0.1480c_y c_m \ . \end{aligned}$$

The equations published by Berns were

$$\begin{aligned} c_c &= -0.19d_c + 2.39d_c^2 - 1.19d_c^3 \ . \\ c_m &= 0.13d_m + 1.39d_m^2 - 0.52d_m^3 \ . \\ c_y &= 0.18d_y + 1.55d_y^2 + 0.73d_y^3 \ . \end{aligned}$$

and

$$\begin{aligned} c_{c.actual} &= 0.03 + 0.51c_c + 0.47c_c^2 - 0.014c_c c_m - 0.20c_c c_y. \\ c_{m.actual} &= 0.02 + 0.74c_m + 0.32c_m^2 - 0.29c_m c_c. \\ c_{y.actual} &= -0.05 + 0.87c_y + 0.19c_y^2. \end{aligned}$$

The coefficients of a_{ij} that describe the relationship between the digital counts and concentrations for the printers are similar for both cyan and magenta dyes. But. the coefficients are quite different for the yellow dye. The reason for this may

be caused by the excess fluorescence of the yellow dye. Berns stated that fluorescent emission of the dyes pose no significant problems for their printer: however, it may not be true for our printer.

For the coefficients of β_{ij} that describe the interactions between the dyes, patterns are found in the coefficients in ours and Berns' printers. Firstly, the actual concentration of a dye is mainly determined by its estimated concentration. Secondly, the coefficients $\beta_{i,3}$ and $\beta_{i,4}$, corresponding to direct interactions, are negligible for both printers. However, the interaction terms related to the covariance of two dyes, which are described by the coefficients $\beta_{i,5}$ and $\beta_{i,6}$, are very different between the two printers. By closely inspecting the coefficients, it seems that there was no interaction between the cyan dye and the others in our printer. This suggests that the first dye transferred by our printer is cyan; whereas, yellow is the first dye transferred by the printer used by Berns. Thus, taking into account the difference in dye transfer order, the equations that described the dye interaction for both printers agree qualitatively. Quantitatively, on the other hand, Berns' printer model fails to represent our printer since its coefficients do not work for our printer.

In general, the Berns' printer model can correctly predict the trend of spectral changes caused by the changes of digital counts. Unfortunately, even with extensive measurement and data fitting we failed to obtain the level of accuracy described by Berns. The average ΔE_{ab} for our model was 7.0 which is quite large compared to 3.0, which was obtained by Berns. As mentioned by Berns, a regression method with the performance of our result produces images of very low colour quality. Such a large error may come from several sources. Possibly, our printer may require a different model than the one Berns used. Even though both printers were from the same manufacturer and use dye diffusion thermal transfer technology, the model described by Berns may not be compatible with our printer. Other problems such as different characteristics of dyes and paper can also cause large errors. The large, hard-to-explain discrepancies illustrates a serious drawback of model-based characterization.

3.1.4 Problems Associated with Models

A mathematical model provides a valuable analytical tool for studying colour reproduction. It can be used to simulate the printing process. Unlike real output devices, the model always produces consistent output without disturbance from environmental factors. Thus, it provides a good platform for testing new ideas for reproduction. However, for several reasons such models are not widely used in reproduction applications.

First, models are very expensive to develop. When a mathematical model is developed for a colour device, it is important to verify that its assumptions are valid for the device. For example, the unmodified Kubelka-Munk model does not work for a dye diffusion thermal transfer printer since it assumes there is no refractive index discontinuity between the coloured layer and its surrounding medium. The Fresnel reflection coefficient must be used to take into account this refractive effect. However, even once the discontinuity in refractive index has been taken into consideration, certain assumptions, such as no fluorescence being present, may not be accurate, thereby degrading the performance of the model, as was illustrated in the previous section. Second, a model developed for a particular device is only valid under restricted operating conditions. Changes in the properties of ink or paper often change the output results so much that the use of the model would be inappropriate. As shown in the experiment that applied Berns' model to a different printer, the large ΔE_{ab} value were mainly caused by dye differences. Third, the inverse of a model is usually very difficult to define and compute. As a result, the backward transformation, which is heavily used in colour reproduction, is effectively unusable. The difficulty of determining the inverse is one of the major problems of model-based characterization. In fact, even if an inverse model exists, it would not be used in practice owing to its high computational cost. For example, consider how the inverse of Berns' printer model is used to determine the device control values for a given reflectance. The reflectance is first converted to its spectral absorption using the Equation 3.4. Equation 3.5 is then solved to determine the actual concentration of each dye. Next, two sets of nonlinear equations, Equation 3.7 and Equation 3.6, must be solved to find the control values.

In general, the measurement cost of model-based characterization is small compared to lookup-table characterization. But the development cost is very large since it is necessary to understand every feature of a device in developing a model. It is possible to obtain an acceptable result with this approach. However, the computational costs of the colour transformations with this approach are usually very high. Thus, it is infeasible to perform the transformations based on a mathematical model in any practical applications. Instead, the transformation is often carried out with a lookup-table approach, which derives colour values from a set of measurement data stored in a CLUT. In this case, models can be used to verify and smooth measured CLUT data.

3.2 Lookup Table Techniques for Colour Characterization

Three steps are needed for colour lookup table (CLUT) characterization. They are *sampling*, *extraction*, and *interpolation*. The process begins with measuring the colour of a large set of samples printed by a device. Sample points may be distributed either uniformly or nonuniformly in the device space. These sample points can be thought of as the vertices of compact cells into which the entire device gamut is divided. The control values and colour values of the samples are used to create the CLUT for the device. Each entry of the CLUT comprises a control value and its corresponding colour value.

To determine a colour value for a given control value, the forward transformation first identifies the cell that encloses the target control value in the device space in an extraction step, the corresponding cell in the colour space is then used to approximate the target colour values by interpolation. For the backward transformation, similar steps can be used to determine the control value for a given colour value, except that the domain and range spaces are interchanged.

Each of these three steps has some impact on the performance of the colour

reproduction process. This section describes the construction of the CLUT. and discusses how the sampling technique affects the accuracy and computational cost associated with the colour transformations.

3.2.1 Colour Lookup Table Construction

Sampling is the first step in CLUT construction. It has large impact on the effectiveness of a colour reproduction process since both extraction and interpolation steps operate on the sample points.

The simplest way to construct a CLUT is to sample points that are uniformly distributed throughout the device coordinate space. This kind of CLUT is easy to construct. but accuracy is a problem for this sampling technique. For example. interpolation errors from uniformly sampled points can be high if the sampling distribution is not dense enough.[1] To solve this problem. the sampling frequency can be increased. However. increased sampling density increases measurement cost since the total number of sampling points increases as n^d. where n is the sampling density in each dimension and d the dimensionality of the colour space. Because reflectance spaces often have high dimensionality. measurement cost can easily be too high for adequate sampling density. An alternative is to use nonlinear interpolation. Higher order interpolation can increase accuracy. but only at the cost of decreased performance because nonlinear interpolation has high computation cost.

Improvement can otherwise be obtained by using nonuniform sampling: denser sampling for regions with high curvature. sparser sampling for others. With the same number of sample points. this approach generates results that have smaller errors compared to those obtained from uniform sampling [Kan96, Chapter 4].

To use nonuniform sampling effectively. some knowledge about the transfer function of a device must be established prior to choosing sample points. A mathematical model of a device can be used to estimate the transfer function. However, the

[1]The relationship between accuracy and sampling density depends on the curvature of the mapping from control values to printed colours.

reliability and high cost problems discussed in the previous section will hinder the effectiveness of this approach. Alternatively. the transfer function can be estimated from empirical data.

By sampling each axis in such a way that the resulting L* values lie evenly in the destination space. Kang [Kan95] demonstrated that this simple nonuniform sampling technique can produce better results compared to those obtained from the uniform sampling techniques. This technique uses sample points that are nonuniformly distributed across the gamut in the device space: however. each cell defined by the sample points is rectangular. which is good for locating an enclosed cell during colour transformation. More sophisticated techniques can be used to provide better results. For example. iterative refinement was used by Allebach. Chang. and Bouman [ACB93]. They repeatedly applied Sequential Scalar Quantization (SSQ) and Sequential Linear Interpolation (SLI). which uses a flexible grid of values to approximate the model. and were able to refine the distribution of sample points until interpolation errors fell below a certain level. Bell and Cowan [BC94] first characterized a printer transfer function with tensor product splines. sample points for which are selected using SLI.

3.2.2 Performance Issues with Colour Lookup Tables

Because the performance of colour transformations is important for any colour reproduction process. the CLUT should be built in a way that allows transformations to be performed as quickly as possible. Both extraction and interpolation must be done once per pixel. Thus. high speed transformation requires good performance in both steps. Linear interpolation is efficient enough for interpolation. There are two methods for extraction. One alternative uses a CLUT with entries uniformly distributed in a domain space. With such a CLUT enclosing cells can be located directly through indexing. But accuracy is lower with this approach. The other alternative uses denser sampling in regions where curvature is high. which requires a search algorithm to identify the enclosing cells.

To build a CLUT with uniformly distributed samples for the forward transfor-

mation. one can simply measure the sample points with equal spacing in the device control space and store them in the CLUT. But. without knowing the transfer function of a device. it is difficult to construct the CLUT for backward transformation. In practice. *remeasuring* or *remapping* is often used to build the CLUT.

Remeasuring is an iterative process to obtain sample points with equal spacing. The process starts with uniform sampling in the device space. After the first measurement. the process uses the sample points to approximate the transfer function of the device. Based on the estimated transfer function. a new set of sample points. which are equally spaced in a colour space with respect to the estimated function. is chosen for the next measurement. The steps of chosing sample points and remeasuring are repeated. terminating only when the set of samples is distributed uniformly enough in the colour space. This approach has been used commercially for producing film editing equipment. and requires as many as six to seven iterations to obtain an acceptable distribution in a one dimensional lightness space. Many more iterations would be required for data in a high dimensional space. making it too expensive for practical applications.

Remapping is another approach commonly used in practice. Like remeasuring. this approach uses sample points that are uniform in device space to estimate the transfer function of a device. Since the function is derived from samples with measurement errors. both measurement and sampling errors are present in the estimated transfer function. Using the estimated transfer function. the control values for a set of regularly distributed points are found. A new CLUT is created with these colour points. Note that the points in the new CLUT are produced from the estimated transfer function. not from the actual measurements. Since resampling uses points that include measurement error to approximate points not in the table. it has double approximation errors. This approach produces results that are lower in accuracy than methods without remapping.

Instead of rebuilding the CLUT. extraction can be improved by using an efficient search algorithm to locate the enclosing cell that contains the target point. A new extraction algorithm is described in Chapter 6. the performance of which is logarithmic in the number of sampling cells. This approach allows fast extraction

without high measurement cost and without sacrificing accuracy. The CLUT is usually built with nonuniform samples in device space to improve accuracy. after which the enclosing cell can be extracted with performance comparable to binary search.

3.2.3 Conclusion

To determine the relationship between device control values and output colours. device characterization must be done. If the transfer function of a device is known. model-based characterization can be used: otherwise. lookup-table characterization is needed.

Different theories are available to model different kinds of output devices. However. these models are expensive to develop. Even when a good model exists for a particular device. problems still exist. such as high computation cost. inflexibility and difficulty in finding the inverse. In contrast. the CLUT approach. which provides low computation and implementation costs. and allows fast processing speed. is widely used in practice.

The CLUT is created from sample points that are uniformly or nonuniformly distributed. Uniform sampling allows fast extraction because direct indexing can be used to locate the enclosing cells. while nonuniform sampling can provide better accuracy by reducing interpolation errors. For high speed applications. a CLUT with uniformly distributed sample points is normally used. Remeasuring or remapping is sometimes used to construct a uniformly sampled CLUT for backward transformation. Unfortunately. high measurement and accuracy cost is always associated with remeasuring and remapping. To maintain accuracy while reducing processing time. a nonuniformly sampled CLUT combined with a fast searching technique is best.

Chapter 4

Gamut Mapping in Reflectance Space

Illuminant dependence is a serious problem when using the CIE colour specifications for colour transformation algorithms of reflective media. When viewing reflective stimuli, the colour signals that enter the eyes, which determine the CIE tristimulus values, are affected by the illuminant. Thus, colour transformations that use the CIE tristimulus values necessarily assume an illuminant. When the viewing illuminant differs from the reference illuminant the results are hard to predict. By reproducing reflectance, an intrinsic surface property that is independent of the source of illumination, the problem of illuminant dependence can be eliminated from gamut mapping.

As mentioned in the previous chapter, reflectance can be expressed as a linear combination of basis functions. To minimize representation errors, basis functions are developed empirically to fit specific output devices. They vary from output device to output device. To match colour across devices, it is necessary to map reflectances from one basis to another.

It is easy to see that two reflectances with similar spectra are likely, when illuminated, to have similar tristimulus values. As a result, the colour difference between

them is expected to be small under a variety of different sources of illumination. Based on this observation, any mapping that minimizes spectral error seems a natural choice for gamut mapping between reflectance spaces. Orthogonal projective transformation is one such mapping. It can be implemented by matrix multiplication, which makes it inexpensive to compute. However, because it does not account for the colour sensitivity of the human visual system, it is a poor choice for gamut mapping between reflectance spaces. It often fails to map to the reflectance that has the smallest tristimulus value difference, and can produce rather large colour differences. This result can be explained in terms of human visual sensitivity space.

To obtain better performance, a gamut mapping for reflectance, based on the fundamental component of reflectance, was developed [CC96]. By using reflectance information, this mapping better preserves the original colours for a variety of illuminants because it maps to the reflectance with the smallest tristimulus value difference.

4.1 Human Visual Sensitivity Space

To study colour reproduction for different illuminants, it is essential to understand human visual sensitivity (HVS) space. HVS space weights reflectance components in proportion to the response of the light sensitive cells in the retina. As such it is derived from the colour matching functions and is illuminant-dependent. As given in Chapter 2, the tristimulus values, $\mathbf{t}$, of any surface can be computed using the matrix equation

$$\mathbf{t} = \mathbf{H}^t \mathbf{E} \mathbf{r},$$

with $\mathbf{H}$ the $3 \times N$ colour matching matrix, $\mathbf{E}$ the $N \times N$ diagonal matrix of the spectrum of an illuminant, and $\mathbf{r}$ the N element vector describing the reflectance of a surface. With $\mathbf{A}_E = \mathbf{H}^t \mathbf{E}$, the above equation can be rewritten as

$$\mathbf{t} = \mathbf{A}_E \mathbf{r}\,. \tag{4.1}$$

The $3 \times N$ matrix $\mathbf{A}_E$ is a transformation matrix from the N-dimensional wavelength space to the 3-dimensional HVS space under the illuminant specified in $\mathbf{E}$. [1] $\mathbf{A}_E$ can be thought of as a sensor that incorporates illuminant information.

For a given illuminant, the N dimensional wavelength space $\mathcal{R}$ can be expressed as a direct sum of the 3 dimensional HVS space, which is spanned by the rows of $\mathbf{A}_E$, and its $N-3$ complement space $\mathcal{N}(\mathbf{A}_E)$, the null space of $\mathbf{A}_E$ with respect to $\mathcal{R}$. Each surface reflectance can thus be divided into two components. One is the fundamental component in the HVS space and another is the metameric black component in $\mathcal{N}(\mathbf{A}_E)$. The metameric black component is invisible to normal observers. Two reflectances are metameric when they have identical fundamental components and different metameric black components. Since the values of matrix $\mathbf{A}_E$ depend on the illuminant, the fundamental component and the metameric black component of the surface reflectance are in general different for different illuminants.

Mathematically, any surface reflectance $\mathbf{r}$ can be expressed as

$$\mathbf{r} = \mathbf{f}_r + \mathbf{b}_r \ .$$

where $\mathbf{f}_r$ is the fundamental component, and $\mathbf{b}_r$ is the metameric black component. The fundamental component can be obtained by using a projection operator, $\mathbf{P}_f$, which is defined as $\mathbf{A}_E(\mathbf{A}_E^t\mathbf{A}_E)^{-1}\mathbf{A}_E^t$. The metameric black component can be obtained by using the projection operator $\mathbf{P}_b = \mathbf{I} - \mathbf{P}_f$. The matrix that represents the projection operator $\mathbf{P}_f$ is commonly referred as the $\mathbf{R}$ matrix. An extensive discussion of its properties can be found in Cohen and Kappauf's paper [CK82, Coh88].

To simplify the discussion that follows, HVS space is referred as the fundamental subspace, denoted by $\mathcal{F}_i$, and $\mathcal{N}(\mathbf{A}_{l_i})$ as the metameric black subspace, denoted by $\mathcal{B}_i$, each for the illuminant l_i.

[1] Under certain special illuminants, it is possible that the HVS space could have a dimensionality less than 3. Since these illuminants are rarely used for viewing colour images, this pathological case will not be further considered in this thesis.

4.2 Orthogonal Projective Mapping

In mapping a reflectance from one reflectance space to another, it is natural to minimize the spectral difference between the mapped reflectance and the original one. With orthogonal projection, a reflectance that has a minimum mean squared spectral error in the target space can be readily found. But, unless the spectrum of the mapped reflectance is exactly the same as the original, minimizing the spectral error does not necessarily preserve the original colours. Thus, projection does not always map reflectance to one that has the same colour appearance even if one exists.

This section describes how to use orthogonal projection for reflectance mapping. Conditions under which projective mappings maintain colour appearance are studied. Unfortunately such conditions are too restrictive for practical applications.

4.2.1 Steps for Orthogonal Projective Mapping

Let $\mathcal{R}_D$ be the reflectance space that is spanned by the orthonormal reflectance basis set $\{c_1(\lambda), c_2(\lambda), \cdots, c_n(\lambda)\}$. Using the orthonormal basis, any reflectance $\mathbf{r} \in \mathcal{R}$ can be projected onto $\mathcal{R}_D$ by a single matrix multiplication. The coordinates of the projected results, $\mathbf{u}_r$, is given by the matrix equation

$$\mathbf{u}_r = \mathbf{B}^t \mathbf{r} .$$

where $\mathbf{B}$ is the $N \times n$ matrix with $c_i(\lambda)$ as its column vectors. The projected reflectance is

$$\mathbf{r}' = \mathbf{B}\,\mathbf{u}_r = \mathbf{B}\,\mathbf{B}^t \mathbf{r} .$$

Thus, the orthogonal projection operator for $\mathcal{R}_D$ can be expressed as a $N \times N$ matrix:

$$\mathbf{P}_D = \mathbf{B}\,\mathbf{B}^t .$$

The spectral error, $\Delta\mathbf{r}$, is

$$\begin{aligned}\Delta\mathbf{r} &= \mathbf{r} - \mathbf{r}' \\ &= \mathbf{r} - \mathbf{P}_D\mathbf{r} \\ &= [\mathbf{I} - \mathbf{P}_D]\mathbf{r}\,. \end{aligned} \tag{4.2}$$

which is equivalent to the projection of $\mathbf{r}$ onto the complementary space of $\mathcal{R}_D$, $\bar{\mathcal{R}}_D$. In fact, the orthogonal projection of any reflectance $\mathbf{r}$ onto $\mathbf{r}' \in \mathcal{R}_D$ is the one that has minimum mean-squared spectral errors, that is $\|\mathbf{s} - \mathbf{r}\| \geq \|\mathbf{r}' - \mathbf{r}\|$ for any $\mathbf{s} \in \mathcal{R}_D$, where $\|\cdot\|$ is defined as: $\|\mathbf{x}\| = \sqrt{x(\lambda_1)^2 + x(\lambda_2)^2 + \cdots + x(\lambda_n)^2}$ for any vector $\mathbf{x}$ in the wavelength space. To see this, let $\mathbf{s} = \mathbf{r}' + \Delta\mathbf{s}$. Since both $\mathbf{s}$ and $\mathbf{r}$ are in $\mathcal{R}_D$, $\Delta\mathbf{s}$ must also be in $\mathcal{R}_D$. Then,

$$\begin{aligned}\|\mathbf{s} - \mathbf{r}\| &= \|\mathbf{r}' + \Delta\mathbf{s} - \mathbf{r}\| \\ &= \|(\mathbf{r}' - \mathbf{r}) + \Delta\mathbf{s}\| \\ &= \|\Delta\mathbf{r} + \Delta\mathbf{s}\| \\ &= \|\Delta\mathbf{r}\| + \|\Delta\mathbf{s}\| \quad \text{as } \Delta\mathbf{s} \in \mathcal{R}_D \text{ and } \Delta\mathbf{r} \in \bar{\mathcal{R}}_D \\ &\geq \|\Delta\mathbf{r}\|\,. \end{aligned}$$

Even though this projective mapping identifies the reflectance that has the most similar spectrum, it may not be the one that is closest in colour appearance because spectral errors do not necessarily correlate well with human colour sensitivity. Differences in the tristimulus values of the spectral errors are not guaranteed to be small. In fact, only under very restrictive conditions can orthogonal projective mapping preserve colour appearance.

4.2.2 Projective Mapping and Colour Matching

Projective mapping is not guaranteed to preserve the original tristimulus values even when there is a reflectance with the same tristimulus values in the target reflectance space. However, under certain conditions the mapping can preserve the tristimulus values. In this section, we study these conditions by examining the

tristimulus values of the spectral errors. It is shown that the conditions under which projective mapping minimizes tristimulus value error are too restrictive for practical applications.

Consider projective mapping between two reflectance spaces of $\mathcal{R}_{D_1}$ and $\mathcal{R}_{D_2}$, each of which is constructed by modified SVD, as discussed in Chapter 2. For $\mathbf{r} \in \mathcal{R}_{D_1}$ and $\mathbf{r}' \in \mathcal{R}_{D_2}$ to have the same colour under illuminant l, the tristimulus values of the spectral error must be zero. The next few paragraphs describe how the tristimulus values are computed.

Let $\mathbf{u}_r$ be the coordinates of $\mathbf{r}$ with respect to the basis of $\mathcal{R}_{D_1}$. $\mathbf{G}_{D_1}$ be the $N \times n$ column matrix of the orthonormal reflectance basis vectors with the unity reflectance, $\mathbf{w}$, the first basis element (see Chapter 2), and $\mathbf{P}_{D_2}$ be the projective operator from $\mathcal{R}_{D_1}$ to $\mathcal{R}_{D_2}$. From the Equation 4.2, the spectral error after projective mapping can be written as

$$\begin{aligned} \Delta\mathbf{r} &= \mathbf{r} - \mathbf{r}' . \\ &= [\mathbf{I} - \mathbf{P}_{D_2}]\,\mathbf{G}_{D_1}\,\mathbf{u}_r . \end{aligned}$$

The corresponding tristimulus values are

$$\begin{aligned} \Delta\mathbf{t}_r &= \mathbf{A}_l\,\Delta\mathbf{r} \\ &= \mathbf{A}_l\,[\mathbf{I} - \mathbf{P}_{D_2}]\,\mathbf{G}_{D_1}\,\mathbf{u}_r \\ &= \mathbf{A}_l\,\mathbf{D}\,\mathbf{u}_r . \end{aligned} \tag{4.3}$$

where $\mathbf{A}_l$ is the $3 \times N$ transformation matrix under l, and $\mathbf{D}$ is the $N \times n$ matrix with values of $[\mathbf{I} - \mathbf{P}_{D_2}]\,\mathbf{G}_{D_1}$, the columns of which represent the projected basis elements onto the complementary space of $\mathcal{R}_{D_2}$, $\bar{\mathcal{R}}_{D_2}$.

Note that for $\mathbf{u}_r$ representing any real reflectance, the condition of $\mathbf{0} \leq \mathbf{G}_{D_1}\mathbf{u}_r \leq \mathbf{1}$ must be satisfied. Thus, $\mathbf{u}_r$ cannot take on arbitrary values. To study the conditions under which $\Delta\mathbf{t}_r$ has zero value, a general formula is needed for computing errors in tristimulus values.

Since $\mathbf{w}$ is the first basis element of $\mathcal{R}_{D_1}$, $\mathbf{r}$ can be expressed as

$$\mathbf{r} = a\,\mathbf{G}_{D_1}\mathbf{v}_r + b\,\mathbf{w} .$$

where $\mathbf{v}_r = (a, u_2, u_3, \cdots, u_n)$ and $b = u_1 - a$. Equation 4.3 can be rewritten as

$$\begin{aligned} \Delta\mathbf{t}_r &= \mathbf{A}_l[\mathbf{I} - \mathbf{P}_{D_2}](a\,\mathbf{G}_{D_1}\mathbf{v}_r + b\,\mathbf{w}) \\ &= a\,\mathbf{A}_l\mathbf{D}\,\mathbf{v}_r + b\,\mathbf{A}_l[\mathbf{I} - \mathbf{P}_{D_2}]\mathbf{w}\,. \end{aligned}$$

Because the white reflectance, $\mathbf{w}$, is one of the basis elements for $\mathcal{R}_{D_2}$, the second term in the equation is zero since $\mathbf{w}$ is orthogonal to the complementary space of $\mathcal{R}_{D_2}$. Thus, the above equation simplifies to

$$\Delta\mathbf{t}_r = a\,\mathbf{A}_l\mathbf{D}\,\mathbf{v}_r\,.$$

The above formula differs from Equation 4.3 by a scalar value. Since $\mathbf{v}_r$ can be any value, the column vectors of $\mathbf{D}$ must be orthogonal to the row vectors of $\mathbf{A}_l$ for the tristimulus values of $\Delta\mathbf{r}$ to be zero. With the column vectors of $\mathbf{D}$ being the projected basis of $\mathcal{R}_{D_1}$ onto the complementary space of $\mathcal{R}_{D_2}$, the above condition states that the basis of $\mathcal{R}_{D_1}$ projected onto the complementary space of $\mathcal{R}_{D_2}$ must be in the metameric black space for the illuminant l.

The necessary condition of colour preservation for projective mapping can be understood by examining an arbitrary basis element of $\mathcal{R}_{D_1}$. Since the wavelength space is a direct sum of $\mathcal{R}_{D_2}$ and $\bar{\mathcal{R}}_{D_2}$, the basis element, $c(\lambda) \in \mathcal{R}_{D_1}$, can be expressed as

$$c(\lambda) = c_{D_2}(\lambda) + \bar{c}_{D_2}(\lambda)\,.$$

where $c_{D_2}(\lambda) \in \mathcal{R}_{D_2}$ and $\bar{c}_{D_2}(\lambda) \in \bar{\mathcal{R}}_{D_2}$. Since the condition states that $\bar{c}_{D_2}(\lambda)$ must be in the metameric black space, the visual sensation of $c(\lambda)$ must come from $c_{D_2}(\lambda)$. This condition ensures that all colours associated with any reflectances in $\mathcal{R}_{D_1}$ must be realizable by the reflectances in $\mathcal{R}_{D_2}$ for the illuminant under consideration.

Unfortunately, the above requirement for the projective mapping to maintain the original colours cannot be satisfied under common viewing illuminants. To understand this, let us rewrite Equation 4.3 as

$$\begin{aligned} \Delta\mathbf{t}_r &= \mathbf{A}_E\mathbf{D}\,\mathbf{u}_r \\ &= \mathbf{H}^t\mathbf{E}\mathbf{D}\,\mathbf{u}_r\,, \end{aligned}$$

where $\mathbf{H}$ is the colour matching matrix, and $\mathbf{E}$ is the diagonal matrix of the spectrum of an illuminant. If the projective mapping preserves colour, $\Delta\mathbf{t}_r$ must be a zero vector for any $\mathbf{u}_r$. Therefore, the result of the matrix multiplication of $\mathbf{H}^t\,\mathbf{E}\,\mathbf{D}$ must be a $3 \times n$ zero matrix. This condition is satisfied only if the spectrum of the viewing illuminant, Φ_λ, is a solution of the homogeneous system

$$\begin{bmatrix} x(\lambda_1)d_1(\lambda_1) & x(\lambda_2)d_1(\lambda_2) & \cdots & x(\lambda_N)d_1(\lambda_N) \\ y(\lambda_1)d_1(\lambda_1) & y(\lambda_2)d_1(\lambda_2) & \cdots & y(\lambda_N)d_1(\lambda_N) \\ z(\lambda_1)d_1(\lambda_1) & z(\lambda_2)d_1(\lambda_2) & \cdots & z(\lambda_N)d_1(\lambda_N) \\ \vdots & \vdots & & \vdots \\ x(\lambda_1)d_n(\lambda_1) & x(\lambda_2)d_n(\lambda_2) & \cdots & x(\lambda_N)d_n(\lambda_N) \\ y(\lambda_1)d_n(\lambda_1) & y(\lambda_2)d_n(\lambda_2) & \cdots & y(\lambda_N)d_n(\lambda_N) \\ z(\lambda_1)d_n(\lambda_1) & z(\lambda_2)d_n(\lambda_2) & \cdots & z(\lambda_N)d_n(\lambda_N) \end{bmatrix} \begin{bmatrix} \Phi_{\lambda_1} \\ \Phi_{\lambda_2} \\ \vdots \\ \Phi_{\lambda_N} \end{bmatrix} = 0\,. \qquad (4.4)$$

where $x(\lambda_i), y(\lambda_i), z(\lambda_i)$ is value of the colour matching function of $\bar{x}, \bar{y}, \bar{z}$, respectively, at the wavelength λ_i, and $d_j(\lambda_i)$ is the value of the jth basis element of $\mathcal{R}_{D_1}$ at λ_i projected onto the complementary space of $\mathcal{R}_{D_2}$, which is the value of the (i, j)th entry of the matrix $\mathbf{D}$.

Given the above equation, we have tested orthogonal projective mapping between our DuPont and Kodak printers. In the experiment, the reflectance basis functions of reflectance spaces for the DuPont and Kodak printers are constructed. The basis construction method is the one proposed in Paeth's thesis [Pae94]. The reflectance basis of the Kodak printer is projected to the complementary reflectance space of the DuPont printer to obtain the matrix $\mathbf{D}$. The entries of the matrix for the above homogeneous system are computed with the 1964 CIE Standard observers. The system is then solved by the SVD method. The solutions represents a set of illuminant basis functions which form a space that contains illuminations under which the projection mapping preserves colour appearance.

Figure 4.1 shows the spectra of illuminants and their residual components for projective mapping. None of the CIE standard illuminants is inside the illuminant

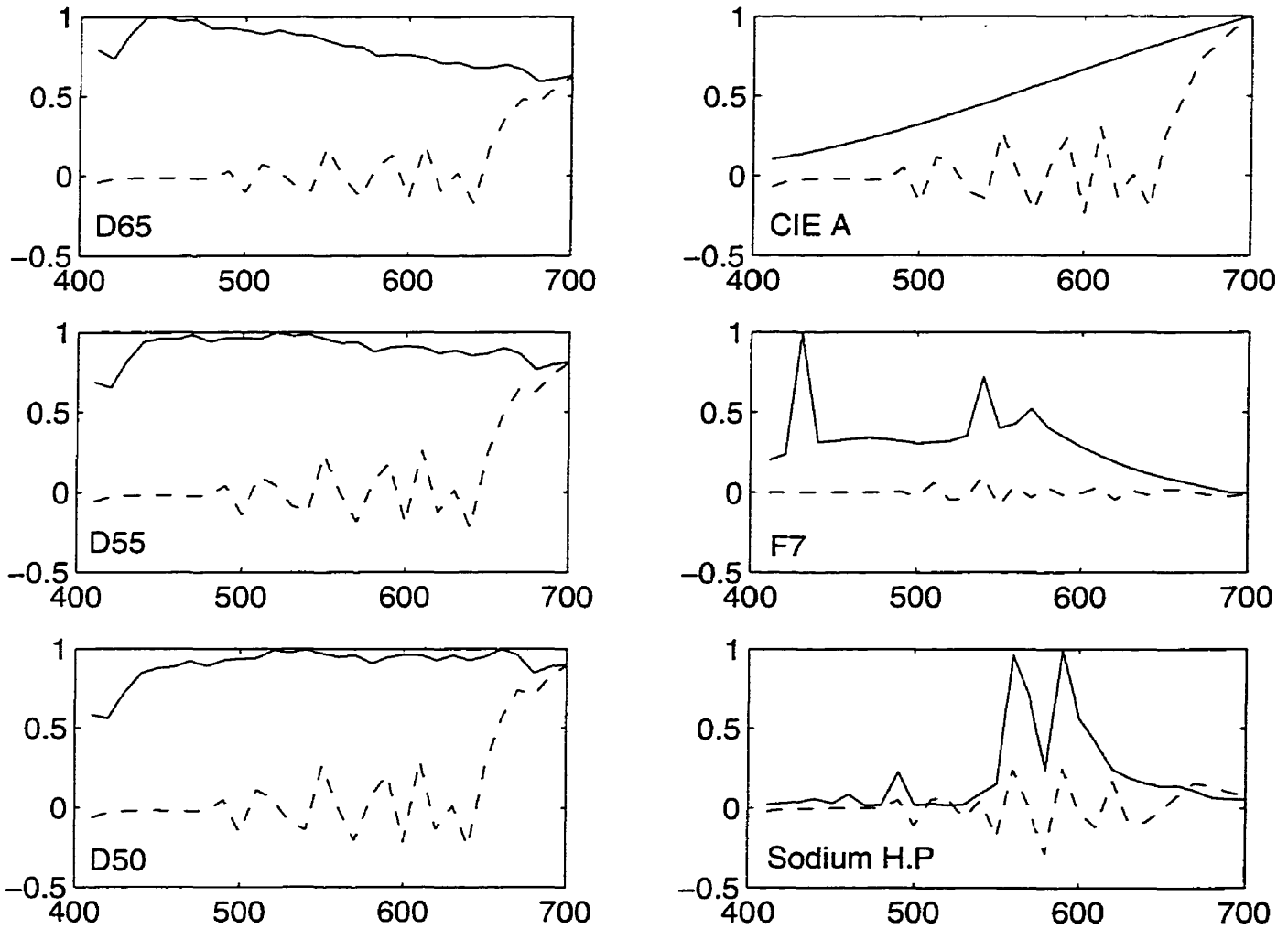


Figure 4.1: Projecting the spectra of each illuminant on the column space of the matrix **D**. The dashed lines represent the residual components of the illuminant that do not satisfy Equation 4.4

space. In general, colours are not maintained after orthogonal projective mapping under normal illuminants. To conserve colour sensation, the mapping that preserves the fundamental component of the reflectance provides a better result.

4.3 Fundamental Component Mapping

As mentioned in the last chapter, the colour appearance of a reflectance is closely related to its fundamental component. Two reflectances that have identical fundamental components under a given illuminant have the same colour appearance under that illuminant. Thus, the problem of finding reflectances that match reflectance $\mathbf{r}$ under illuminant l_i consists of finding reflectances, $\mathbf{r}'$, with the same fundamental component as $\mathbf{r}$. This section describes how to use the fundamental component for reflectance mapping. Fundamental component mapping is better than projective mapping in two ways: first, when colour identity is possible within the given reflectance gamuts, it always finds it: second, when colour identity is not possible, empirical results show that it consistently outperforms projective mapping.

4.3.1 Basic Concepts of Fundamental Component Mapping

Let $\mathcal{R}$ be the reflectance space generated by the output of an output device. To determine the fundamental components of the reflectances in $\mathcal{R}$ under l_i, we represent $\mathcal{R}$ as the direct sum of two subspaces $\mathcal{F}_{\mathcal{R}_i}$ and $\mathcal{B}_{\mathcal{R}_i}$:

$$\mathcal{R} = \mathcal{F}_{\mathcal{R}_i} \oplus \mathcal{B}_{\mathcal{R}_i} .$$

Here, $\mathcal{B}_{\mathcal{R}_i}$ is the intersection between the reflectance space $\mathcal{R}$ and the metameric black subspace $\mathcal{B}_i$, and $\mathcal{F}_{\mathcal{R}_i}$ is the subspace of $\mathcal{R}$ orthogonal to $\mathcal{B}_{\mathcal{R}_i}$ (Figure 4.2). Note that $\mathcal{F}_{\mathcal{R}_i}$ is not the fundamental component space $\mathcal{F}_i$ intersected with $\mathcal{R}$. The definition ensures that every non-zero reflectance in $\mathcal{F}_{\mathcal{R}_i}$ is made up of a fundamental component and a possibly zero black component. The basis of $\mathcal{F}_{\mathcal{R}_i}$

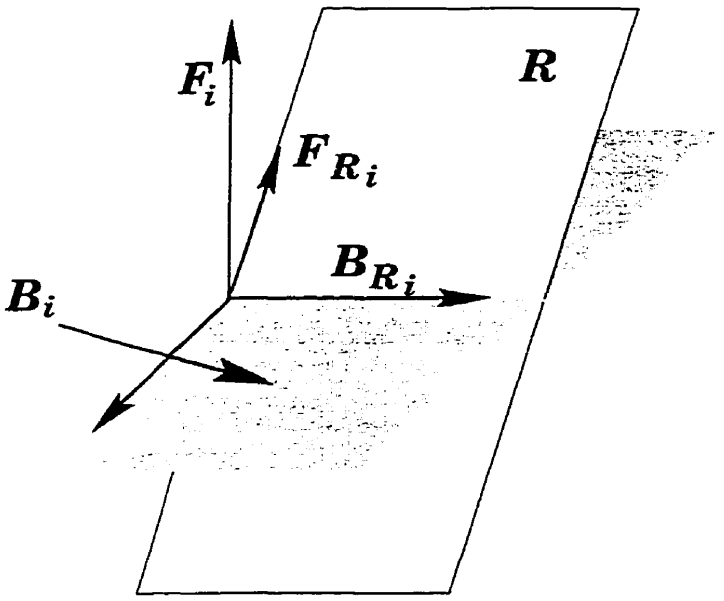


Figure 4.2: Each reflectance space $\mathcal{R}$ can be represented as the direct sum of two subspaces $\mathcal{F}_{\mathcal{R}_i}$ and $\mathcal{B}_{\mathcal{R}_i}$ under illuminant l_i. $\mathcal{B}_{\mathcal{R}_i}$ is the intersection between the reflectance space $\mathcal{R}$ and the metameric black subspace $\mathcal{B}_i$, and $\mathcal{F}_{\mathcal{R}_i}$ is the subspace of $\mathcal{R}$ orthogonal to $\mathcal{B}_{\mathcal{R}_i}$

is the set of reflectances that always cause some kind of colour sensation, whereas that of $\mathcal{B}_{\mathcal{R}_i}$ is the set of reflectances that are invisible to normal observers. (The elements in both sets may not be physically realizable.) The computation of $\mathcal{F}_{\mathcal{R}_i}$ and $\mathcal{B}_{\mathcal{R}_i}$ can be carried out by singular value decomposition (SVD), which provides both basis sets in a single computation [GVL83].

Every trichromatic reflectance space, $\mathcal{R}$,[2] has a 3-dimensional subspace $\mathcal{F}_{\mathcal{R}_i}$. Now let $\{\mathbf{f}'_1, \mathbf{f}'_2, \mathbf{f}'_3\}$ be the basis of $\mathcal{F}_{\mathcal{R}_i}$. Since each $\mathbf{f}'_j$ contains both a fundamental component and a metameric black component, it can be expressed as

$$\mathbf{f}'_j = \mathbf{f}_j + \mathbf{b}_j \ ,$$

where $\mathbf{f}_j \in \mathcal{F}_i$ and $\mathbf{b}_j \in \mathcal{B}_i$. Because $\mathcal{R}$ produces a three dimensional colour sensation, the reflectances $\mathbf{f}_j$ must span at least a three dimensional space. Since $\mathcal{F}_i$ is a 3-dimensional space, any three linear independent reflectances in it can be used as its basis. The set $\{\mathbf{f}_1, \mathbf{f}_2, \mathbf{f}_3\}$ is chosen here as the basis of $\mathcal{F}_i$.

Now consider the problem of finding a reflectance $\mathbf{r}' \in \mathcal{R}$ that has the same fundamental component as that of $\mathbf{r}$. Let $\mathbf{f}_r$ be the fundamental component of $\mathbf{r}$. It can be expressed in terms of $\mathbf{f}_i$:

$$\mathbf{f}_r = a_1\mathbf{f}_1 + a_2\mathbf{f}_2 + a_3\mathbf{f}_3 \ .$$

Every element $\mathbf{r}' \in \mathcal{F}_{\mathcal{R}_i}$ that has the same coefficients a_i with respect to the basis $\{\mathbf{f}'_1, \mathbf{f}'_2, \mathbf{f}'_3\}$ has a fundamental component identical to that of $\mathbf{r}$. To see this express $\mathbf{r}'$ as

$$\begin{aligned} \mathbf{r}' &= a_1\mathbf{f}'_1 + a_2\mathbf{f}'_2 + a_3\mathbf{f}'_3 + \mathbf{b}_{\mathbf{r}'} \\ &= a_1(\mathbf{f}_1 + \mathbf{b}_1) + a_2(\mathbf{f}_2 + \mathbf{b}_2) + a_3(\mathbf{f}_3 + \mathbf{b}_3) + \mathbf{b}_{\mathbf{r}'} \\ &= a_1\mathbf{f}_1 + a_2\mathbf{f}_2 + a_3\mathbf{f}_3 + \mathbf{b}_{\sum \mathbf{r}'} \qquad \text{for} \quad \mathbf{b}_{\sum \mathbf{r}'} = a_1\mathbf{b}_1 + a_2\mathbf{b}_2 + a_3\mathbf{b}_3 + \mathbf{b}_{\mathbf{r}'} \ , \end{aligned}$$

where $\mathbf{b}_{\mathbf{r}'} \in \mathcal{B}_{\mathcal{R}_i}$. Since $\mathbf{b}_{\sum \mathbf{r}'} \in \mathcal{B}_{\mathcal{R}}$, $\mathbf{r}'$ has the same fundamental component as $\mathbf{r}$. Their colours match under illuminant l_i. In fact any reflectance $\tilde{\mathbf{r}} \in \mathcal{R}$ matches the

[2]Trichromatic reflectance space refers to a reflectance space generated by the output of a device which causes 3-dimensional colour sensation.

colour appearance of $\mathbf{r}$ if $\tilde{\mathbf{r}}$ can be expressed as

$$\tilde{\mathbf{r}} = a_1\mathbf{f}'_1 + a_2\mathbf{f}'_2 + a_3\mathbf{f}'_3 + \mathbf{b}_{\tilde{\mathbf{r}}} .$$

for any $\mathbf{b}_{\tilde{\mathbf{r}}} \in \mathcal{B}_{\mathcal{R}_i}$. Among these reflectances, it is possible that the spectral reflectance of $\tilde{\mathbf{r}}$ may be different from that of $\mathbf{r}$. A large spectral difference is undesirable because the larger the difference in spectral reflectance, the more likely it is that the two reflectances do not match under other illuminants. The reflectance in $\mathcal{R}$ that has the same fundamental component with smallest amount of difference in the spectral distribution is the best mapped value of $\mathbf{r}$.

To find such a reflectance, the residual reflectance, $\Delta\mathbf{r} = \mathbf{r} - \mathbf{r}'$, is first computed. Then a spectral distribution similar to $\Delta\mathbf{r}$ is added to $\mathbf{r}'$. To maintain the fundamental component, the added reflectance must be chosen from $\mathcal{B}_{\mathcal{R}_i}$. This can be done by orthogonal projection of $\Delta\mathbf{r}$ onto $\mathcal{B}_{\mathcal{R}_i}$. The result is the metameric black component in $\mathcal{R}$ that is closest to $\Delta\mathbf{r}$ in terms of least squared spectral error.

4.3.2 Fundamental Component Mapping under Several Illuminants

Now let us consider the two-illuminants case first, which can be easily extended to several illuminants. Let $\mathbf{s} \in \mathcal{R}$ be a reflectance that matches the colour of $\mathbf{r}$ under illuminants l_1 and l_2. Then $\mathbf{s}$ can be expressed as

$$\mathbf{s} = \mathbf{f}'_{s_1} + \mathbf{b}_{s_1} \text{ for illuminant } l_1 .$$

and

$$\mathbf{s} = \mathbf{f}'_{s_2} + \mathbf{b}_{s_2} \text{ for illuminant } l_2 .$$

where $\mathbf{b}_{s_i} \in \mathcal{B}_{\mathcal{R}_i}$, and $\mathbf{f}'_{s_i} \in \mathcal{F}_{\mathcal{R}_i}$ which is same as the fundamental component of $\mathbf{r}$ under the illuminant l_i. By combining the above two equations, we have

$$\begin{aligned} \mathbf{f}'_{s_2} - \mathbf{f}'_{s_1} &= \mathbf{b}_{s_1} - \mathbf{b}_{s_2} \\ &= \mathbf{P}_{b_1}\mathbf{s} - \mathbf{P}_{b_2}\mathbf{s} \\ &= (\mathbf{P}_{b_1} - \mathbf{P}_{b_2})\,\mathbf{s} , \end{aligned} \tag{4.5}$$

where $\mathbf{P}_{b_1} . \mathbf{P}_{b_2}$ is the projection transformation matrix that maps $\mathbf{s}$ to $\mathbf{b}_{s_1}$ and $\mathbf{b}_{s_2}$. respectively. Since the values of $\mathbf{f}_{s_i}$ and $\mathbf{P}_{b_i}$ are known once the reflectance space $\mathcal{R}$ and the illuminants are defined. the reflectance $\mathbf{s}$ can be found by solving the above linear equation. Like the single illuminant case. a metameric black component for both illuminants. i.e.. $\mathbf{b}_{12} \in (\mathcal{B}_{\mathcal{R}_1} \cap \mathcal{B}_{\mathcal{R}_2})$. can be added to $\mathbf{r}$ to reduce the spectral error. In fact. $\mathcal{R}$ can be expressed as

$$\mathcal{R} = \mathcal{F}_{\mathcal{R}_{12}} \oplus \mathcal{B}_{\mathcal{R}_{12}} .$$

where $\mathcal{B}_{\mathcal{R}_{12}} = (\mathcal{B}_{\mathcal{R}_1} \cap \mathcal{B}_{\mathcal{R}_2})$. $\mathcal{F}_{\mathcal{R}_{12}}$ contains reflectances orthogonal to the elements in $\mathcal{B}_{\mathcal{R}_{12}}$ and which have nonzero fundamental components under at least one of the illuminants.

The above approach can be easily extended to several illuminants. For instance. in the three illuminants case. the left hand side of the Equation 4.5 can be defined as

$$\begin{bmatrix} \Delta \mathbf{f}'_{s_{21}} \\ \Delta \mathbf{f}'_{s_{32}} \end{bmatrix} = \begin{bmatrix} \mathbf{P}_{b_1} - \mathbf{P}_{b_2} \\ \mathbf{P}_{b_2} - \mathbf{P}_{b_3} \end{bmatrix} \times \mathbf{s} .$$

The reflectance $\mathbf{r}$ can be obtained as in the two illuminants case.

Note that the possibility of finding a reflectance that matches colours of a given reflectance decreases rapidly as the number of illuminants considered increases. Consider the subspace of $\mathcal{F}_{\mathcal{R}_\mathcal{I}}$ for k illuminants. Since every element $\mathbf{x} \in \mathcal{F}_{\mathcal{R}_\mathcal{I}}$ has nonzero fundamental components under at least one of the illuminants. $\mathbf{x}$ must be in $\cup_{i \in \mathcal{I}} \mathcal{F}_i$. For $\mathcal{R}$ be a trichromatic reflectance space under each illuminant. the subspace that contains $\cup_{i \in \mathcal{I}} \mathcal{F}_i$ may have dimension as large as $3k$. As a result, the dimension of $\mathcal{F}_{\mathcal{R}_\mathcal{I}}$ may be as large as $3k$. Certainly. if the illuminants in $\mathcal{I}$ are similar to one another. the dimension of $\mathcal{F}_{\mathcal{R}_\mathcal{I}}$ is less than $3k$. In general, however, the possibility of finding a reflectance $\mathbf{s} \in \mathcal{R}$ with the same colours as $\mathbf{r} \notin \mathcal{R}$ under illuminants in $\mathcal{I}$ decreases as the number of illuminants in $\mathcal{I}$ increases.

When no reflectance matches the colour of $\mathbf{r}$ under the complete set of illuminants. the linear equation has no solution. However. by using SVD to solve the equation. it is possible to get the least-squares best approximation of $\mathbf{r}$. Since it

is difficult, perhaps impossible, to derive an error model for fundamental component mapping, experiments are used to show the performance of the mapping for multiple illuminants.

4.4 Experimental Results

Both orthogonal projection and fundamental component mappings were implemented. Experiments were conducted to test their relative performance empirically. This section describes the results, which show that fundamental component mapping consistently outperforms projective mapping.

To test the effectiveness of fundamental component mapping, two reflectance spaces were constructed using Paeth's modified SVD. Two sets of illuminants were used. One set comprised CIE Standard Illuminant A, F7 fluorescent light, and a high pressure sodium light. The other comprised CIE Standard Illuminants D50, D55, and D65. Two reflectance spaces were constructed. One of the spaces was constructed based on the reflectances of 40 real objects, and the other based on a set of output colours from a Kodak dye sublimation printer. Each reflectance space serves as a target space in one of our two experiments. The input reflectances obtained from the 24 patches of the Macbeth Colorchecker and the 40 real objects were then transformed to the target reflectance spaces.

For each reflectance space, three transformations were performed.

1. Projective Mapping. The original reflectances were mapped to the target reflectance space using projective mapping. The average CIELAB colour difference, ΔE_{ab}, between the original and the mapped reflectances were computed for each of the six illuminants in the two illuminant sets. The results are listed in Table 4.1 labelled "Proj.".

2. Fundamental Component Mapping for the First Illuminant Set. The original reflectances were mapped to the space using fundamental component mapping for the illuminant set containing the CIE D50, CIE D55, and CIE D65.

Reflectance Samples	CIE D50		CIE D55		CIE D65	
	F.M.	Proj.	F.M.	Proj.	F.M.	Proj
Real Object	0.000	0.364	0.000	0.357	0.000	0.346
Macbeth	0.000	0.809	0.000	0.810	0.000	0.810

(a)

Reflectance Samples	CIE A		F7		HP Sodium	
	F.M.	Proj.	F.M.	Proj.	F.M.	Proj
Real Object	0.289	0.352	0.011	0.432	0.023	0.490
Macbeth	0.072	0.700	0.054	1.144	0.054	1.077

(b)

Table 4.1: The average CIELAB colour differences for the fundamental mapping (F.M.) and directed projection (Proj.) under two set of illuminants. The reflectances of 40 real objects and 24 patches of Macbeth Colourchecker were mapped to the reflectance space which constructed based on the reflectances from 40 real objects.

The average ΔE_{ab} over the test reflectances were computed for the three illuminants in the set. The results are listed in Table 4.1(a) labelled "F.M."

3. Fundamental Component Mapping for the Second Illuminant Set. The original reflectances were mapped to the space using fundamental component mapping for the illuminant set contains the CIE A, F7 fluorescent light, and the sodium light. The average ΔE_{ab} between over the test reflectances were computed for the three illuminants in the set. The results are listed in Table 4.1(b) labelled "F.M."

Reflectance Samples	CIE D50		CIE D55		CIE D65	
	F.M.	Proj.	F.M.	Proj.	F.M.	Proj
Real Object	0.000	2.658	0.000	2.627	0.000	2.582
Macbeth	0.000	0.942	0.000	0.895	0.000	0.840

(a)

Reflectance Samples	CIE A		F7		HP Sodium	
	F.M.	Proj.	F.M.	Proj.	F.M.	Proj
Real Object	0.126	2.486	0.146	2.072	0.038	2.402
Macbeth	0.187	1.253	0.251	1.372	0.043	2.005

(b)

Table 4.2: The average CIELAB colour differences for the fundamental mapping (F.M.) and directed projection (Proj.) under two set of illuminants. The reflectances of 40 real objects and 24 patches of Macbeth Colourchecker were mapped to the reflectance space which constructed based on the reflectances of the evenly sampled printer output colours.

	D50 vs D55	D50 vs D65	D55 vs D65
1st min. angle	1.0000	1.0000	1.0000
2nd min. angle	0.9998	0.9991	0.9997
3rd min. angle	0.9994	0.9961	0.9986

	A vs F7	A vs H.P. Sodium	F7 vs H.P. Sodium
1st min. angle	0.9663	0.8945	0.8832
2nd min. angle	0.9039	0.8643	0.7195
3rd min. angle	0.7818	0.5849	0.4765

Table 4.3: Cosine of the principal angles between the fundamental component subspaces of the pairs of illuminants within a set. When the cosine of principal angle equals to 1. it means two vectors in the two subspaces coincide with each other

4.4.1 Illuminant Differences

The principal angles between the fundamental component subspaces within each set of illuminants have been computed. The principal angles describe the similarity between two subspaces. The computed principal angles provide the qualitative measurement of how different the light source would be with each illuminant set. From Table 4.3. which shows the cosine of principal angles between two illuminants. it shows that the fundamental component subspaces for the first set of illuminants are very similar. whereas the illuminants of the second set are quite different.

The first set is daylight illuminants. all of each have good colour rendering index. the largest principal angle is 3°. In contrast the first minimum principal angles among the second set of illuminants. which contains artificial illuminants. lies between 15° and 27°. and the third principal is as large as 62°. Thus, it is

difficult to reproduce colours with small colour differences under the second set of illuminants.

4.4.2 Mapping Results

As shown in Tables 4.1 and 4.2, the fundamental component mapping provides much better results than simple projective transformation. In our experiments for the daylight illuminants, the fundamental component mapping always identifies the reflectances with the same colour as the original, whereas the projective mapping does not always map to the ones with the same colours. The average colour difference using the fundamental component mapping less than 0.0005, and using projective mapping is 1.17. For the second set of illuminants, the results, as expected, are not as good as the first one. However, the largest average colour difference using the fundamental component mapping is 0.289, whereas the projective mapping is 2.486. In most cases, the average colour differences for the fundamental component mapping are ten times smaller than those for the projective mapping. The projective transformation sometimes maps to reflectances objectionably different from the original, but the fundamental mapping never does.

The fundamental mapping does well for the following reasons. When the viewing illuminants are similar, the fundamental mapping performs effectively because of the overlay of large portion of the fundamental component subspaces for the illuminants (see Tables 4.1a & 4.2a). Even when the illuminants are very different, the mapping is still able to find a suitable reflectance that matches the original colour because the fundamental component of the reflectance is similar to the original one for the given illuminants. (see Tables 4.1b & 4.2b).

Since the fundamental component is directly related to the CIE XYZ tristimulus values, the fundamental component mapping in essence is trying to maintain the tristimulus values. However, the XYZ values are not commonly used to measure colour difference since the XYZ space is not perceptually uniform. Instead, CIELAB or CIELUV are a better choice for measuring colour difference. Mappings that are developed to preserve the CIELAB or CIELUV values are believed to produce better

results. However, the nonlinearity of these colour spaces substantially increases the complexity of the algorithms. As a result, their performances is unlikely to be suitable for practical applications. Fortunately, the differences in the XYZ values obtained from the fundamental component mapping are usually very small which leads to small differences in the CIELAB and CIELUV spaces as well. Therefore, the fundamental component mapping is a very useful approach for preserving the colour appearance of reflectively defined images.

4.5 Conclusions

Reflectance spaces are constructed to provide representations that have minimal errors in spectral reflectance. Thus, it is natural to minimize spectral errors when mapping a reflectance from one reflectance space to another. This objective is achieved by orthogonal projective mapping, which maps the original reflectance to the one that has minimum mean squared spectral errors in the target space. However, without taking into account the illuminant and the colour sensitivity of the human visual system, this simple transformation does not, in general, map reflectances to the ones that have the same colour appearance even when they exist in the target space. This problem can be avoided by using the fundamental component mapping, which tries to preserve the fundamental component of the reflectances. Colours are preserved by the mapping when possible. When an exact colour match is not possible, our experimental results shows that fundamental component mapping consistently outperforms projective mapping in terms of perceived colour difference.

Chapter 5

Colour Attributes in Reflectance Space

As discussed in Chapter 1. there are two different approaches to gamut mapping for colour reproduction. One minimizes an objective function. such as ΔE_{ab}. that is a CIE measure of perceived colour difference: another uses models of colour appearance to maintain the perceptual colour attributes. The previous chapter showed that objective functions can be extended to reflectance space using the fundamental component mapping. This chapter discusses how to evaluate perceptual colour attributes in reflectance space. In doing so we establish the relationships between a reflectance and its colour attributes. Since the colour attributes are always more or less affected by the viewing illuminant. issues such as how the attributes vary due to the change of illuminant. and how to choose the reflectances for colour reproduction under different illuminants are important. Unless stated otherwise. the arguments for reflectances in this chapter apply to both physically realizable and nonrealizable reflectances.

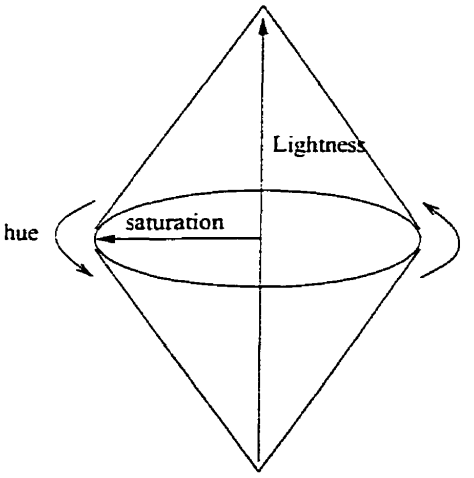
All colour spaces have similar topological properties for colour attributes. For example. a circuit around the neutral axis sees hue changing through the sequence. blue. cyan. green. yellow. orange. red. magenta in all colour spaces. The pattern of

hues. placed circularly following the above order. is referred as the hue circle. Similarly. lightness changes from dark to light along the neutral axis: and saturation increases along radial lines running from the neutral axis to the most saturated colours (Figure 5.1). Furthermore. transformations between colour spaces are continuous and 'monotonic' in the sense that the relative strengths of colour attributes between nearby colour points are preserved in the transformations. By studying the relationship between a reflectance and its hue. lightness and saturation. we show that very similar topological properties can be realized in a high dimensional reflectance space. Based on this fact. relative colour appearance between reflectances can be controlled even when it is not possible to specify the exact appearance of an illuminated reflectance. As a result. gamut mapping ideas that were developed based on the colour attributes of trichromatic spaces can be extended to reflectance spaces.

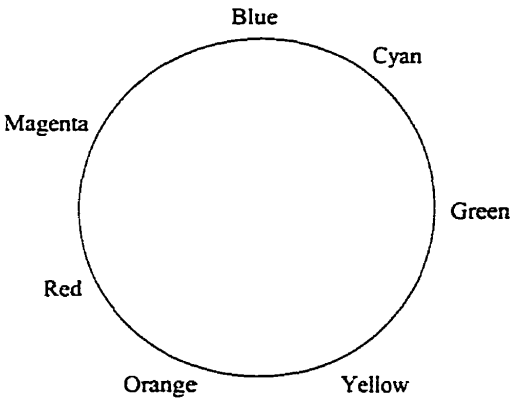
5.1 Constant Hue in Reflectance Space

Because the human visual system is very sensitive to hue changes. it is important to preserve the hues of an original image. Deviation of hue from original to reproduction jeopardizes reproduction quality. Many gamut mapping algorithms for trichromatic colour spaces are implicitly designed to operate within constant hue planes to simplify hue relationships. Thus. it is important for colour reproduction processes to identify all reflectances in a reflectance space that have the same hue.

Because colour constancy in the human visual system is incomplete. affected by both illuminant and the viewing context [BW91]. the appearance of a reflectance changes when the viewing illuminant changes. Thus. there is no definite relationship between the reflectance and hue in general. Fortunately. absolute hue sensation is often less important than hue relationships. Specifically. it is most important to know whether or not two reflectances have the same hue for the given set of illuminants. which is the focus of this section.

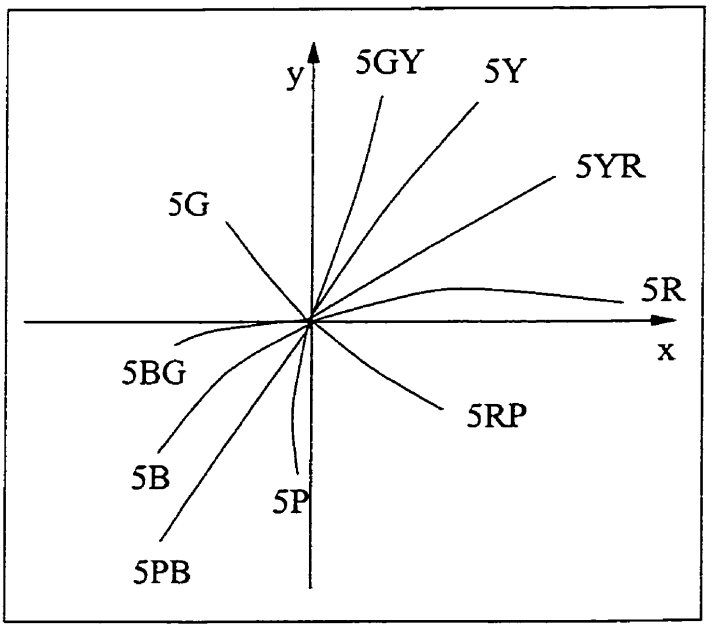


(a)

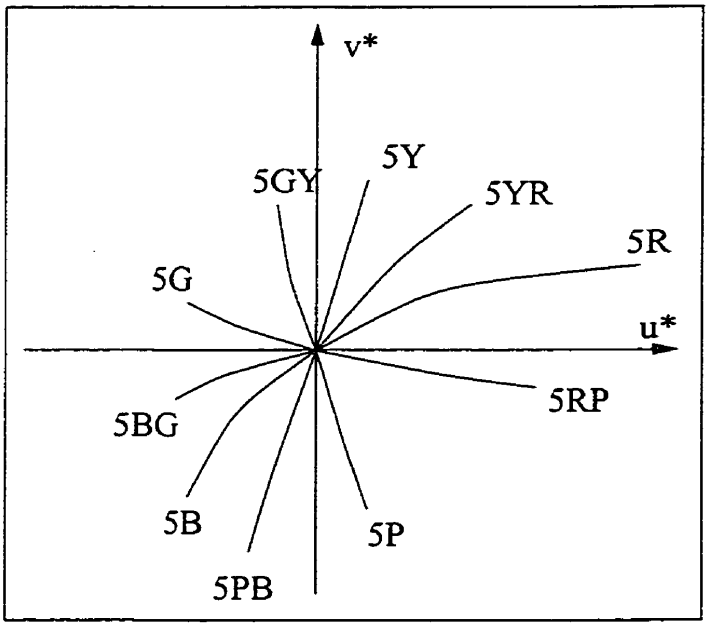


(b)

Figure 5.1: Common topological properties for colour attributes. (a) Lightness changes from dark to light along the neutral axis: and saturation increases along radial lines running from the neutral axis to the most saturated colour. (b) Hue changes from blue, cyan, green, yellow, orange, red, and magenta.



(a)



(b)

Figure 5.2: The constant hue lines for Munsell Value 5 are slightly curved in the CIE (x,y) chromaticity diagram and the CIE (u*,v*) chromaticity diagram.

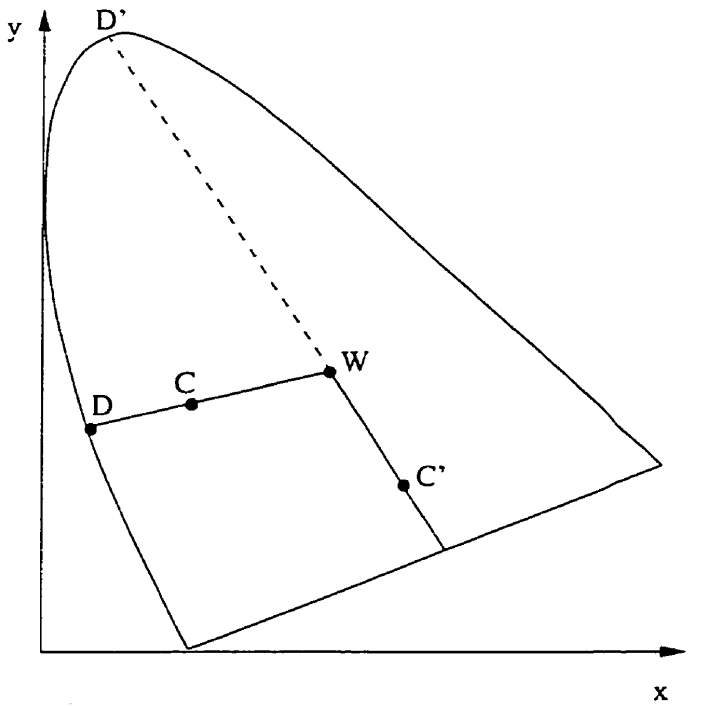


Figure 5.3: The dominant wavelength (D) of the colour (C) is the wavelength of intersected locus from a radial line extending out from the white point (W) to a colour point. The complement wavelength (D') of the colour (C') is the wavelength of intersected locus from a radial line extending out from C' to W

5.1.1 Hue Sensation and Colour Spaces

Wyszecki and Stiles [WS82] summarize research on hue sensation in CIE colour spaces by examining the distribution of colours having the same hue. They showed that the set of colours of constant hue for any lightness are slightly curved lines in the chromaticity diagram of CIELUV and the constant lightness plane of CIELAB (Figure 5.2). Similarly, the lines of constant hue are also slightly curved in the (x,y)-chromaticity diagram. To simplify computation, the CIE specifies radial lines in the (u',v') and (a^*,b^*) plane that approximate the true constant hue lines [WS82]. Similarly, the German Standard *DIN Colour System* [RW86] defines hue based on the dominant (or complementary) wavelength. Dominant and complementary wavelengths are based on the observation that any colour can be uniquely created as the additive mixture of a monochromatic colour and a neutral colour. The dominant wavelength of the colour is the wavelength of the monochromatic colour (Figure 5.3). Thus, all points on a radial line extending out from the white point in the (x,y)-chromaticity diagram are defined, in these systems, to have the same hue, a close approximation to constant perceived hue. The points on a line of constant hue defined above do not exactly have constant hue perceptually. Their hues in fact vary slightly. But, because the curvatures of the lines of constant hue are small, the amount of hue difference is less than the hue shift caused by chromatic induction and adaptation [Wys86].

In this thesis, we adopt the idea of the DIN Colour System that hue does not change when a colour is mixed additively with achromatic colours. As shown in Section 5.1.2, this approach allows us to specify the set of reflectances with same hue under a given set of illuminants as a linear expression.

The ideas developed in this chapter are based on the following definitions.

Definition 1 (Achromatic Hue Set). *The set of reflectances, which may or may not be physical realizable that have uniformly distributed spectra, called* $\mathcal{H}_A$.

The ideal white, $\mathbf{w}$, is an element in this set. All elements in $\mathcal{H}_A$ can be obtained by scaling the spectrum of white. They appear as achromatic under most light sources.

Definition 2 (Constant Hue). *Two reflectances have the same hue if they are related to one another by changing intensity and/or by additive mixing with any amount of achromatic reflectance in* $\mathcal{H}_A$. *The set of reflectances with the same hue as a reflectance* $\mathbf{r}$ *is defined as the constant hue set of* $\mathbf{r}$. $\mathcal{H}_\mathbf{r}$.

Using the DIN Colour System definition of hue. the above definition ensures that elements in $\mathcal{H}_\mathbf{r}$ have the same hue as $\mathbf{r}$ under all illuminants.

Mathematically. the definition states that

$$\mathbf{r} \in \mathcal{H}_\mathbf{r} \Longrightarrow a\,\mathbf{r} \in \mathcal{H}_\mathbf{r} .$$

and

$$\mathbf{r} \in \mathcal{H}_\mathbf{r} \Longrightarrow \mathbf{r} + b\mathbf{n} \in \mathcal{H}_\mathbf{r} .$$

where a. and b are any positive scalars. $\mathbf{n}$ is any reflectance in the achromatic set $\mathcal{H}_A$. and $+$ means additive mixture. The above two statements can be combined as

$$\mathbf{r} \in \mathcal{H}_\mathbf{r} \Longrightarrow a\mathbf{r} + b\mathbf{n} \in \mathcal{H}_\mathbf{r} .$$

Note that $\mathcal{H}_\mathbf{r}$ does not relate to a single hue sensation: instead. it relates to the set of hue sensations associated with $\mathbf{r}$ under different illuminants.

Constant hue for reflectance as defined above is analogous to hue defined for emitted lights using dominant wavelength. In fact. when reflectances with a constant hue are projected on the $(x.y)$ plane for a given illuminant. they form radial lines exactly like hue in the DIN Colour system. Since the set $\mathcal{H}_\mathbf{r}$ is closely related to lines of constant hue. the hues of reflectances in $\mathcal{H}_\mathbf{r}$ are *almost* perceptually identical.

Definition 3 (Complementary Hue). *The complementary reflectance* $\tilde{\mathbf{r}}$ *of a given reflectance* $\mathbf{r}$ *is defined as* $\mathbf{w} - \mathbf{r}$ *over the visible spectrum. The complementary hue is the hue associated with the complementary reflectance of a given reflectance.*

From the above two definitions. the following theorem must be true:

Theorem 1. *Whenever two reflectances have the same hue, so do their complementary reflectances.*

Proof. Let $\mathbf{r}_1$ and $\mathbf{r}_2$ be two reflectances with the same hue. By Definition 2, the relationship of $\mathbf{r}_1$ and $\mathbf{r}_2$ can be expressed as

$$\mathbf{r}_1 = a_1\mathbf{r}_2 + a_2\mathbf{n} \,. \tag{5.1}$$

where a_i are real numbers and $\mathbf{n}$ belongs to $\mathcal{H}_A$. Now consider the complementary reflectance of $\mathbf{r}_1$:

$$\begin{aligned}
\tilde{\mathbf{r}}_1 &= \mathbf{w} - \mathbf{r}_1 \,. \\
&= \mathbf{w} - (a_1\mathbf{r}_2 + a_2\mathbf{n}) \,. \\
&= a_1(\mathbf{w} - \mathbf{r}_2) + [(1 - a_1)\mathbf{w} - a_2\mathbf{n}] \,. \\
&= a_1(\mathbf{w} - \mathbf{r}_2) + \mathbf{n}' \qquad \text{for } \mathbf{n}' = [(1 - a_1)\mathbf{w} - a_2\mathbf{n}] \,. \\
&= a_1\tilde{\mathbf{r}}_2 + \mathbf{n}' \,.
\end{aligned}$$

By the definition of achromatic hue, $\mathbf{n}'$ belongs to $\mathcal{H}_A$. Thus, $\tilde{\mathbf{r}}_1$ and $\tilde{\mathbf{r}}_2$ have the same hue. □

From the above theorem, it can be seen that complementary hue is uniquely determined by the constant hue set. The above definition of complementary hue for a reflectance is based on its spectral distribution. Roughly speaking, the complement of green is magenta, and yellow is cyan. Notice that this definition is different from the complement of unique hue sometimes used in psychophysical literature, where the complement of green is red, and the complement of yellow is blue. The complementary hue concept in Definition 2 is analogous to complementary hue as defined for lights within the DIN colour system.

With the concepts of constant and complementary hue in place, a constant hue space can now be defined:

Definition 4 (Constant Hue Space). *A constant hue space $\mathcal{H}_{\mathbf{r}}^{\mathcal{E}}$ is the space that contains all reflectances that have the same hue as $\mathbf{r}$ or $\tilde{\mathbf{r}}$ under a set of illuminants $\mathcal{E}$.*

At first, it seems strange that a constant hue space includes reflectances associated with the complementary hue. As discussed in Section 5.1.3 constant hue spaces defined like this are subspaces of linear reflectance spaces. This greatly simplifies our later analysis.

5.1.2 Matching Hue under an Unknown Illuminant

Like other colour attributes, the hue sensation of a reflectance is affected by the viewing illuminant. Because of surface metamerism, reflectances with the same hue for one illuminant may appear to have different hues under other illuminants. However, hue difference is not necessary. Based on our definition of constant hue, it is possible for two reflectances to have identical hue for every illuminant. This occurs if they are related to each other in one of the two following ways: their spectra differ only by a constant scale factor: or one reflectance can be obtained by mixing another with an uniformly distributed reflectance, known as ideal white spectrum $\mathbf{w}$, which is achromatic.

Thus, when $\mathbf{r}$ and $\mathbf{r}_i$ have the same hue under all illuminants, $\mathbf{r}_i$ can be expressed as

$$\mathbf{r}_i = b_1\mathbf{r} + b_2\mathbf{w} \; . \tag{5.2}$$

If each reflectance is considered as a vector in the wavelength space, the equation indicates that all reflectances in the space spanned by the vectors $\mathbf{r}$ and $\mathbf{w}$ have the same hue as $\mathbf{r}$ regardless of the viewing illuminant. A special case occurs when $b_1 = 0$. In this case, $\mathbf{r}_i = b_2\mathbf{w}$ is achromatic.

The mathematical equations described so far in this chapter apply to both physical realizable and nonrealizable reflectances. Now consider how Equation 5.2 can be used to restrict the results to physical reflectances. If the values of b_1 and b_2 are restricted to positive real numbers, reflectances that are more saturated than $\mathbf{r}$ cannot be expressed even though they have the same hue as $\mathbf{r}$. This problem can be solved by using negative values for b_2. However, this complicates the process of determining whether or not a reflectance is physically realizable. Alternatively, it

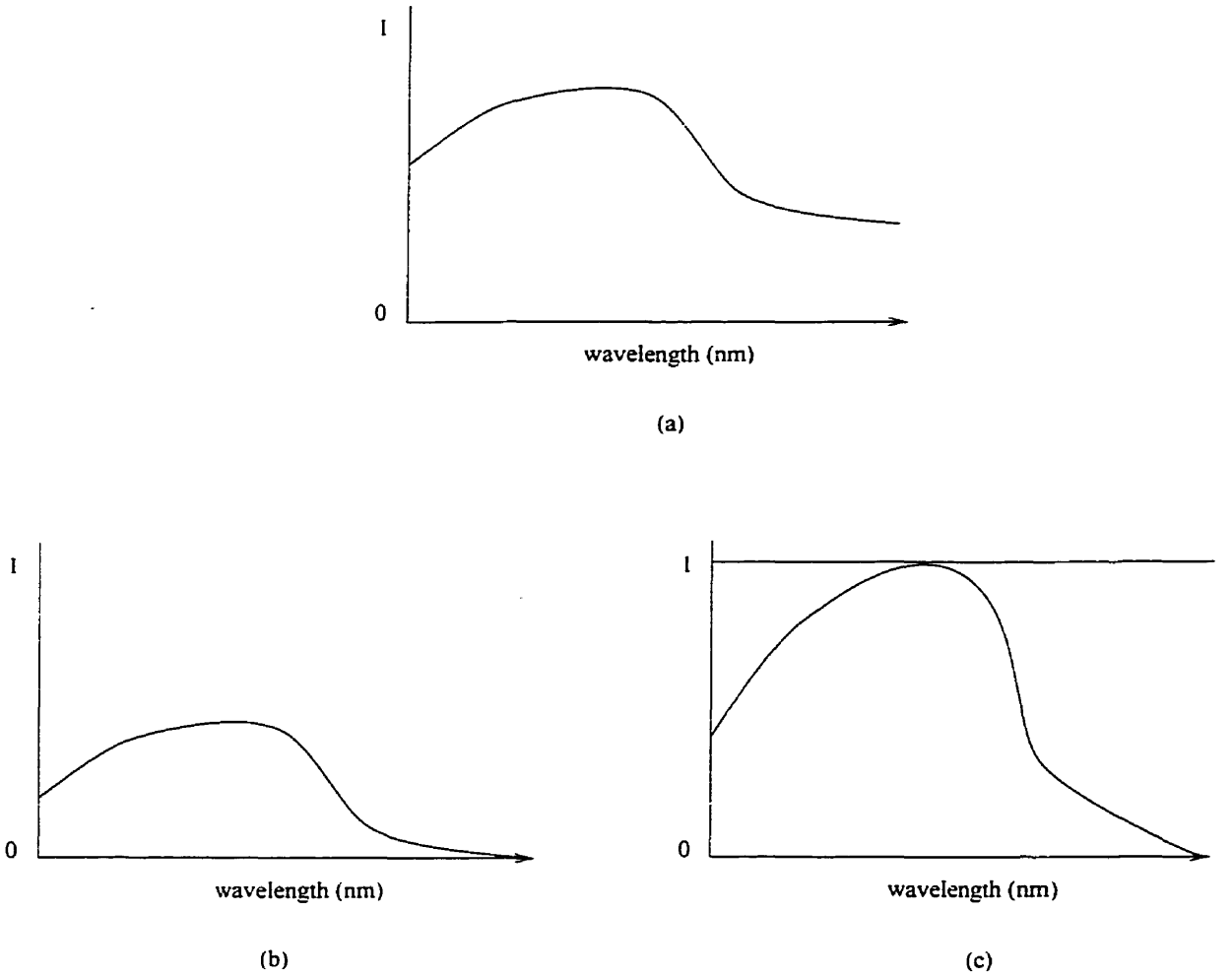


Figure 5.4: Saturated reflectance corresponding to a reflectance (shown in (a)) can be obtained by first subtracting its neutral component (b), followed by scaling (c).

is possible to use the reflectance with maximum saturation $\mathbf{r}_s$ to express all other reflectances of same hue. The variable $\mathbf{r}$ in the above equation is then replaced by $\mathbf{r}_s$ (Figure 5.4).

The spectrum of any maximally saturated reflectance $\mathbf{r}_s$ has 0 as its minimum value, and 1 as its maximum value, i.e., $\min_\lambda r_s(\lambda) = 0$ and $\max_\lambda r_s(\lambda) = 1$. $\mathbf{r}_s$ is thus determined by the following two steps:

$$\mathbf{r}_1 = \mathbf{r} - \min_\lambda r(\lambda)\ \mathbf{w}$$

and

$$\mathbf{r}_s = \frac{\mathbf{r}_1}{\max_\lambda r_1(\lambda)}$$

Note that the above procedure does not work for reflectances with spectra of which are uniformly distributed. In such cases, $\mathbf{r}_s$ is simply defined as 0.

When $\mathbf{r}$ is in a reflectance space $\mathcal{R}$, the saturated reflectance defined above is also in $\mathcal{R}$ since it is obtained by adjusting the coefficient of the first basis vector in $\mathbf{r}$, followed by scalar multiplication. Every $\mathbf{r} \in \mathcal{R}$ can be expressed as

$$\mathbf{r} = b_1\mathbf{r}_s + b_2\mathbf{w}\ .$$

Using this representation, any reflectance that is not physically realizable can easily be identified. Since every saturated reflectance has the value zero somewhere in its spectrum, any negative value in the resultant reflectance $\mathbf{r}$ is contributed by the white component. Thus, any reflectance that has negative values in its spectrum has $b_2 < 0$, and every $b_2 < 0$ has negative values and is therefore unphysical. On the other hand, since both $\mathbf{r}_s$ and $\mathbf{w}$ have the maximum value of 1 in their spectra, any $(b_1 + b_2)$ value larger than 1 results in a spectrum with values higher than 1. Consequently, any physically realizable reflectance $\mathbf{r}_p$ that has the same hue as $\mathbf{r}_s$ can be expressed as

$$\mathbf{r}_p = b_1\mathbf{r}_s + b_2\mathbf{w}\ . \tag{5.3}$$

with $0 \leq b_1, b_2 \leq 1$ and $(b_1 + b_2) \leq 1$. Conversely, when $0 \leq b_1, b_2 \leq 1$ and $(b_1 + b_2) \leq 1$, the smallest possible value in the spectrum of $\mathbf{r}_p$ is 0, and the largest

is 1. Thus, $\mathbf{r}_p$ is physical realizable. In summary, a reflectance $\mathbf{r}_p$ is physical realizable if and only if it can be expressed as Equation 5.3 with $0 \leq b_1, b_2 \leq 1$ and $(b_1 + b_2) \leq 1$.

In fact, $\mathbf{r}_p$ can also be represented in parametric form:

$$\mathbf{r}_p = r(\alpha, \beta) = \beta(\alpha \mathbf{r}_s + (1 - \alpha)\mathbf{w}) \ .$$

for $0 \leq \alpha, \beta \leq 1$. Notice that the complementary reflectance $\tilde{\mathbf{r}}_p$ of $\mathbf{r}_p$, which is defined as $\tilde{\mathbf{r}}_p = \mathbf{w} - \mathbf{r}_p$, also lies in the space spanned by $\mathbf{r}_s$ and $\mathbf{w}$. Consider the following equations:

$$\begin{aligned} \tilde{\mathbf{r}}_p &= \mathbf{w} - \mathbf{r}_p \\ &= \mathbf{w} - (b_1 \mathbf{r}_s + b_2 \mathbf{w}) \qquad \text{for } \mathbf{r}_p = b_1 \mathbf{r}_s + b_2 \mathbf{w} \\ &= -b_1 \mathbf{r}_s + (1 - b_2)\mathbf{w} \\ &= c_1 \mathbf{r}_s + c_2 \mathbf{w} \qquad \text{for } c_1 = -b_1 \quad \text{and } c_2 = 1 - b_2 \ . \end{aligned}$$

Since $0 \leq b_1, b_2 \leq 1$, it follows that $-1 \leq c_1 \leq 0$ and $0 \leq c_2 \leq 1$. Furthermore, $0 \leq c_1 + c_2 \leq 1$. The last equation shows that all reflectances with the same hue as the complement of $\mathbf{r}$ lie in the space spanned by $\mathbf{r}_s$ and $\mathbf{w}$.

With the saturated reflectance $\mathbf{r}_s$ and the ideal white reflectance $\mathbf{w}$, all reflectances that can be represented as a linear combination of $\mathbf{r}_s$ and $\mathbf{w}$ have the same hue as $\mathbf{r}_s$ or as its complement $\tilde{\mathbf{r}}_s = \mathbf{w} - \mathbf{r}_s$, regardless of the viewing illuminant. By simple linear algebra, the constant hue space of $\mathbf{r}_s$ is a 2-dimensional linear subspace in the wavelength space. The achromatic reflectance, $\mathbf{w}$, is an exception. Its constant hue space is a one dimensional space aligned with the achromatic axis.

As discussed above, the constant hue space is a 2-dimensional subspace. In fact, this is the most restricted case in the sense that the reflectances in the subspace match in hue under all viewing illuminants. This 2 dimensional space is called the universal hue plane to emphasize that it is illuminant independent. In the following sections, we will investigate what happens to the constant hue space for a specific set of illuminants.

5.1.3 Matching Hue with a Single Light Source

Most commonly used device independent colour spaces are 3-dimensional. all colours being specified with respect to a given viewing illuminant. Colours with the same hue as defined by Definition 2 are a 2-dimensional subset of the colour space. As shown in the following paragraph. the manifold of constant hue lies on a plane in any colour space that is a linear transformation of the CIEXYZ space: whereas. the manifold lies on a curved surface in nonlinear spaces. such as the CIELAB space.

In any 3-dimensional linear colour space. the set of reflectances identical in hue. with respect to the Definition 2. can be easily identified. Consider the colour point P_r. in CIEXYZ colour space. the colour of reflectance $\mathbf{r}$ under an illuminant $\mathbf{l}_i$. Any reflectance that has the same hue as $\mathbf{r}$ is a linear combination of $\mathbf{r}$ and the ideal white reflectance $\mathbf{w}$. Because tristimulus value computation is linear. the set of colour points with the same hue as P_r can be expressed as a linear combination of P_r and the white point P_w. In other words. they lie in the plane defined by the achromatic axis and the line segment connecting the colour point P_r and the ideal black point P_b in the colour space. Thus. the colours produced by illuminating a constant hue space $\mathcal{H}_r^i$ are a 2-dimensional subspace of CIEXYZ space spanned by the vectors $\overline{P_bP_r}$ and $\overline{P_bP_w}$. In effect. an illuminant imposes a single linear equation of constraint that defines the colours in a constant hue space.

Now consider the constant hue space generated by a given reflectance $\mathbf{r}_x$ in a N dimensional linear reflectance space $\mathcal{R}$. Let $\mathbf{l}_i$ be the illuminant under consideration. As described in Chapter 4. $\mathbf{r}_x$ can be divided into two components: a pseudo fundamental component $\mathbf{f}'_{x_i} \in \mathcal{F}_{\mathcal{R}_i}$ and a metameric black component $\mathbf{b}_{x_i} \in \mathcal{B}_{\mathcal{R}_i}$. Recall that $\mathcal{F}_{\mathcal{R}_i}$ is a 3-dimensional subspace that contains reflectance components that always cause non-zero colour sensation. and $\mathcal{B}_{\mathcal{R}_i}$ is a $N-3$ dimensional subspace that contains the components invisible to normal observers. For any reflectance $\mathbf{r}_y \in \mathcal{R}$ that has the same hue as $\mathbf{r}_x$ under $\mathbf{l}_i$. the pseudo fundamental component $\mathbf{f}'_{y_i} \in \mathcal{F}_{\mathcal{R}_i}$ can be expressed as

$$\mathbf{f}'_{y_i} = a_x \mathbf{f}'_{x_i} + a_w \mathbf{f}'_{w_i} .$$

where $\mathbf{f}'_{w_i}$ is the pseudo fundamental component for the ideal white reflectance, and a_x and a_w are real numbers. When $\mathbf{r}_x$ is not an achromatic colour, $\mathbf{f}'_{x_i}$ is linearly independent of $\mathbf{f}'_{w_i}$. The pseudo fundamental components of the set of reflectances with the same hue as $\mathbf{r}_x$ thus make up a 2-dimensional subspace in $\mathcal{F}_{\mathcal{R}_i}$. Any reflectance that can be expressed as a linear combination of $\mathbf{f}'_{x_i}$, $\mathbf{f}'_{w_i}$ and the basis of $\mathcal{B}_{\mathcal{R}_i}$, $\mathbf{b}_{ij}$, is in the constant hue space $\mathcal{H}^i_{r_x}$.

Since $\mathcal{B}_{\mathcal{R}_i}$ is a $N-3$ dimensional subspace and both $\mathbf{f}'_{x_i}$ and $\mathbf{f}'_{w_i}$ are orthogonal to $\mathcal{B}_{\mathcal{R}_i}$ by definition, it follows that the constant hue space in $\mathcal{R}$ under the illuminant $\mathbf{l}_i$ is a $N-1$ dimensional subspace spanned by $\mathbf{f}'_{x_i}$, $\mathbf{f}'_{w_i}$ and $\mathbf{b}_{ij}$.

To determine the constant hue space H_{x_i} for a reflectance $\mathbf{r} \in \mathcal{R}$ under an illuminant $\mathbf{l}_i$, the following procedure can be used: (1) partition $\mathcal{R}$ into the pseudo fundamental subspace $\mathcal{F}_{\mathcal{R}_i}$ and the metameric black subspace $\mathcal{B}_{\mathcal{R}_i}$ using the methods discussed in Chapter 2. (2) compute the pseudo fundamental components of $\mathbf{r}$ and ideal white reflectance $\mathbf{w}$. (3) use the pseudo fundamental components of $\mathbf{r}$, $\mathbf{w}$, and the basis of $\mathcal{B}_{\mathcal{R}_i}$ as a basis to construct the constant hue space $\mathcal{H}_{x_i}$.

5.1.4 Matching Hue with Multiple Light Sources

With a method for constructing a constant hue space for a single illuminant, the constant hue space for multiple illuminants can be easily found. Consider finding the constant hue space of $\mathbf{r}$ for illuminants $\mathbf{l}_1$ and $\mathbf{l}_2$. Let $\mathcal{H}^i_r$ be the constant hue space of $\mathbf{r}$ under illuminant $\mathbf{l}_i$. Then the set of intersection of $\mathcal{H}^1_r$ and $\mathcal{H}^2_r$ contains all reflectances that have the same hue as $\mathbf{r}$ for both $\mathbf{l}_1$ and $\mathbf{l}_2$.

The same idea can be extended to several illuminants. In that case, the constant hue space $\mathcal{H}^E_r$ is defined as

$$\mathcal{H}^E_r = \bigcap_{i=1}^{N} \mathcal{H}^i_r \,.$$

where E represents the illuminant set under consideration. Since the intersection of subspaces is always a subspace [FIS89], $\mathcal{H}^E_r$ is a subspace of $\mathcal{R}$.

In general, as the number of illuminants increases, the dimension of $\mathcal{H}_r^E$ decreases. However, when a constant hue space is constructed from the basis of a illuminant space, the dimensionality of the constant hue space is not reduced for any additional illuminant from the illuminant space. As shown by Wyszecki [WS82], daylight is well approximated as a linear combination of three spectral distributions. As a result, the constant hue space in R for these basis spectra has dimension $N-3$, which is invariant with respect to the number of daylight illuminants. In fact, when a new illuminant is added only the part of it that is linearly independent of illuminants already taken into account affects the constant hue space. Since artificial illuminants often have components independent of the daylight basis, the dimension of a constant hue space is usually decreased when artificial illuminants are added. This is one of the reasons why "daylight" is so commonly used as reference in graphic arts applications [AFR96]. Note that the lowest dimension of a constant hue space is two since both $\mathbf{r}$ and $\mathbf{w}$, which are linearly independent of each other, are always in every subspace of $\mathcal{H}_r^i$.

5.1.5 Summary

We have found a way to to determine whether two reflectances have the same hue under a given set of illuminants. Given the definition of constant hue space, the set of reflectances with same hue can be found by intersecting the constant hue space for each illuminant. Thus, it is possible for a reproduction process to retain the original hue for a set of illuminants by using reflectances from the same constant hue space.

5.2 Lightness in Reflectance Space

Lightness is a second important attribute that affects the colour appearance of an object. As discussed in Chapter 1, many gamut mapping algorithms try to preserve the lightness of original colours, while others change lightness depending on the

saturation of original colours. To accommodate these different requirements for reflective data, it is important to understand how lightness fits into a reflectance space. In this section, the subspace of constant lightness in a reflectance space is discussed. I show that chromatic and achromatic colours do not, in general, retain relative lightness under different illuminants. In fact, the rate of of lightness change due to illuminant change depends on how far a reflectance is away from the achromatic axis in the reflectance space, which is a measure of its saturation (Section 5.3).

5.2.1 Constant Lightness in Reflectance Space

The usual equations for computing the lightness of a reflectance **r** are restated below:

$$L^* = 116.0 \times (\frac{Y}{Y_n})^{\frac{1}{3}} \quad \text{for } \frac{Y}{Y_n} > 0.008856 \ . \tag{5.4}$$

$$L^* = 903.3 \times (\frac{Y}{Y_n})^{\frac{1}{3}} \quad \text{for } \frac{Y}{Y_n} \leq 0.008856 \ . \tag{5.5}$$

The luminance, Y, and the reference white luminance, Y_n, are computed using Equation 2.1:

$$Y = \sum_{i=1\cdots N} r(\lambda_i)\Phi_{\lambda_i}\bar{y}_{\lambda_i} \qquad \text{and} \qquad Y_n = \sum_{i=1\cdots N} w(\lambda_i)\Phi_{\lambda_i}\bar{y}_{\lambda_i}$$

The above equations state that the lightness of a given reflectance is proportional to the cube root of its luminance divided by the luminance of reference white. Since each reflectance is obtained by normalizing the measured spectrum with respect to the spectrum of reference white, the normalized reference white reflectance is unity across the visible spectrum, and its luminance value is constant for any given illuminant. L^* can thus be rewritten as $a \times Y^{\frac{1}{3}}$ with $a = 116.0 \times (1/Y_n)^{\frac{1}{3}}$ or $903.3 \times (1/Y_n)^{\frac{1}{3}}$, depending on the ratio of Y and Y_n. As a consequence, two reflectances that have the same luminance always have equal lightness. Since constant luminance implies constant lightness, and since luminance can be calculated linearly, luminance is used for discussing constant lightness.

The computation of luminance can be expressed in matrix form. Let Y_i be the luminance of a reflectance $\mathbf{r}$ under illuminant Φ_i. As in Chapter 2. Y_i can be expressed as

$$Y_i = \mathbf{y}^t \mathbf{E}_i \mathbf{r} = \mathbf{g}_i \cdot \mathbf{r} \,. \tag{5.6}$$

where $\mathbf{y}$ is a vector of the luminance function. $\bar{y}(\lambda_j)$. and $\mathbf{E}_i$ is the $N \times N$ diagonal matrix with $\Phi_i \lambda_j$ in its $(j.j)$ entry. and $\mathbf{g}_i = \mathbf{y}\mathbf{E}_i$ is the luminous vector of Φ_i.

When $\mathbf{g}_i$ is considered as the generator of a one dimensional subspace $\mathcal{G}_i$ in a wavelength space. the wavelength space $\mathcal{W}$ is the direct sum of $\mathcal{G}_i$ and the null space of $\mathbf{g}_i$. i.e.. $\mathcal{W} = \mathcal{G}_i \oplus \mathcal{N}(\mathbf{g}_i)$. Equation 5.6 can be considered as the projection of $\mathbf{r}$ on the subspace $\mathcal{G}_i$. Clearly. $\mathcal{N}(\mathbf{g}_i)$ is a $N-1$ dimensional subspace of $\mathcal{W}$ that contains all reflectances with zero luminance under illuminant Φ_i. The following theorem shows that the coset of $\mathbf{r} + \mathcal{N}(\mathbf{g}_i)$ defines all reflectances that have the same luminous values as $\mathbf{r}$.

Theorem 2 (Equal Luminance). *A reflectance $\mathbf{r}_i$ has the same luminance as $\mathbf{r}$ under Φ_i if and only if $\mathbf{r}_i$ is in the coset of $\mathbf{r} + \mathcal{N}(\mathbf{g}_i)$.*

Proof. Suppose $\mathbf{r}_i \in \mathbf{r} + \mathcal{N}(\mathbf{g}_i)$. Then. there exists a $\Delta\mathbf{r} \in \mathcal{N}(\mathbf{g}_i)$ such that $\mathbf{r}_i = \mathbf{r} + \Delta\mathbf{r}$. The luminance difference between $\mathbf{r}_i$ and $\mathbf{r}$ is: $\Delta Y_i = \mathbf{g}_i (\mathbf{r}_i - \mathbf{r}) = \mathbf{g}_i \cdot \Delta\mathbf{r} = 0$.

Conversely. let $\mathbf{r}_i$ be any reflectance that has the same luminance as $\mathbf{r}$. i.e.. $\Delta Y_i = 0$. For $\Delta\mathbf{r} = \mathbf{r}_i - \mathbf{r}$. $\Delta\mathbf{r}$ must be in the null space $\mathcal{N}(\mathbf{g}_i)$ since $\Delta Y_i = \mathbf{g}_i \cdot \Delta\mathbf{r} = 0$. Thus. $\mathbf{r}_i$ must be in the coset of $\mathbf{r} + \mathcal{N}(\mathbf{g}_i)$. □

In follows from the above theorem that a reflectance $\mathbf{r}^*$ equal in luminance to $\mathbf{r}$ for n different illuminants must be in every coset of $\mathbf{r} + \mathcal{N}(\mathbf{g}_j)$ for $j = 1, \ldots, n$. That is $\mathbf{r}^* \in \bigcap_j (\mathbf{r} + \mathcal{N}(\mathbf{g}_j)) = \mathbf{r} + \bigcap_j \mathcal{N}(\mathbf{g}_j)$. The elements in the the subspace of $\bigcap_j \mathcal{N}(\mathbf{g}_j)$ are those that have zero luminous values for the n illuminants. Consider the multiple illuminants version of Equation 5.6:

$$Y = \mathbf{L}\,\mathbf{A}_y \mathbf{r} = \mathbf{G}\mathbf{r} \,. \tag{5.7}$$

where $\mathbf{L}$ is the $n \times N$ matrix obtained by stacking the n row vectors of $\mathbf{l}_i$. and $\mathbf{G} = \mathbf{L}\,\mathbf{A}_y$ is the luminous matrix of the illuminants. As mentioned before. any $\mathbf{r}$ that is mapped to 0 value of Y associates with a reflectance in $\bigcap_j \mathcal{N}(\mathbf{g}_j)$. Therefore. $\mathcal{N}(\mathbf{G})$. the null space of $\mathbf{G}$. corresponds to the set of $\bigcap_j \mathcal{N}(\mathbf{g}_j)$. Once $\mathcal{N}(\mathbf{G})$ is determined. reflectances that have the same luminance as $\mathbf{r}$ can be obtained by adding $\mathbf{r}$ with any reflectance difference $\Delta\mathbf{r} \in \mathcal{N}(\mathbf{G})$.

The dimension of $\mathcal{N}(\mathbf{G})$ depends on the rank of row space of $\mathbf{G}$. $rank(\mathbf{G})$. It is equal to $N - rank(\mathbf{G})$. If. for example. the sources of illuminations for viewing are natural daylight. which can be effectively represented by a linear combination of three spectra [WS82]. $\mathcal{N}(\mathbf{G})$ is a $N - 3$ dimensional space. Generally speaking. the more illuminants used. the smaller the dimension of $\mathcal{N}(\mathbf{G})$. As a result. there are fewer reflectances that preserve luminance under all the illuminants.

5.2.2 Changes of Lightness Due to Illuminant Changes

Unless the spectral difference between two reflectances belongs to $\mathcal{N}(\mathbf{G})$. the lightness relationship between two reflectances can vary with changes of illuminant. How this happens can be understood by inspecting Figure 5.5. In the figure. the luminous vectors. g_1 and g_2. for two illuminants Φ_1 and Φ_2 are shown. These vectors make up a 2-dimensional projection space. Each point in the space corresponds to a unique luminance pair. For example. the luminance pair for $\mathbf{r}$ is (Y_{r1}, Y_{r2}). which corresponds to the projections of $\mathbf{r}$ on the luminous vector $\mathbf{g}_1$ and $\mathbf{g}_2$. respectively.

As shown in the figure. the projection space for the two illuminants is divided into four regions by the projection lines. Any reflectance that has a projected value lying below the projection line for $\mathbf{g}_1$ is smaller in luminance than $\mathbf{r}$ under Φ_1; any reflectance that has a projected value lying on the left side of the projection line for $\mathbf{g}_2$ is smaller in luminance than $\mathbf{r}$ under Φ_2. Thus. the region marked as B in the figure contains all projected reflectances that are smaller in luminance than $\mathbf{r}$ for both illuminants. Similarly. region C contains all reflectances with higher luminance than $\mathbf{r}$ for both illuminants. Reflectances in region A are higher in luminance than $\mathbf{r}$ under Φ_1. but lower than $\mathbf{r}$ under Φ_2. Reflectances associated

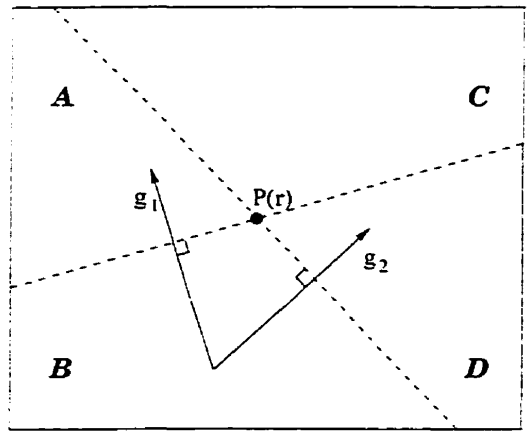


Figure 5.5: The projection space for two illuminants. g_1 and g_2. is divided into four regions which associated with certain luminance relationship with the reflectance **r**. For reflectances associated with regions B and C. the luminance relationship with **r** remains the same under both illuminants. For reflectances in regions A and D. the relative illuminance depends on the illuminant.

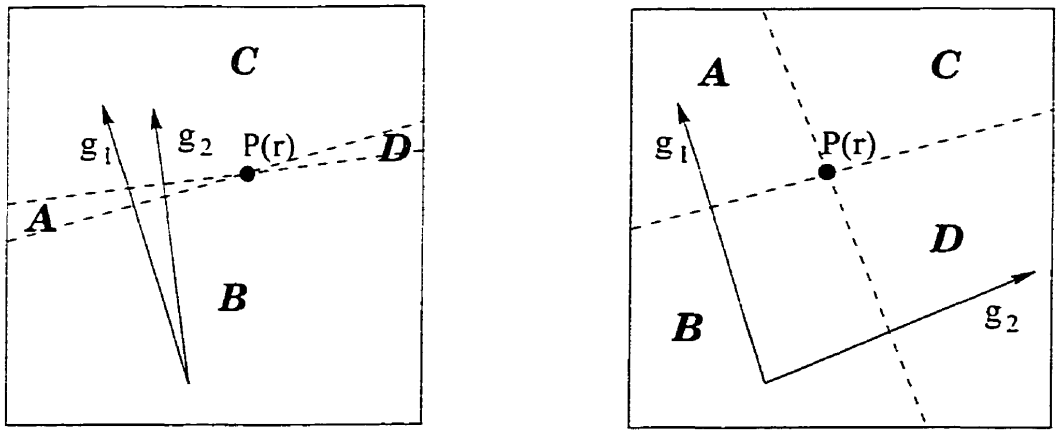


Figure 5.6: The sizes of regions A and D determine the number of useful reflectances available for colour reproduction. The two luminous vectors are very close to each other (a), which corresponds to the much smaller regions of A and D compared to those have luminous vectors separated wide apart (b).

with the region D are the reverse. In summary, for reflectances associated with regions B and C, the luminance relationship with $\mathbf{r}$ remains the same under both illuminants. However, for reflectances in regions A and D, the relative illuminance depends on the illuminant.

Changes of lightness relationships when the illuminant changes cause problems for colour reproduction. Imagine, for example, that an original has two colours, one darker than the other. The relative lightness should be preserved in the reproduction. If the lighter reproduced colour lies in region A, as defined by the darker colour, it is lighter under Φ_1. However, if the illuminant is changed to Φ_2, it is darker, which is not desired. To avoid unexpected changes of lightness, reproduction algorithms should use only those reflectances that have consistent lightness relationships for all relevant illuminants. Specifically, only reflectances that correspond to regions of B and C should be used.

	A	D50	D65	F7	H.P. Sodium
A	-	12°	16°	22°	42°
D50	12°	-	3°	17°	49°
D65	16°	3°	-	18°	51°
F7	22°	17°	18°	-	50°
HP Sodium	42°	49°	51°	50°	-

Table 5.1: Angles between luminous vectors of two light sources

The sizes of regions A and D, compared to the size of B and C, determine the number of useful reflectances available for colour reproduction. The more similar the spectra of two illuminants, the smaller the sizes of regions A and D. The measurement of closeness can be done by computing the angle between the corresponding luminous vectors. Figure 5.6(a) shows two vectors that are very close to each other, producing small regions A and D. By contrast Figure 5.6(b) shows luminous vectors widely separated. As shown in Table 5.1, luminous vectors of natural illuminants, such as D50 and D65, are close together; whereas, the luminous vectors among the artificial illuminants are far apart. Thus, when the reproduction is to be viewed under artificial lighting, great care must be taken in selecting the reproduction reflectances.

5.2.3 Lightness Changes for Chromatic Colours

From Equation 5.6, it is easy to see that the ratio of Y/Y_n for uniformly distributed reflectances remains constant when the illuminant changes. As a result, the lightness of these reflectances are constant for all illuminants. However, the lightnesses of other reflectances vary with illuminant.

The rate of change of lightness depends on its relative position with respect to

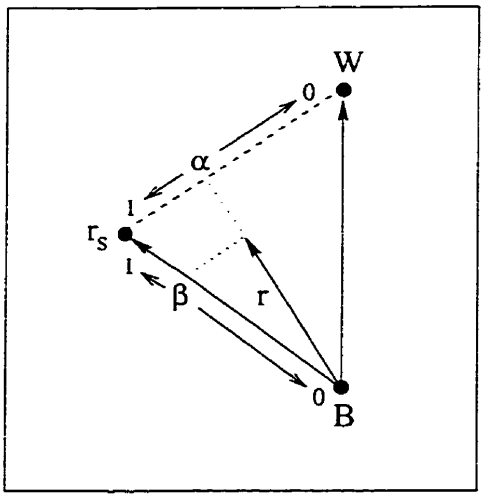


Figure 5.7: The changing of illuminant has different impact on luminance for different reflectances depending on their relative location in its universal hue plane. The luminance of the most saturated reflectance ($\alpha \rightarrow 1$) in a constant hue plane is more sensitive to illuminant change, while the luminance of the desaturated reflectances ($\alpha \rightarrow 0$) are less sensitive to illuminant change.

the ideal white $\mathbf{w}$ and the most saturated reflectance $\mathbf{r}_s$ in the universal hue plane, which was defined in the Section 5.1.2. Now consider the change of luminance of a reflectance $\mathbf{r}$. Assume the luminance of $\mathbf{r}_s$ to be Y_{s1} and Y_{s2} under illuminants Φ_1 and Φ_2, respectively. $\mathbf{r}$ can be expressed as a linear combination of $\mathbf{r}_s$ and $\mathbf{w}$. Its luminous values, Y_{r1} and Y_{r2}, are the same linear combination of Y_{s1} and Y_{n1} under Φ_1, and of Y_{s2} and Y_{n2} under Φ_2. When $\mathbf{r}$ is expressed as $\mathbf{r} = \beta(\alpha\mathbf{r}_s + (1-\alpha)\mathbf{w})$, for $0 \leq \beta, \alpha \leq 1$ (Figure 5.7), the change of luminous value is

$$\begin{aligned}
\Delta Y_r &= \mathbf{g}_1\mathbf{r} - \mathbf{g}_2\mathbf{r} \\
&= \mathbf{g}_1[\beta(\alpha\mathbf{r}_s + (1-\alpha)\mathbf{w})] - \mathbf{g}_2[\beta(\alpha\mathbf{r}_s + (1-\alpha)\mathbf{w})] \\
&= \alpha\beta(\mathbf{g}_1\mathbf{r}_s - \mathbf{g}_2\mathbf{r}_s) + \beta(1-\alpha)(\mathbf{g}_1 - \mathbf{g}_2)\mathbf{w} \\
&= \alpha\beta(Y_{s1} - Y_{s2}) + \beta(1-\alpha)\Delta Y_n \\
&= \alpha\beta\Delta Y_s + \beta(1-\alpha)\Delta Y_n \\
&= \beta(\alpha\Delta Y_s + (1-\alpha)\Delta Y_n)
\end{aligned}$$

The above equation shows that changing the illuminant has different impacts on the luminance of different reflectances, and that the difference depends on relative location in the universal hue plane. For a fixed α value, ΔY_r increases as the value of β increases. Thus, larger changes in luminance are expected for reflectances with larger β values. In other words, larger changes in lightness are expected for reflectances with larger β values.

For a fixed β value, the α value can be viewed as varying the ratio of luminance change of the saturated reflectance and of the ideal white reflectance. The value of ΔY_n reflects the difference in luminance between the two illuminants. We want to factor out this effect because it is common to the whole image. We adjust the brightness of the second illuminant until $\Delta Y_n = 0$. Then the change of lightness due to the change of illuminant is larger for reflectances with larger α values, in which the saturated reflectance has larger influence. In summary, the most saturated reflectance in a constant hue plane always has the largest lightness change owing to the change of illuminant.

5.2.4 Summary

In brief. it is possible to retain the luminance of a reflectance in the reproduction process. However. if maintaining luminance is not wanted. care must be taken to ensure the relationship between the original and reproduction luminances is consistent under the possible viewing illuminants. As shown in the previous section. luminance changes due to change of illuminant are varied across a constant hue plane. This may explain why maintaining lightness is not as important as hue. which is changed in the same direction as illuminant changes.

5.3 Saturation in Reflectance Space

Saturation is the last colour attribute that affects colour appearance. Even though saturation is not as important as hue or lightness for colour reproduction. it still has a major impact on the quality of a reproduction. This section describes the relationship between the spectrum of a reflectance and its saturation. and studies how saturation changes within a hue plane.

5.3.1 Reflectance and Saturation

Saturation describes the colorfulness of a colour. Basically the more achromatic component a reflectance has the less saturated it is. The Commission Internationale de l'Éclairage defines an objective function for saturation in the CIELUV space as follows:

$$s_{uv} = 13 \left[(u' - u'_n)^2 + (v' - v'_n)^2 \right]^{\frac{1}{2}} ,$$

where

$$\begin{aligned} u' &= 4\,X/(X + 15Y + 3Z) , \\ v' &= 9\,Y/(X + 15Y + 3Z) , \end{aligned}$$

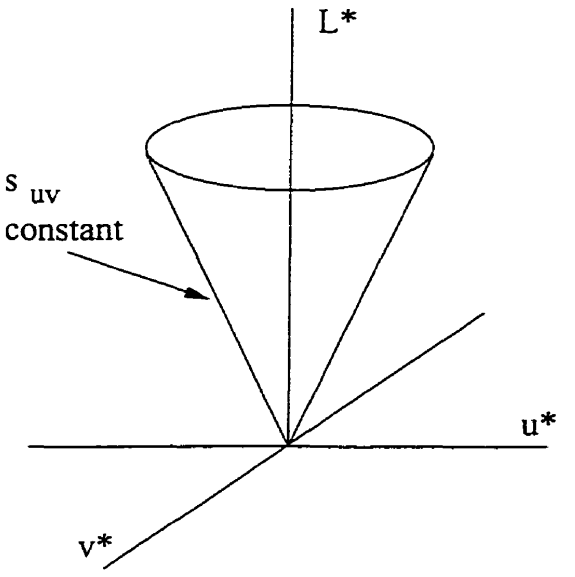


Figure 5.8: The chromaticity diagram of CIELUV. Saturation increases as colour points are located further away from the lightness axis.

with X, Y, Z the tristimulus values of the target colour, and u'_n and v'_n the value of u' and v' of the reference white, respectively. As shown in Figure 5.8, saturation increases as colour points are located farther away from the lightness axis.

To determine how the position of a reflectance **r** on a constant hue plane relates to its saturation, s_{uv}, we express **r** as a linear combination of the ideal white reflectance **w** and the most saturated reflectance $\mathbf{r}_s$ of the plane (Equation 5.3). Now consider the set of reflectances with a fixed α value. Let (s_X, s_Y, s_Z) and (w_X, w_Y, w_Z) be the CIE XYZ values for $\mathbf{r}_s$ and **w**, respectively. For any reflectance $\mathbf{r} = \beta\,(\,\alpha\mathbf{r}_s + (1-\alpha)\,\mathbf{w})$, the tristimulus values (r_X, r_Y, r_Z) are

$$\begin{aligned} r_X &= \beta\,(\,\alpha s_X + (1-\alpha)\,w_X) \\ r_Y &= \beta\,(\,\alpha s_Y + (1-\alpha)\,w_Y) \\ r_Z &= \beta\,(\,\alpha s_Z + (1-\alpha)\,w_Z)\,. \end{aligned}$$

Let $r_{XYZ} = r_X + 15\,r_Y + 3\,r_Z$ and $w_{XYZ} = w_X + 15\,w_Y + 3\,w_Z$. The value of $(\,u'_r - u'_n\,)$ is

$$u'_r - u'_n = \frac{4\,r_X}{r_{XYZ}} - \frac{4\,w_X}{w_{XYZ}} \tag{5.8}$$

$$= 4\left[\frac{\beta\,(\,\alpha s_X + (1-\alpha)\,w_X)}{\beta\,(\,\alpha s_{XYZ} + (1-\alpha)\,w_{XYZ})} - \frac{w_X}{w_{XYZ}}\right] \tag{5.9}$$

$$= 4\left[\frac{(\,\alpha s_X + (1-\alpha)\,w_X)}{(\,\alpha s_{XYZ} + (1-\alpha)\,w_{XYZ})} - \frac{w_X}{w_{XYZ}}\right]. \tag{5.10}$$

and the value of $(\,v'_r - v'_n\,)$ is

$$v'_r - v'_n = 9\left[\frac{(\,\alpha s_Y + (1-\alpha)\,w_Y)}{(\,\alpha s_{XYZ} + (1-\alpha)\,w_{XYZ})} - \frac{w_Y}{w_{XYZ}}\right]. \tag{5.11}$$

The above equations show that the values of $(u'_r - u'_n)$ and $(v'_r - v'_n)$ are independent of the β value. Consequently, saturation of a reflectance is not affected by the changes of β value. In other words, the points that lie on a line emerging from the null point in a reflectance space, which all have a constant α value, always define a set of reflectances having constant saturation (Figure 5.7). As shown in the equations, reflectance saturation is determined by the value of α.

Equation 5.8 and Equation 5.11 can be viewed as a projection from CIEXYZ to CIELUV spaces. The projection is monotonic in the sense that the values of $(u'_r - u'_n)$ and $(v'_r - v'_n)$ increase as α increases. This feature is often found in a trichromatic colour space [Hun95].

5.3.2 Summary

Saturation varies with α. but remains constant as β changes. As the result. reflectance has high saturation when it is located farther away from the ideal white axis within a constant hue plane. This topological property for saturation is commonly found in other colour spaces. Thus. ideas about how to handle saturation for conventional colour space can be adopted easily in a reflectance space.

5.4 Possible Mapping Methods

From the discussion of sections 5.1 to 5.3. we see that developing a satisfactory gamut mapping algorithm for reflectance data is possible. but nontrivial. In this section. two mapping methods are discussed to illustrate how reflectance data can be used in the colour reproduction process. Both methods maintain hue. which is the most critical colour attribute for colour reproduction.

5.4.1 Hue Mapping that Minimizes Surface Metamerism

The basic idea of this approach is to choose the reflectance that most closely matches the original reflectance spectrum while maintaining its hue.

As shown in Section 5.1. those reflectances that have the same hue under a set of given illuminants are a subspace of the reflectance space. This subspace is easily found once the fundamental component of the original reflectance for each illuminant is known. The original reflectance is then projected orthogonally to the

subspace. The result of projection is the reflectance that has the minimum mean squared spectral errors. This reflectance should be used to reproduce the original reflectance.

This approach preserves hue. However, the relative lightness and saturation among the reflectances may not be maintained since closeness of spectral reflectance does not guarantee identity of lightness and saturation.

5.4.2 Barycentric Mapping on the Universal Hue Plane

An alternative approach that better preserves the relative lightness and saturation uses barycentric coordinates. To map a given reflectance into a reflectance space, the barycentric coordinates of the reflectance are defined with respect to a triangle, the vertices of which are defined by the ideal white and black points and the point of the most saturated reflectance in the corresponding hue plane. A corresponding target triangle lying on the hue plane with the same hue as the original in the output reflectance space is also found. The same barycentric coordinates define a point in the target triangle to reproduce the original reflectance.

This mapping is similar to the triangular gamut mapping defined by Morovic and Luo [ML97] except that the mapping is applied in reflectance space instead of a trichromatic space. This approach is able to maintain relative lightness and saturation, and also to maximize luminance contrast since the whole luminance output range is used. In addition, saturation is maximized in the reproduction since reflectances lying on the gamut boundary are mapped onto the boundary of the output gamut. However, the possibility that lightness will be altered excessively, noted by Morovic and Luo, exists when the shapes of input and output gamuts are very different.

5.5 Conclusion

To develop a colour reproduction process based on perceptual colour attributes in reflectance space. the relationships between reflectance and colour attributes must be understood. Since colour attributes are affected by the viewing illuminant. the colour attribute of a reflectance viewed under several illuminants is not unique.

Fortunately. in most cases the absolute values of the colour attributes are less important for the colour reproduction process than are relative values. For example. the exact perceived hue of a reflectance does not have to be known in order to find reflectances with the same hue under several different illuminants: the hue subspace in reflectance space identifies them easily.

This chapter identifies how to determine the constant hue subspace. and the coset space for reflectances that are identical in lightness. Thus. reproduction algorithms that preserve hue and lightness are possible in reflectance space. Furthermore. the distribution of saturation within constant hue planes in reflectance space is similar to that of other colour spaces. Since the topological properties of the colour attributes are very similar in reflectance spaces and in illuminant dependent colour spaces. conventional algorithms that operate on a constant hue plane in trichromatic spaces are easily extended to reflectance space.

Chapter 6

Device Control Values for Reflective Images

Once the output colours are determined, a backward transformation is needed to calculate corresponding device control values. For reflective images, pixels are represented in reflectance coordinates. The domain of the backward transformation is a reflectance space rather than the usual CIE colour space. Except for operating in a different space, backward transformations for reflective images and for normal colour images are very similar. Thus, current techniques for backward transformation are expected to perform well for reflective images.

As mentioned in Chapter 2, either model based or colour lookup table (CLUT) approaches can be used to determine the relationship between control values and output colours. If a mathematical model is available for a device, it may be possible to determine control values from the inverse of the model; otherwise, control values are approximated by interpolating data in a CLUT.

Since the backward transformation has to be performed for every pixel while printing, it must be efficient for any practical application. Because of its high complexity, the model-based approach is seldom used for the backward transformation in practice; instead, the CLUT approach, which provides high speed performance,

is the most common choice.

Speed and accuracy are the two most important factors for developing an effective backward transformation. Unfortunately, these two factors are in conflict with one another. This conflict is exacerbated further for reflective image reproduction because images are represented in a higher dimensional space. For reflective image reproduction to be possible in practice, further improvements in backward transformation technique are needed. To address this problem, a new cell-finding algorithm based on a divide-and-conquer strategy is developed in this section. It finds the correct cell using an amount of processing that is logarithmic in the number of CLUT cells. This performance does not depend on evenly spaced samples in a reflectance space. Given this performance, the size of the CLUT can be increased. As a result, higher accuracy conversion using this search algorithm is possible.

In this chapter, I describe the concepts of backward transformation using a CLUT. The relationship between accuracy and speed is examined. In the later sections, the newly developed algorithm is described. An analysis of its performance is also presented.

6.1 Backward Transformations Using Colour Lookup Tables

As for the forward transformation, CLUT-based backward transformations determine the device control values of a given colour by first locating the cell that encloses the colour point. The corresponding cell in the device space, identified through the CLUT, is then used to approximate the target control values. The operation that locates the enclosing cell is referred to as *extraction*; approximation is done by *interpolation*.

Extraction and *interpolation* are the two critical operations that determine the performance of a backward transformation. Specifically, extraction most influences speed, while interpolation most influences accuracy. However, the two operations

are related in the sense that they are both affected by the size of the CLUT. A large CLUT allows data to be approximated more accurately by the interpolation step. but a longer time is needed to locate the cell during extraction. In contrast. a small CLUT allows fast extraction but poor interpolation. Backward transformation can be improved by increasing the speed of extraction or the accuracy of interpolation. This section compares different ways of doing these two operations. emphasizing their effect on the performance of backward transformation.

6.1.1 Extraction

The sole purpose of extraction is identification of the vertices of an enclosing cell in a CLUT. Thus. speed is paramount for extraction. Data can be found in a CLUT by searching or indexing. The performance of either process depends strongly the structure of the sampling distribution used to construct the CLUT. In general. locating an individual point from a well structured sampling distribution is much easier than from an unstructured one.

CLUT sampling distributions with N sample points in a d-dimensional colour space can be classified into the following five categories.

Uniform Sample points are equally spaced in each dimension of a colour space. $N = n_1 \times n_2 \times \cdots \times n_d \approx n^d$. where n_i is the number of sampling points in dimension i. and n is the average number of sampling points in each dimension.

Orthogonal Sampling locations are the cartesian products of the nonevenly distributed spacing in each dimension of a colour space. The distribution can be visualized as a set of parallel planes orthogonal to each axis of a colour space. As for the uniform distribution. $N \approx n^d$.

Pseudo-uniform Sample points are obtained from a *uniform sampling* in device coordinates. The corresponding distribution in the colour space is not regular. but systematically deviates from a set of parallel planes. With n the average number of sampling points in each dimension. $N \approx n^d$.

Pseudo-orthogonal Sample points are obtained from an *orthogonal sampling* in device coordinates. The corresponding distribution in the colour space is not regular, but systematically deviates from a set of parallel planes. Similar to a pseudo-uniform distribution. $N \approx n^d$.

Random Sample points are not structured, either in device coordinates or in colour space. The average number of sampling points in each dimension, n, is approximately equal to $\sqrt[d]{N}$.

For uniform CLUT, indexing locates the entry of a given data point. By stripping off the low order bits of the data values in each dimension, the position of the corresponding entry is identified directly. Since no searching is done, the processing time is independent of the size of the CLUT. The computational cost, which depends only on the dimensionality of the colour space, is $O(d)$. With this regular structure, a large CLUT can be used to improve accuracy of interpolation without affecting the speed of extraction.

For orthogonal CLUTs, a series of comparisons is performed, one series per dimension, to determine the range in which a given point lies. The set of comparisons identifies the cell. With binary search, the total number of comparisons needed is $d\log(n)$. Since the number of comparisons increases with the number sample points in each dimension, the performance decreases as the size of CLUT increases.

For pseudo-uniform and pseudo-orthogonal distributions, the CLUT is created by measuring a set of sample data regularly spaced in device coordinates. Thus forward transformations are easily made efficient. As for the random CLUTs, however, the corresponding distribution in colour space is unstructured. Thus, it is difficult to obtain high speed extraction for backward transformations. To solve this problem, remapping is usually performed to construct a more structured CLUT. However, the accuracy of this approach is limited by cumulative approximation errors: one from measurement errors when constructing the CLUT, the other from interpolating colour values within a cell. Thus, a fast searching algorithm that does not compromise accuracy is often needed.

Several techniques have been proposed to speed up extraction. One widely used method is bounding box detection. the same idea that speeds up ray tracing in computer graphics. The idea is to enclose each cell by a regularly shaped polyhedron for fast detection of enclosure [NKP92. Hun93]. For example. when a rectangular bounding box is used. points that are not located between three sets of parallel planes associated with the bounding box of a cell are simply rejected. after which a further test for cell enclosure is performed. Because most bounding boxes do not contain the target point. the simplified enclosure test provides better performance by reducing the number of costly operations needed to determine point enclosure in an irregularly shaped cell. However. the need to check every individual bounding box for every pixel is still very expensive.

Improvement is possible if each cell is a simplex. an $(m+1)$-vertex polytope in a m dimensional space. Using Delaunay tetrahedrization. Bell and Cowan [BC93] developed a walking algorithm that can find the enclosing tetrahedron much faster. Any point outside a given tetrahedron has at least one negative barycentric coordinate when represented in terms of the four vertices. Based on this observation. after finding the point is not inside the current tetrahedron. the algorithm checks the tetrahedron that shares the facet with the most negative coordinate. The process finds the enclosing tetrahedron by walking through the tetrahedra until all barycentric coordinates are positive. Bell and Cowan showed that on average it needs to traverse $O(n)$ tetrahedra. where n is the number sample points on each axis. They also discussed using a binary space-partitioning algorithm to locate the enclosing tetrahedron. but the computation cost was higher than for the walking algorithm. Even with these fast algorithms. the computational cost for extraction from an unstructured sample distribution is too high.

6.1.2 Interpolation

After the cell that contains the target point is located. interpolation is performed to approximate the desired control values. Interpolation approximates between the sample points. Speed and accuracy are the two major criterion for evaluating

interpolation technique in a colour reproduction process. Of linear and nonlinear interpolation. linear interpolation provides faster performance. whereas nonlinear interpolation provides better accuracy.

Because of its simple implementation and excellent performance. linear interpolation is widely used. Many researchers have developed linear interpolation techniques specifically for colour reproduction. All algorithms are multiple applications of one dimensional linear interpolation. These techniques can be differentiated by the way the sample points are chosen for computing a target value. i.e.. how cells are constructed for interpolation.

When the entire 3D device gamut is made up of cubic cells. the eight corner points are used as input for trilinear interpolation [Kan96]. Four linear interpolations are first applied to determine four interpolated points along the parallel edges of the cube. then two linear interpolations are applied on these. using two pairs of edge points to locate another two points on the opposite faces of the cube. The target point is then approximated by linearly interpolation of the last two interpolated points (Figure 6.1(a)).

Other interpolation techniques [Pyg74. SI78. Fla82. KFK92] use cells of prisms or tetrahedra. Six and four lattice points form a cell for prismatic and tetrahedral interpolation. respectively. The cells are created by slicing a cubic cell into several polyhedra. For prismatic interpolation. a cube is first sliced into two halves to obtain two triangular prisms. interpolation is then applied to whichever prism contains the target point. Linear interpolations are performed along two axes to obtain a point on each triangular face. The target point is obtained by the linear interpolation of these two points (Figure 6.1(b)).

For tetrahedral interpolation. a cubic cell is sliced into six tetrahedra. Since the tetrahedron is the 3-D simplex. its interpolation scheme amounts to determining barycentric coordinates of the target point within the tetrahedron. Using the following equation the target point P_t is represented by a linear combination of the four vertices:

$$P_t = a_1 v_1 + a_2 v_2 + a_3 v_3 + a_4 v_4 \ .$$

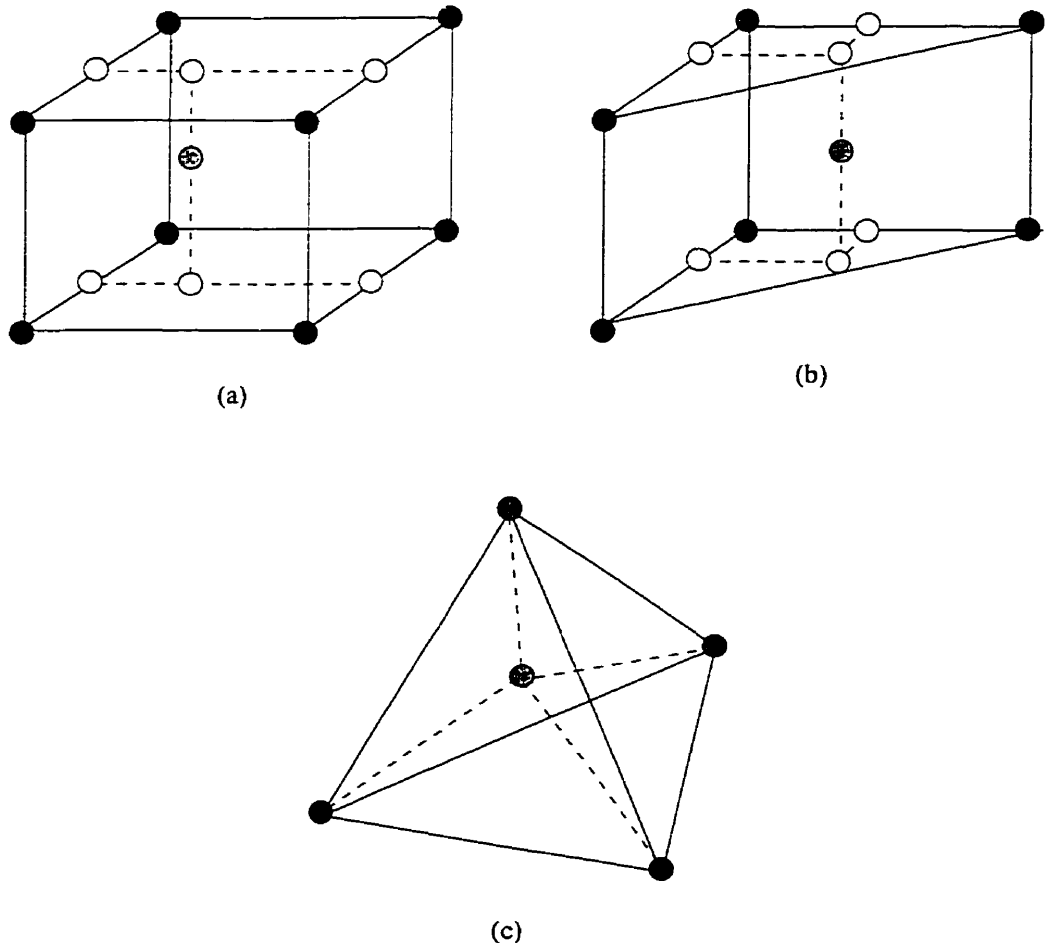


Figure 6.1: (a) Trilinear interpolation: (b) prism interpolation: and (c) tetrahedral interpolation are shown in the figure. Sample points are represented in dark circles. the intermediate interpolated points are in white circles. and the source points are in shaded circles.

where a_i are positive coefficients, with $\sum_i a_i = 1$. Compared to other geometric interpolations, tetrahedral interpolation is the least expensive to compute (Figure 6.1(c)).

The major challenge for linear interpolation is ensuring that interpolation errors are low enough to produce satisfactory accuracy. The success of linear interpolation relies heavily on the assumption that surfaces in a device gamut are well approximated by linear surfaces. When this condition is not met, interpolation errors can be high. When non-linearity is present, the sample points in the CLUT must be dense to avoid excessive errors. Usually this is not possible without excessive measurement cost. To solve this problem, nonlinear interpolation can be used.

As discussed in Chapter 3, nonlinear interpolation generally performs much better for colour devices with nonlinear transfer functions. To improve efficiency, however, nonlinear interpolation is not applied directly to sample data during printing. Instead, a CLUT large enough for linear interpolation is constructed by interpolating the sample points nonlinearly.

The procedure is the following.

1. Measure a small number of sample points, usually evenly distributed in the device space.
2. Choose a suitable nonlinear function to model the transfer function of a device.
3. Determine the parameters of the function from the sample point values.
4. Use the function to compute the values of extra points that lie between the sample points.
5. Use these extra points to build the large CLUT.

Step (3) is a data fitting process that determines a set of parameters of the function chosen in step (2). Many nonlinear functions have been used to approximate the transfer function, including Bell functions [RK93], third-order polynomials [Hun93], and cubic spline functions [BC94]. These nonlinear functions can

produce better results than simple linear interpolation methods. However, there are no guidelines for determining which nonlinear function should be used for a given device. Further research is needed in this area.

6.2 A Fast Extraction Algorithm for the Backward Transformation

Except uniform CLUTs, the processing time required for the backward transformation is often directly proportional to the size of a CLUT. With a large CLUT, better accuracy can be obtained from linear interpolation, but the time required for extraction is longer; with a smaller CLUT, extraction time decreases at the cost of worse accuracy. This tradeoff poses a constraint for the speed of extraction at a given level of accuracy. For high dimensional colour reproduction to be practical, this constraint must be loosened. To achieve this, a new searching algorithm was developed [CC97]. This algorithm provides high speed searching, with cost roughly logarithmic in the size of CLUT. As a result, high speed performance can be obtained without sacrificing accuracy.

6.2.1 Basic Idea

The proposed algorithm provides a fast colour transformation method for all colour reproduction processes. For illustration purpose, a CMY device space and the CIELAB colour space are used to describe it. The problem is to determine the CMY value corresponding to a given L*a*b* value within the printer gamut. It assumes only that the forward transformation from a CMY value to its L*a*b* value is cheap to evaluate. As discussed earlier, this is easily accomplished by using a uniform CLUT followed by interpolation.

The proposed extraction algorithm uses a divide-and-conquer approach, analogously to binary subdivision. Initially, the algorithm uses the minimum and max-

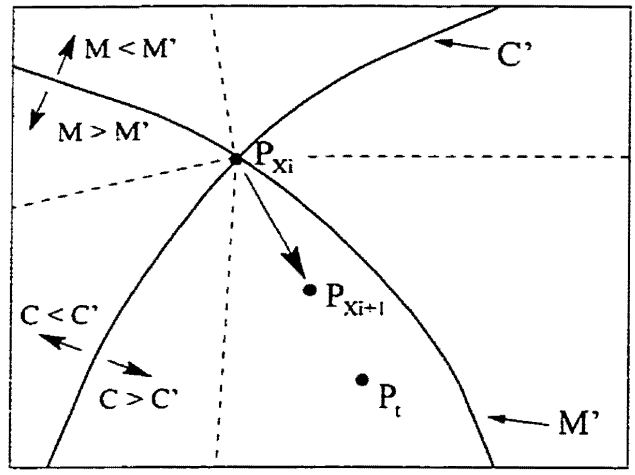


Figure 6.2: Regions defined by the contour curves of C_0 and M_0. Each region has a well-determined relationship on one of the CMY coordinates. The current point $(CMY)_0$ advances to the next point $(CMY)_1$ based on the region in which the target L*a*b* value locates.

imum colour values as the lower and upper bound for the colour components of the target CMY value. It starts with an initial CMY value, $(CMY)_0$, for which L*a*b* has been measured to have the value $(Lab)_0$. In the neighbourhood of $(Lab)_0$ the entire L*a*b* space is partitioned into regions, with each region having a well-determined relationship to one of the CMY coordinates. For example, one region has $C > C_0$, another has $M > M_0$, and so on (Figure 6.2). The colour space is completely filled by the partition, which is approximated using only local information so that partitioning can be performed in constant time. Depending on which partition contains the desired L*a*b* value, one of the colour components of $(CMY)_0$ becomes the new lower or upper bound for the target CMY value. For instance, if the desired L*a*b* value lies in a region that has a smaller C value, then C_0 is the new upper bound for the C component while the bounds on the M and Y components do not change. The mid-point of the current lower and upper bounds of each colour component is chosen to be the updated CMY value, $(CMY)_1$. This value has an improved estimate for whichever of the CMY values was indicated by the partition. This process continues until the point that has the closest CMY value related to the desired L*a*b* colour has been identified. Interpolation is then used to find the correct CMY value within the cell.

As described above, there are three basic operations in each iteration, namely, gamut partition, region detection, and point advancement. These operations are discussed in detail in the next few sections.

6.2.2 Gamut Partition

Since fast convergence depends on effective region subdivision, a robust partition method is essential. The following partition method is based on geometric features of printer gamuts in the CIELAB space.

Consider the set of CMY values having a specified value of a particular colour component, say C. These colour values define a plane in CMY space, which corresponds to a smooth continuous surface (iso-C-surface) in the CIELAB space. As the values of the M and Y components change across this surface, their L*a*b*

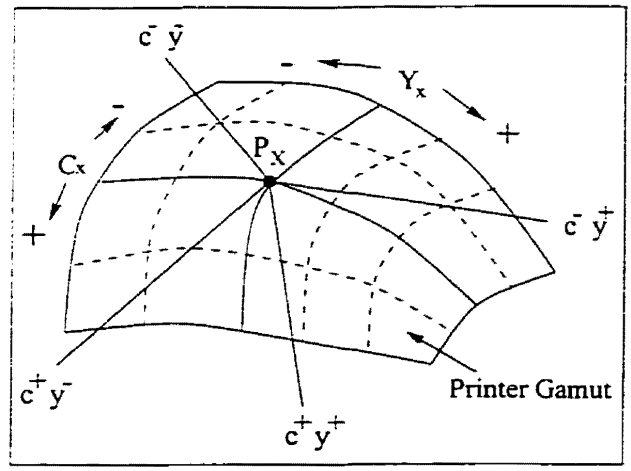


Figure 6.3: Partition of 2D printer gamut. Four boundary lines divide the 2D printer gamut into four regions. Each region is defined such that it corresponds to a portion of the gamut that has either a smaller or a larger amount of one of the colour components than does P_x.

values vary continuously. The curvatures of such surfaces are usually small but not negligible. This assumption, which holds for well-behaved printers, underpins the partition method described below.

To simplify the description of the partition procedure, let us first consider the 2 dimensional case. Imagine that there is a 2D device independent colour space, similar to the CIELAB space, covering all the colours generated by the two inks, for example cyan (C) and yellow (Y). Any printer using only these two inks has a gamut that is a closed region in the colour space. Figure 6.3 shows a possible printer gamut. Each curve in the figure is a contour curve for a constant C or Y value. Now consider a point P_x inside the printer gamut, with C_x and Y_x its C and Y components. The printer gamut can be divided into four regions based on the location of P_x. Each region contains points that have a fixed relationship with one of the colour components of P_x. One such partition is shown in Figure 6.3, in which

the regions are defined by four boundary lines c^-y^-, c^-y^+, c^+y^-, and c^+y^+. The points inside the region bounded by the lines c^-y^- and c^-y^+ have C smaller than C_x, while the points inside the region bounded by the c^+y^+ and c^-y^+ have Y larger than Y_x, and so on. In general, each region corresponds to a portion of the gamut that has either a smaller or a larger amount of one of the colour components than does P_x. A partition is not unique, but every partition must meet the following two conditions: (1) the boundary lines do not cross the contours defined by $C = C_x$ and $Y = Y_x$. (2) only two boundary lines lie on the same side of the region separated by the C_x or Y_x contour curves. The first condition ensures that all points from the same side of a boundary line have the same relationship with one of the colour components of P_x, and the second condition ensures that each one of four gamut regions bounded by the two contour curves has one and only one boundary line in it. As a result, the segment of contour line that runs from P_x to the gamut border is inside a single region.

Applying the above criteria strictly, it is potentially costly to define a suitable set of boundary lines. A better alternative approximates the boundary lines on local values of P_x. Because printers use inks with chromaticities that are far apart in the colour space, the contour curves of different inks are almost perpendicular to each other in the region close to P_x. If the lines that evenly divide the cross contour angles are chosen to be the boundary lines, the criteria are met locally. The local region is very large if the curvature of the contours is small, as it normally is. (Figure 6.4)

To obtain the angles of two cross contour curves, the tangents of the contours at the cross point have to be computed. When a precise mathematical model of the printer is not available, it is impossible to compute the tangents in general. And even when a model is available precise tangent computation is costly. However, tangent-defined boundary lines are not the only way to partition the gamut; close approximations to them serve equally well. One workable solution uses the four lines that connect the current P_x point to the point $(C_x - \Delta U, Y_x - \Delta U)$, $(C_x - \Delta U, Y_x + \Delta U)$, $(C_x + \Delta U, Y_x - \Delta U)$ and $(C_x + \Delta U, Y_x - \Delta U)$, respectively, where ΔU is a fixed value.

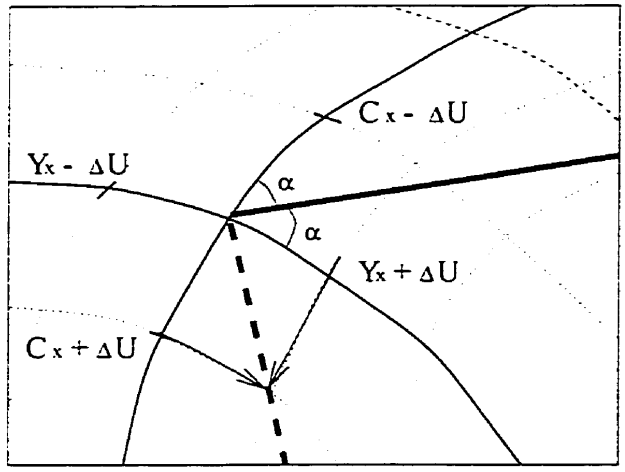


Figure 6.4: Boundary lines that partition the 2D printer gamut. Lines (thick solid line) that evenly divide the cross contour angles are good candidates for boundary lines. These lines are inexpensively approximated by joining the current point with a point offset by a fixed amount for each component (dash line). The thin solid and dotted lines represent the lines for iso-surfaces.

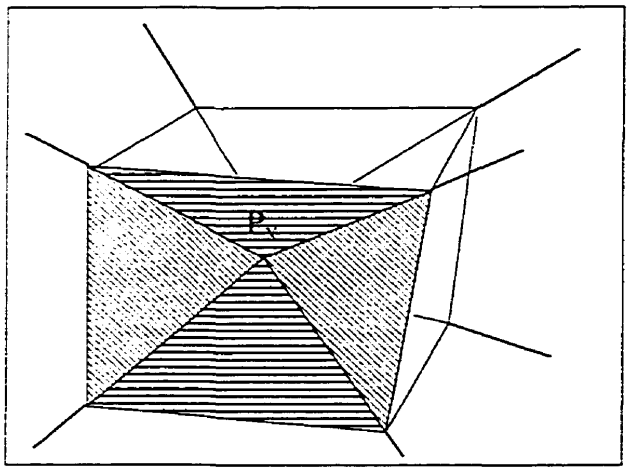


Figure 6.5: Boundary planes of gamut partition in 3D colour space. Similar to the 2D case, the boundary planes defined by two neighbouring lines which connecting the current point P_x to any two points in the set $\{(C_x \pm \Delta U, M_x \pm \Delta U, Y_x \pm \Delta U)\}$ that differ by only one component.

Partitioning the printer gamut in the 3D CIELAB space is analogous to the 2D case described above. Instead of four boundary lines, twelve boundary planes are using to partition the gamut. Each region in the gamut is confined by four planes (Figure 6.5). The criteria for choosing these planes is the following: (1) the boundary planes do not cross any iso-surface of the colour components of P_x, and (2) four and only four planes lie on the same side of the region separated by each iso-surfaces. As for the 2D case, one possible way to partition the gamut is to use the boundary planes defined by two neighbouring lines which connecting the current point P_x to pair of points in the set $\{(C_x \pm \Delta U, M_x \pm \Delta U, Y_x \pm \Delta U)\}$ that differ by only one component. For example, one boundary plane is defined by the line connecting P_x to $(C_x - \Delta U, M_x - \Delta U, Y_x - \Delta U)$ and the line connecting P_x to $(C_x - \Delta U, M_x - \Delta U, Y_x + \Delta U)$. With the set of eight points $\{(C_x \pm \Delta U, M_x \pm \Delta U, Y_x \pm \Delta U)\}$, twelve planes are defined to partition the gamut in the CIELAB space. If P_x lies on the boundary of gamut, the outside gamut boundary planes can be obtained by extrapolating the inside gamut planes through P_x.

The value chosen for ΔU is not critical. In practice, we choose for ΔU the interval used to build the CLUT. The boundary planes defined based on this ΔU value accurately partition the gamut for any colour point P_x.

6.2.3 Region Detection

Once the regions are defined it is necessary to find out which region contains the target point P_t. Based on this information, the direction for point advancement can be determined. Since each region is bounded by four planes and each plane divides the colour space into two half spaces, the region detection problem amounts to calculating which half space P_t occupies for each boundary plane. Using a fixed normal vector convention, and computing the dot product of the normal vector of a plane and the vector, defined by the difference of the points P_x and P_t, the half space containing the target point is cheaply identified. For example, if the dot product is positive, then P_t lies on the same side as the normal vector; otherwise, P_t is on the opposite side. Repeating this calculation for each boundary plane, the

partition region containing P_t is found.

6.2.4 Point Advancement

Knowing which region contains P_t. the components of P_x can be updated. If. for instance. the P_t is in the region in which all points have less magenta component. M_x. than the P_x. then the magenta component of P_x should be reduced and the cyan and yellow components maintained to define the new P_x. Note that. in this case. the current magenta component can be used to define the upper bound of the magenta component for P_t. Conversely. if the magenta component is too small. it should be increased to define the new P_x. The current level of the magenta component is the lower bound for P_t. The amount of change to the colour component is calculated based on the current upper and lower bound values of the colour component. The new colour component value is most effectively placed at the mid-point of the bounding values. When the colour relationship between the CMY and L*a*b* spaces is defined by the CLUT. the L*a*b* value of the mid-point may not be available without interpolation. In this case. the nearest sample point is used as the new P_x. Notice that the region in which the new P_x is centered is necessarily smaller after point advancement. The operations of gamut partition. region detection and point advancement are repeated until the point that has the closest CMY value related to the desired L*a*b* colour has been identified. Interpolation is then used to find the correct CMY value within the cell.

6.2.5 Performance Analysis of the Algorithm

Table 6.1 shows pseudocode of the algorithm. Steps 2 to 10 are performed for each iteration. The total number of iterations depends on the precision required. As mentioned in ther previous subsection. the new colour component value is the mid-point of its upper and lower bound. This approach is similar to binary search which has running time the order of $\log(M)$. where M is the number of points being searched. To determine the final CMY value. this algorithm requires $O(d\log(n))$

1. Set up the initial point of P_x and compute its Lab values
2. If $P_x = P_t$, go to step (11)
3. Determine 12 boundary planes based on the 8 neighbour points of P_x
4. Compute the normal vector of each plane
5. Compute the dot products of the vector (P_t - P_x) with the normal vector of each plane
6. Determine the region in which P_t lies
7. If P_t lies in the outside gamut region, go to step (12)
8. Adjust the lower or upper bound of P_t based on the result of (6)
9. Update the colour component of P_x based on the bounding values of (8)
10. Go to step (2)
11. Return the CMY value of P_x
12. Return out of gamut status

Table 6.1: Pseudocode of the extraction algorithm

	Expected Cost	Worst-Case Cost
Tetrahedral Walk	$O(n)$	$O(d^2 \log n)$
Tetrahedral BSP	$O(n^{d^2/2})$	$O(d^3 \log n)$
Iterative Extraction	$O(d\log(n))$	$O(d\log(n))$

Table 6.2: Compare the expected and worst-case costs of extraction for the tetrahedral walking and binary space partitioning tree algorithms with the iterative extraction algorithm.

iterations. where n is the number of sample points for each colour component. and d is the dimension of the colour space. For printer with 8^3 entries in a CLUT. the maximum number of iterations needed to find the CMY value is $3\log(8) = 9$. The expected and worst-case costs of this algorithm compared to the walking algorithm and binary space partitioning tree approaches [BC93] are shown in Table 6.2. The algorithm is fast enough that colour transformation in high dimensional spaces is possible for practical applications.

6.2.6 Applying the Extraction Algorithm in Reflectance Space

As discussed in the previous section. the success of the extraction algorithm relies on the iso-surfaces of the device gamut being smooth. It works well as long as the smoothness criterion is met. Thus. the algorithm works for a high dimensional reflectance space with little modification. In such a case. (d-1)D planes. hyperplanes are used to partition the regions. However. the complexity of gamut partition and region detection increases. and performance decreases. It is better to project a printer gamut into a space with dimension equal to the number of colour channels. The algorithm then works for any three ink printer with the performance described above. The latter approach is used in our studies and is described below.

In a reflectance space. a three-ink printer gamut is a 3-dimensional manifold in a high dimensional space. To use the extraction algorithm. the manifold should be projected into a space such that the smoothness property of the iso-surfaces is maintained. This can be achieved by projecting each iso-surface onto its tangent plane. The projection plane can be obtained by averaging the tangent planes of the iso-surfaces for different component values. Unfortunately. unless a mathematical model of the printer is known. the tangent planes cannot be computed. However. any close approximation of the planes serves equally well. The planes are defined by the gradient vectors of the iso-surfaces. which are computed by averaging the spectral differences between two reflectances. one of a colour with full amount of ink x. and the other with no ink x. The other two inks are kept constant. These

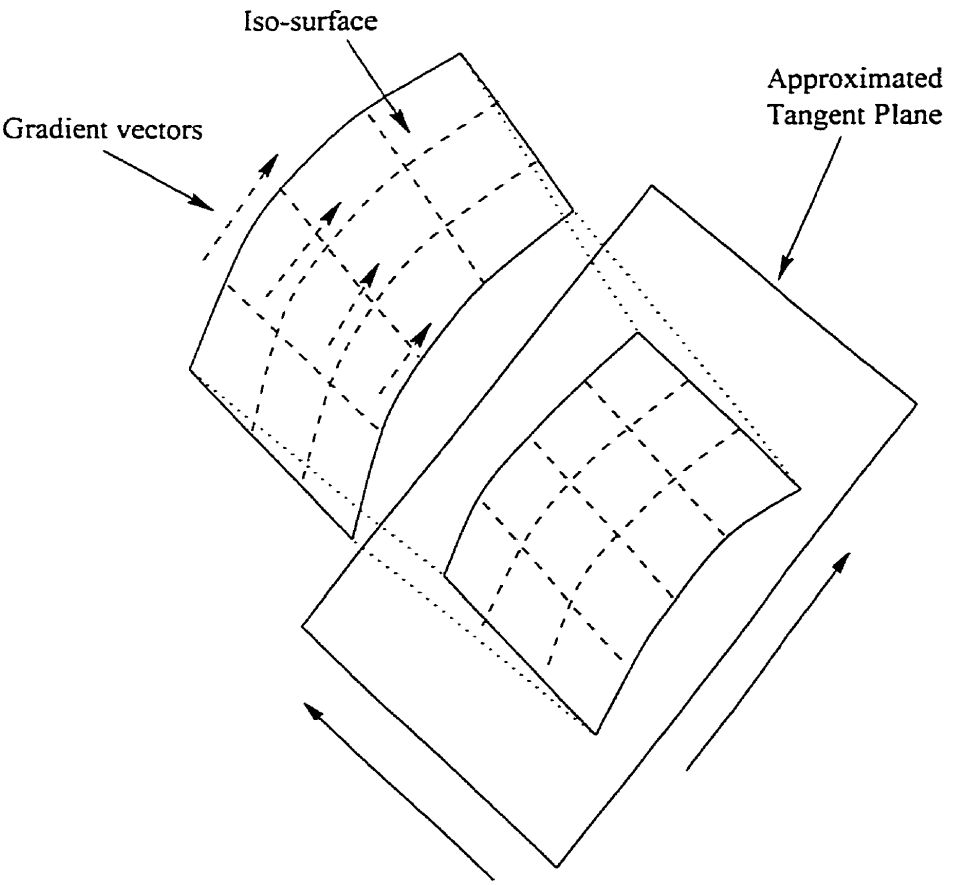


Figure 6.6: To maintain the smoothness property of an iso-surface, the surface is projected onto a tangent plane. However, since the printer model is not known in most cases, it may not be possible to compute the tangent plane. An approximation of the tangent plane is obtained by using gradient vectors.

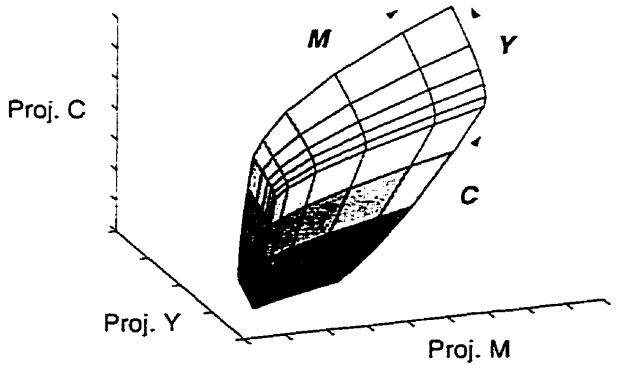


Figure 6.7: Projection of printer gamut in a reflectance space. Each projection direction is determined from the average gradients for the corresponding ink.

gradient vectors serve as the axes of a projection space. Any two axes define a projection plane in the reflectance space (Figure 6.6).

Once a projection space is defined. reflectances are projected into the space. The control value of any given reflectance is determined by the extraction algorithm operating as it does in CIELAB space.

The above procedure has been implemented and tested for the DuPont printer model discussed in Chapter 1. Figure 6.7 shows the printer gamut in the projection shape. The smoothness of the iso-surfaces is maintained by the projection. Each plot of Figure 6.8 is the orthogonal projection of an iso-surface for a given C value onto the projected plane defined by the gradient vectors of M and Y components. It shows that the points with constant C component are distributed in an orderly fashion. For testing purpose. the algorithm was applied to the 1000 randomly distributed colour samples of our DuPont printer. All results were converged to the target points. Thus. the extraction algorithm can be applied to the gamut in the projection space without any problems.

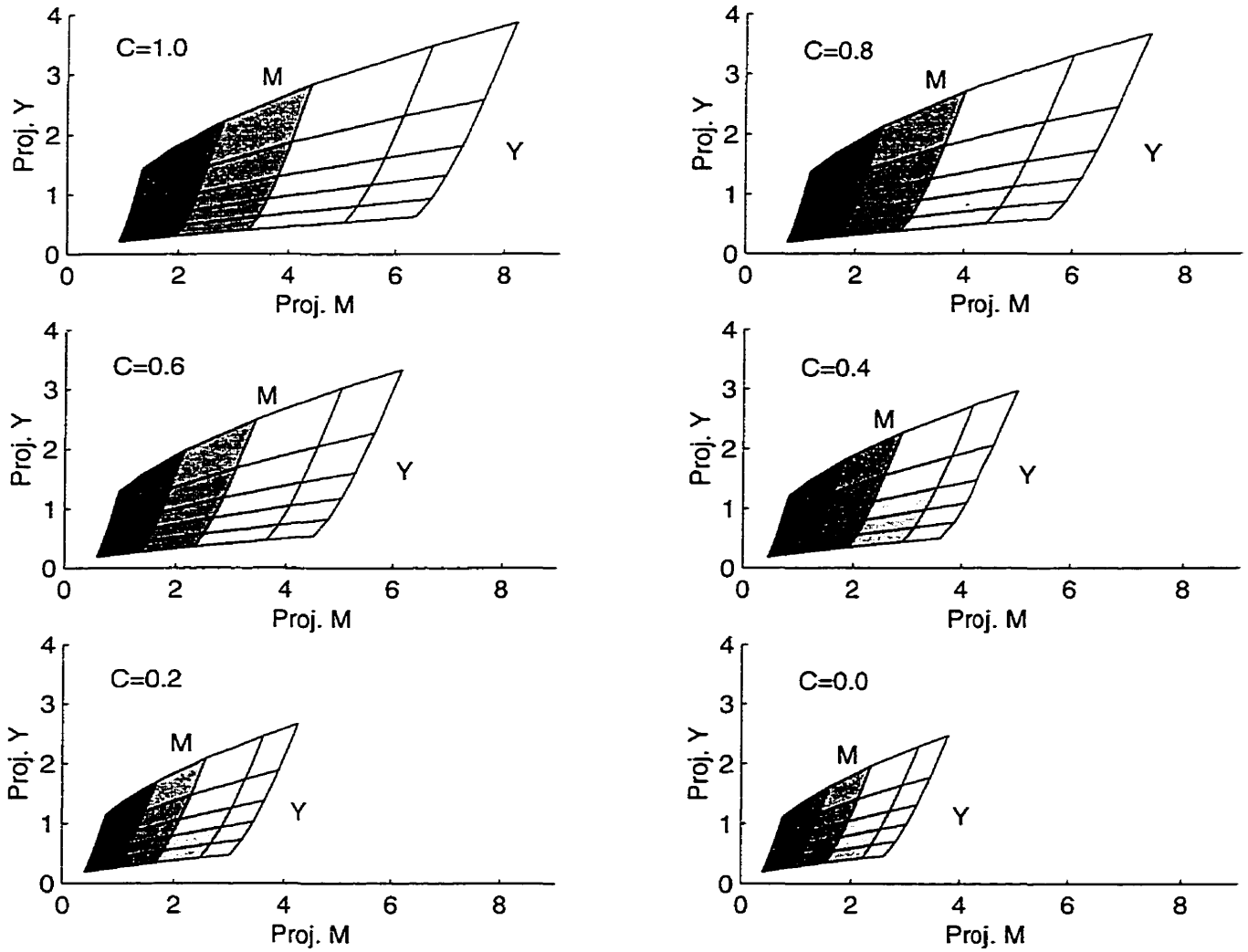


Figure 6.8: Orthogonal projection of printer gamut onto a plane. The smoothness of the iso-surfaces is maintained after projection.

6.3 Conclusion

The backward transformation is needed to compute the control values for a given output colour or reflectance. The CLUT method is commonly used for the transformation. To determine the control values. extraction first identifies the cell that contains the target point. after which the target control value is approximated by interpolation. Since the backward transformation has to be performed on every pixel. speed is important.

A fast extraction algorithm for backward transformation was developed. Its computation cost is logarithmic in the number of cells in the CLUT. and its performance is robust provided that the printer gamut in the colour space is sufficiently smooth. It was shown experimentally that printer models currently in use are adequately smooth. Measurement error can upset this condition. of course. and the gamut fitting techniques previously investigated in our laboratory [Bel96] can be used to condition measured data so that the new algorithm is guaranteed to converge. As shown in Section 6.2.6. the algorithm also works for reflective images.

The speed of the new algorithm makes it possible to increase the size of pseudo-uniform and pseudo-orthogonal CLUTs. Thus. higher accuracy conversion can be obtained.

Chapter 7

Conclusion

7.1 Summary of the Thesis

Digital colour image reproduction is one of the most active research areas in the printing industry. Those reproduction problems that are most difficult to solve occur because of differences in colour gamut from one device to another. This thesis studies how the gamut difference problem can be handled for colours specified as spectral reflectances. The following reproduction model is used. Devices are first characterized with respect to a device independent colour space. Input colours are then transformed to output colours by a gamut mapping defined in the device-independent space. Finally, output colours are converted to the device control signals through a backward transformation.

The two most common strategies for gamut mapping are discussed in Chapter 2. Based on the idea that colours with similar tristimulus values invoke similar colour sensations, one strategy seeks to minimize differences between reproduction and original in a colour space based on tristimulus values. The other is to match in the reproduction the colour relationships of the original image. Whichever strategy is used, most current algorithms perform the gamut mapping step on data specified directly or indirectly by CIE tristimulus colour values, which are derived from

emitted light, and depend on the source of illumination. If the human visual system has no colour constancy, perceived colours are solely based on the tristimulus values. Matching tristimulus values then provide a general solution for colour image reproduction. But the results are likely to be upset by changes in illumination, particularly when the spectral compositions of illuminants are significantly different. On the other hand, if the visual system exhibits perfect colour constancy, then matching appropriate aspects of surface reflectance is the best general solution for colour image reproduction. The human visual system exhibits good, but imperfect, colour constancy. Thus, gamut mapping techniques that take into account both reflectance and illumination may be expected to produce better results.

As an initial step towards making this possible the thesis develops the basic concepts of colour image reproduction in reflectance space. Both model-based and lookup-table methods for reflective characterization are described in Chapter 3. Compared to lookup-table methods, model-based characterization has lower measurement cost. However, the development cost of a device model is very high. Furthermore, the complexity of the model is usually too high to allow efficient colour transformation. Lastly, as demonstrated by the results of applying Berns' dye diffusion thermal transfer printer model to a similar printer, a general device model is very hard to find. Nevertheless, a device model that produces consistent output without disturbance by environmental factors is a valuable tool for studying colour image reproduction. In particular, even an incomplete device model can verify and smooth data measured for lookup tables.

Despite its larger measurement cost, a colour lookup-table (CLUT) characterization is most often used in practice because it provides very fast colour transformation. To construct a CLUT, samples can be chosen uniformly or nonuniformly throughout the device gamut. Uniform sampling allows fast data access with lower accuracy for nonlinear devices; nonuniform sampling provides higher accuracy with slower data access because of the high cost of extracting the cell within which interpolation is done.

After a CLUT is constructed, interpolation and extraction are used to identify target colours for colour transformation, a process that must be fast for both

forward and backward characterization transformations. A CLUT with uniformly sampled data is an intuitive choice. However, for the backward transformation it is difficult to obtained a CLUT with uniformly distributed data since the transfer function of the device is usually not known. Remeasuring or remapping can be used to build the CLUT. Remeasuring often needs several iterations before a final CLUT is built, which is too expensive to use with high dimensional colour spaces. On the other hand, remapping increases measurement errors that are present in the estimated control values because extensive resampling is required. Thus, a CLUT with nonuniformly distributed samples is likely to be preferred for colour spaces based on reflectance. In this case, fast interpolation and extraction are needed to provide good performance. Linear interpolation handles interpolation efficiently. The new iterative searching algorithm for extraction proposed in Chapter 6 can be used to improve extraction performance.

Once the input and output devices have been characterized, gamut mapping can be applied. The two common strategies for gamut mapping, matching trichromatic colour specifications and matching colour appearance, are studied for reflective data in Chapter 4 and Chapter 5. Since the reflectance spaces of colour devices are usually constructed to minimize spectral errors in the representation of reflectances, orthogonal projective mapping, which minimizes spectral errors, is a natural choice for gamut mapping between reflectance spaces. Chapter 4 shows that projective mapping produces perfect colorimetric matches only under restricted sets of illuminants. It does not always map to the reflectance that has the smallest trichromatic difference. Sometimes, it can produce rather large colour differences.

By taking account of the colour sensitivity of the human visual system, a gamut mapping based on the fundamental component of a reflectance was developed. This mapping preserves the fundamental component of a reflectance whenever possible. If no reproducible reflectance has the same fundamental component as the original, it finds the one that has minimal spectral errors as weighted by human visual sensitivity. This mapping is extended to multiple illuminants. Experiments to study its performance were conducted for two sets of illuminants, each having three different illuminants. The results show that fundamental component mapping consistently

outperforms projective mapping in terms of CIELAB colour differences.

To develop gamut mapping for matching appearance, the relationship between a reflectance and its perceived colour attributes must be known. Since colour attributes vary somewhat with illuminant while reflectance does not, there is not a fixed relationship between a reflectance and its colour attributes. Nevertheless, it turned out to be possible to develop useful concepts for colour attributes of different reflectances.

Most gamut mapping algorithms based on colour attributes reproduced colour lightness, hue and saturation. This thesis defined methods for identifying sets of reflectances that are constant in these attributes. To begin, it defines a procedure to identify constant hue spaces within a reflectance colour space. A constant hue space is a linear subspace that contains the set of reflectances that are identical in hue under a given set of illuminants. To retain the hue of an original reflectance, the reproduced reflectance is chosen from the subspace.

Similarly, luminance can be maintained by choosing the reproduced reflectance from cosets of spaces of constant luminance. However, when reproducing relative lightness care must be taken because relative luminance varies with illuminant. Our results show that luminances of colours far from the achromatic axis are more sensitive to illuminant change, making it important to ensure that luminances of saturated colours are mapped correctly.

By examining relative saturations of reflectances in a constant hue plane, we see that the distribution of saturation in a reflectance space is similar to the distribution of saturation in colour spaces based on tristimulus values. The further away a reflectance is from the achromatic axis, the higher saturation it has, although there is a variable monotonic scaling factor. In fact, the topological properties of lightness and saturation in a constant hue plane of a colour space based on reflectance are similar to those of trichromatic colour spaces.

As a result, many current gamut mapping algorithms can be easily adopted for reflectance space. As a proof of this concept, two basic mapping algorithms based on colour attributes have been defined for reflective images. Both methods ensure

that the hues of the original reflectances are maintained.

Once the desired reflectance is known, the control values of an output device corresponding to the reflectance must be found using the backward transformation. As mentioned previously, transformations using a CLUT created with nonuniform sampling are preferred for colour spaces based on reflectance. However, algorithmic inefficiencies associated with nonuniformly sampled CLUTs must be overcome to obtain acceptable performance. For this reason, a general cell-finding algorithm based on the divide-and-conquer concept of binary subdivision has been developed for extraction. Its computation cost is logarithmic in the number of cells in the CLUT. The algorithm identifies cells for extraction from any smooth printer gamut. The procedure for using the algorithm in a reflectance space was given in Chapter 6.

7.2 Future Work

Research in colour image reproduction has expanded rapidly because of recent advances in desktop technology. It was not possible to investigate all aspects of image reproduction in reflective colour spaces during this research. A complete reflective image reproduction solution will not be possible until further research has been done. Here are some of the important issues that need further study.

1. Device gamuts in reflectance space. The gamut mapping algorithms developed in this thesis focus on the physically realizable reflectances, which may or may not be producible by a specific output device. A mapping from reflectances to printable colours should be defined. Thus, it is important to find a compact representation for device gamuts in a high dimensional reflectance spaces.

2. Gray component replacement. Gray component replacement, which replaces mixtures of cyan (C), magenta (M), and yellow (Y) inks with appropriate amounts of black (K) ink, has been widely used for enhancing reproduction quality. It is often done in two steps [HPK89, Hun94a, Say87]. First, the

required amount of C. M. and Y inks are determined. Then the amount of black ink to replace part of the C. M. Y inks is calculated. Gray component replacement is complicated by there being more than one possible mixture of inks for a given colour in a trichromatic colour space. Because reflective colour specifications are more resistant to metamerism there are fewer mixtures that match reflectance components. Future research may able to find gray component replacement solution that improve resistance to metamerism.

3. Additional inks for better colour image reproduction. Colour image reproduction process using more than four inks have been studied [Ost93. Bol94]. As more inks are used. the printer gamut becomes larger. However. part of the extra gamut is hidden in a trichromatic space because some colours can be produced by more than one possible mixture of inks. This hidden gamut is revealed in reflectance space. Future study would able to provide multiple illuminant solutions for extra inks using concepts developed in Chapter 4.

Even after such issues have been resolved. image reproduction using colour spaces based on reflectance fails to guarantee a general solution of colour image reproduction. Better understanding of the working of the human visual system. and particularly of colour constancy. is essential for future advance in colour image reproduction. With this knowledge. algorithms for colour reproduction can take into account both illuminant and reflectance information to produce better results.

7.3 Final Conclusions

This research developed the basic concepts of colour image reproduction in colour spaces based on reflectance. It examined each of the major image reproduction steps for reflective images. including device characterization. gamut mapping. and backward colour transformation. The findings of this research provide a basic framework for developing future colour image reproduction in reflectance space.

By studying model-based and colour CLUT characterization methods, this research concludes that device characterization based on a CLUT is preferred to model-based characterization. Specifically, CLUT with nonuniform sampling should be used since it provides better accuracy without incurring the high measurement cost of uniform sampling.

Reflectance space gamut mapping algorithms based on objective measurement, such as the colour difference between the original and reproduced colours in the CIELAB colour space, and ones based on subjective criterion, matching colour appearance, were investigated. For minimizing colour difference, this research shows that the seemingly *neutral* choice of orthogonal projective mapping should be avoided. By taking into account the human visual system, a novel algorithm that preserves fundamental component was developed. It was proven to exhibit consistently smaller colour differences for multiple illuminants. For matching colour appearance, useful concepts, such as constant hue space, relative luminance and saturation for reflectances, were developed in this thesis. These concepts are essential for developing appearance matching gamut mapping algorithms in colour spaces based on reflectance. As demonstrated in this thesis, gamut mapping algorithms based on perceived colour attributes in the CIE tristimulus colour spaces can be easily adapted for reflectance colour spaces because of luminance and saturation distributions are similar in constant hue planes of both kinds of colour spaces.

Since nonuniformly sampled CLUTs, which increase the cost of extracting colour cells for the backward transformation, are recommended for reflectance colour spaces, it is essential for practical applications to have a fast backward transformation. A novel algorithm for cell-finding was developed. This algorithm improves the speed of extraction, which must be done once per image pixel. As a result, better performance of the backward transformation can be obtained.

As mentioned in the previous section, a general colour image reproduction system based on reflectance is far from complete. However, this research provides the starting point for developing reproduction systems for reflective images. The basic concepts and the novel algorithms for gamut mapping and backward transformation developed in this thesis set up the groundwork for future development of colour

reproduction for reflective images.

Bibliography

[ACB93] J. P. Allebach. J. Z. Chang. and C. A. Bouman. Efficient implementation of nonlinear color transformations. In *Proc. IS&T/SID 1st Color Imaging Conference: Transforms & Transportability of Color*. pages 143–148. 1993.

[AFR96] J. M. Adams. D. D. Faus. and L. J. Rieber. *Printing Technology*. An International Thomson Publishing Company. New York. 1996.

[All80] E Allen. Colorant formulation and shading. In F. Grum and C.J. Bartleson. editors. *Optical Radiation Measurement. Volumn 2. Color Measurement*. Academic Press. New York. 1980.

[BC93] I. E. Bell and W. Cowan. Characterizing printer gamuts using tetrahedral interpolation. In *Proc. IS&T/SID 1st Color Imaging Conference: Transforms & Transportability of Color*. pages 108–113. 1993.

[BC94] I. E. Bell and W. Cowan. Device characterization using spline smoothing and sequential linear interpolation. In *Proc. IS&T/SID 2nd Color Imaging Conference*. pages 29–32. 1994.

[Bel96] Ian E. Bell. *Spline-Based Tools For Conventional and Reflective Image Reproduction*. PhD thesis. University of Waterloo. 1996.

[Ber93] Roy S. Berns. Spectral modeling of a dye diffusion thermal transfer printer. *Journal of Electronic Imaging*. 2:359–370. 1993.

[BF95] K. M. Braun and M. D. Fairchild. Evaluation of five color-appearance transforms across changes in viewing conditions and media. In *Proc. IS&T/SID 3st Color Imaging Conference*. pages 93–96. 1995.

[BF97] D. H. Brainard and W. T. Freeman. Bayesian color constancy. *Journal of the Optical Society of America. A*. 14:1393–1411. 1997.

[Bok97] S. M. Boker. A measurement of the adaptation of color vision to spectral environment. *Psychological Science*, 8(2):130–134, 1997.

[Bol94] H. Boll. A color to colorant transformation for a seven ink process. In *SPIE*. volume 2170. pages 108–118. 1994.

[BS81] W. Jr. Billmeyer and M. Saltzman. *Principles of Color Technology*. John Wiley & Sons. Inc.. 2nd edition. 1981.

[BW91] D. H. Brainard and B. A. Wandell. A bilinear model of the illuminant's effect on color appearance. In J. A. Movshon and M. S. Landy. editors. *Computational Models of Visual Processing*. MIT Press. Cambridge. MA. 1991.

[CC96] W. Chau and W. Cowan. Gamut mapping based on the fundamental components of reflective image specificiation. In *Proc. IS&T/SID 4th Color Imaging Conference: Color Science. Systems and Applications*. pages 67–70. 1996.

[CC97] W. Chau and W. Cowan. A fast iteration algorithm for mapping l*a*b* to cmy values. In *Proc. IS&T/SID 5th Color Imaging Conference: Color Science. Systems and Applications*. pages 92–95. 1997.

[CIE78] CIE (Commission Internationale de l'Eclairage). Bureau Central de la CIE. Paris. *CIE Recommendations on Uniform Color Spaces. Colour-difference Equations. and Psychometric Colour Terms*. 1978. Supplement No. 2 to Publication CIE No. 15. Colrimetry.

[CK82] J. B. Cohen and W. F. Kappauf. Metameric color stimuli. fundamental metamers. and wyszecki's metameric blacks. *American Journal of Psychology*. 95(4):537–564. 1982.

[Coh88] J. B. Cohen. Color and color mixture: Scalar and vector fundamentals. *Color Research and Application*. 13(1):5–39. 1988.

[CY55] F. R. Clapper and J. A. C. Yule. Reproduction of color with halftone images. In *TAGA Proceedings*. pages 1–12. 1955.

[Dan92] J. L. Dannemiller. Spectral reflectance of nautral objects: how many basis functions are necessary ? *Journal of the Optical Society of America. A*. 9(4):507–515. 1992.

[D'Z92] M. D'Zmura. Color constancy: Surface color from changing illumination. *Journal of the Optical Society of America. A*. 9:490–493. 1992.

[Fai91] M. D. Fairchild. Formulation and testing of an incomplete-chromatic adaptation model. *Color Research and Application*. 16:243–250. 1991.

[Fai93] M. D. Fairchild. Rlab: A color appearance space for color reproduction. In *Proceedings of SPIE: Device Independent Color Imaging Systems Intergration*. volume 1909. pages 19–29. 1993.

[FIS89] S.H. Friedberg. A.J. Insel. and L. E. Spence. *Linear Algebra.* Prentice-Hall International. Inc. 2nd edition. 1989.

[Fla82] P. Flanklin. Interpolaiton methods and apparatus. US Patent 4334240. 1982.

[Fun93] B. V. Funt. Modelling reflectance by logarithmic basic functions. In *Proc. IS&T/SID 1st Color Imaging Conference: Transforms & Transportability of Color.* pages 68–71. 1993.

[GB82] F. Grum and C. J. Bartleson. editors. *Optical Radiation Measurements.* John Wiley & Sons. Inc.. 1982.

[GHP87] J. Gordon. R. Holub. and R. Poe. On the rendition of unprintable colors. In *TAGA Proceedings.* pages 186–195. 1987.

[Gra95] E. M. Granger. Gamut mapping for hard copy using the atd color space. In *Proceedings of SPIE.* volume 2414. pages 27–35. 1995.

[Gua92] Randall G. Guay. Method of color correction which preserves perceived color differences. In *Proceedings of the SPIE: Color Hard Copy and Graphic Arts.* volume 1670. pages 335–343. 1992.

[Gut91] S. L. Guth. Model for color vision and light adaptation. *Journal of the Optical Society of America. A.* 8:976–993. 1991.

[GVL83] G. H. Golub and C. F Van Loan. *Matrix Computations.* The Johns Hopkins University Press. Maryland. 1983.

[GWA90] R. S. Gentile. E. Walowit. and J. P. Allebach. A comparison of techniques for color gamut mismatch compensation. *Journal of Imaging Technology.* 16(5):176–181. 1990.

[HB93] T. Hoshino and R.S. Berns. Color gamut mapping techniques for color hard copy images. In *Proceedings of SPIE: Device Independent Color Imaging Systems Intergration.* volume 1909. pages 152–164. 1993.

[HFD90] J. Ho. B. V. Funt. and M. S. Drew. Separating a color signal into illumination and surface reflectance components: Theory and application. *IEEE Trans. Pattern Anal. Mach. Intell..* PAMI-12:966–977. 1990.

[HPK89] R. Holub. C. Pearson. and W Kearsley. The black printer. *Journal of Imaging Technology.* 15(4):149–158. 1989.

[HRV97] B. Hill. T. Roger. and F. W. Vorhagen. Comparative analysis of the quantization of color spaces on the basis of the cielab color-difference formula. *ACM Transaction on Graphics.* 16(2):109–154. 1997.

[Hun89] J. R. Huntsman. A planar-vector based color space for graphic arts color analysis and reproduction. *Color Research and Application.* 14:240–259. 1989.

[Hun91a] R. W. G. Hunt. Revised colour-appearance model for related and unrealted colours. *Color Research and Application*. 16:146–165. 1991.

[Hun91b] Robert W. G. Hunt. *Measuring Colour*. Ellis Horwood. England. 2th edition. 1991.

[Hun93] Po-Chieh Hung. Colorimetric calibration in electronic imaging devices using a look-up-table model and interpolation. *Journal of Electronic Imaging*. 2:53-61. 1993.

[Hun94a] Po-Chieh Hung. Smooth colorimeteric calibration technique utilizing the entire color gamut of cmyk printers. *Journal of Electronic Imaging*. 3:415–424. 1994.

[Hun94b] R. W. G. Hunt. An improved predictor of colourfulness in a model of colour vision. *Color Research and Application*. 19:23–26. 1994.

[Hun95] Robert W. G. Hunt. *The Reproduction of Colour*. Fountain Press. Kingston-upon-Thames. UK. 5th edition. 1995.

[Kan95] Henry R. Kang. Comparisons of three-dimensional interpolation techniques by simulations. In *SPIE*. volume 2414. pages 104–114. 1995.

[Kan96] Henry R. Kang. *Color Technology for Electronic Imaging Devices*. SPIE. Bellingham. Washington. USA. 1996.

[KFK92] K. Kanamori. T. Fumoto. and H. Koter. A color transformation algorithm using prism interpolation. In *IS&T 8th International Congress on Advances in Non-Impact Printing Technologies*. pages 477–482. 1992.

[Kri47] E. L. Krinov. Spectral reflectance properties of natural formations. Technical report. Technical Translation TT-439 (National Research Council of Canada. 1953). 1947.

[Lai93] Pekka Laihanen. A new approach to the manipulation of colour display images. In *Proceedings of SPIE: Device Independent Color Imaging Systems Intergration*. volume 1909. pages 31–43. 1993.

[LM71] E. H. Land and J. J. McCann. Lightness and retinex theory. *Journal of the Optical Society of America*. 61(1):1–11. 1971.

[Mac93] Lindsay W. MacDonald. Gamut mapping in perceptual colour space. In *Proc. IS&T/SID 1st Color Imaging Conference: Transforms & Transportability of Color*. pages 193–196. 1993.

[ML97] J. Morovic and M. R. Luo. Gamut mapping algorithms based on psychophysical experiment. In *Proc. IS&T/SID 5nd Color Imaging Conference: Color Science. System and Application*. pages 44–49, 1997.

[Mun46] A. H. Munsell. *A Color Notation.* Baltimore: Munsell Color Company. Inc.. 1946.

[MW86] L. T. Maloney and B. A. Wandell. Color constancy: A method for recovering surface spectral reflectance. *Journal of the Optical Society of America. A.* 3:29–33. 1986.

[NKP92] S. I. Nin. J. M. Kasson. and W. Plouffe. Printing cielab images on a cmyk printer using tri-linear interpolation. In *SPIE.* volume 1670. pages 316–323. 1992.

[NTS90] Y. Nayatani. K. Takahama. and H Sobagaki. Color-appearance model and chromatic-adaptation transform. *Color Research and Application.* 15:210–221. 1990.

[Ost93] V Ostromoukhov. Chromaticity gamut enhancement by heptatone multi-color printing. In *Proceedings of SPIE: Device Independent Color Imaging Systems Intergration.* volume 1909. pages 139–151. 1993.

[Pae94] A. W. Paeth. *Linear Models of Reflective Colour.* PhD thesis. University of Waterloo. 1994.

[PS86] J. Pokorny and V. Smith. Colorimetry and color discrimination. In K.R. Buff. L. Kaufman. and J. P. Thomas. editors. *Handbook of Perception and Human Performance. Volumn 1.* John Wiley & Sons Inc.. 1986.

[Pyg74] P. C. Pygsley. Image reproduction methods and apparatus. British Patent 1.369.702. 1974.

[RK93] S. A. Rajala and A. P. Kakodkar. Interpolation of color data. In *Proc. IS&T/SID 1st Color Imaging Conference: Transforms & Transportability of Color.* pages 180–183. 1993.

[RW86] M. Richter and K Witt. Din colour system. *Color Research and Application.* 11:138. 1986.

[Say87] K. Sayanagi. Black printer. ucr and uca. In *TAGA Proceedings.* pages 711–724. 1987.

[SCB88] M.C. Stone. W.B. Cowan. and J.C. Beatty. Color gamut mapping and the printing of digital color images. *ACM Transactions on Graphics.* 7(4):249–292. 1988.

[Sch86] William F. Schreiber. A color prepress system using appearance variables. *Journal of Imaging Technology.* 12(4):200–211. 1986.

[SFB92] M. Stokes. M. D. Fairchild. and R. S. Berns. Precision requirements for digital color reproduction. *ACM Transaction on Graphics.* 11(4):406–422. 1992.

[SI78] T. Sakamoto and A. Itooka. Interpolation method for memory devices. Japanese Patent Disclosure 53-123201. 1978.

[Smi78] A. R. Smith. Color gamut transform pair. *Computer Graphics*. 12:12–19. 1978.

[SW91] M.C. Stone and W.E. Wallace. Gamut mapping computer generated imagery. In *Proceedings of Graphics Interface*. pages 32–39. 1991.

[VGI94] M. J. Vrhel. R. Gershon. and L. S. Iwan. Measurement and analysis of object reflectance spectra. *Color Research and Application*. 19(1):4–9. 1994.

[VW92] J.A.S. Viggiano and C.J. Wang. A comparison of algorithms for mapping color between media of differing luminance ranges. In *TAGA & ISCC Proceedings*. volume 2. pages 959–973. 1992.

[WAB94] M. Wolski. J.P. Allebach. and C.A. Bouman. Gamut mapping: Squeezing the most out of your colour system. In *Proc. IS&T/SID 2nd Color Imaging Conference: Color Science. System and Application*. pages 89–92. 1994.

[Wan87] B. A. Wandell. The synthesis and analysis of color images. *IEEE Trans. Pattern Anal. Mach. Intell.*. PAMI-9:2–13. 1987.

[WG93] D. Walker and Scott Gregory. The effects of illuminant spectra on desktop color reproduction. In *Proceedings of SPIE: Device Independent Color Imaging Systems Intergration*. volume 1909. pages 236–246. 1993.

[WS82] G. Wyszecki and W. S. Stiles. *Color Science: Concepts and Methods. Quantitative Data and Formulae*. John Wiley & Sons. Inc.. 2nd edition. 1982.

[Wys86] G. Wyszecki. Color apperance. In K.R. Buff. L. Kaufman. and J. P. Thomas. editors. *Handbook of Perception and Human Performance. Volumn 1*. John Wiley & Sons Inc.. 1986.

[YN51] J. A. C. Yule and W. J. Nielsen. The penetration of light into paper and its effect on halftone reproduction. In *TAGA Proceedings*. pages 65–75. 1951.

[Yul67] J.A.C. Yule. *Principles of Color Reproduction*. John Wiley & Sons. 1967.